

University of Nevada, Reno

**Spatial and Temporal Variation of Dissolved Arsenic Concentrations in the
Intermediate Aquifer of the Lahontan Valley, Nevada**

A thesis submitted in partial fulfillment of the
requirements for the degree of Master of Science in
Hydrogeology

By

Michael S. Meinert

Dr. Mark J. Walker, Ph.D./Thesis Advisor

August, 2009

© by Michael S. Meinert
All Rights Reserved



THE GRADUATE SCHOOL

We recommend that the thesis
prepared under our supervision by

MICHAEL S. MEINERT

entitled

**Spatial And Temporal Variation Of Dissolved Arsenic Concentrations In The
Intermediate Aquifer Of The Lahontan Valley, Nevada**

be accepted in partial fulfillment of the
requirements for the degree of

MASTER OF SCIENCE

Mark J. Walker, Ph.D., Advisor

Lisa L. Stillings, Ph.D., Committee Member

Glenn C. Miller, Ph.D., Graduate School Representative

Marsha H. Read, Ph. D., Associate Dean, Graduate School

August, 2009

Abstract

A study was conducted in the intermediate-depth alluvial aquifer (50-500 ft) of Lahontan Valley, Nevada, to determine if there is temporal and spatial stability of dissolved arsenic concentrations, and if chemical mechanisms commonly associated with arsenic mobility are responsible for any trends observed. This aquifer is an alkaline and reducing environment that is chemically distinct from hydrologic units above and below it. Five wells previously observed to have substantial concentrations of both As(V) and As(III) were chosen to represent a groundwater flow-path and were sampled monthly from February 2004 – August 2005. Arsenic concentrations were observed to be statistically unchanged for the sampling period at each well, as were the majority of other chemical constituents and physical characteristics. Spatially, total arsenic activities $[As_T]$ increased nearly seven-fold along the flow-path, and the ratio of the concentration of arsenic as arsenite to total arsenic ($[As(III)]/[As_T]$) decreased. The concentration of total arsenic correlated with dissolved organic carbon (DOC), $[HCO_3^-]$, and distance along flow-path ($p = 0.04, 0.01, 0.02$, respectively).

NETPATH 2.0 and Visual MINTEQ 2.3 geochemical models were employed to model geochemical reactions controlling potential arsenic release to the aquifer using both field -measured and modeled electric potential (Eh) values. Models show minor desorption of AsO_4^{3-} from hydrous ferric oxides (HFO) along the flow-path (~0.5%), and to a lesser degree with increased pH. H_3AsO_3 desorbed to a greater degree along the flow-path according to models, with little pH dependence. Arsenic out-competed phosphate for sorption sites according to the models. Competition from other ligands was also likely. Model analysis indicated that reductive dissolution of HFO did not occur at

field-measured Eh and average pH for each well. However, under MINTEQ-computed Eh values that were considerably lower, HFO reductive dissolution was shown to occur, potentially releasing arsenic to groundwater. Further research into the strong correlation of As_T with DOC and HCO_3^- is suggested.

to my father, Richard J. Meinert, Jr.

Acknowledgements

- Thesis Advisor: Dr. Mark J. Walker
Department of Natural Resources and Environmental Science
College of Agriculture, Biotechnology, and Natural Resources
- Thesis Committee: Dr. Lisa L Stillings
U.S. Geological Survey
Department of Geological Sciences and Engineering
College of Science
- Dr. Glenn C. Miller
Department of Natural Resources and Environmental Science
College of Agriculture, Biotechnology, and Natural Resources
- Funding: This project is based upon work supported by the U.S. Department of Agriculture, with a grant funded through the National Water Program.
- Any opinions, findings, conclusions, or recommendations expressed in this publication are those of the author and do not necessarily reflect the view of the U.S. Department of Agriculture
- Special Thanks: Mae Gustin
Jerry Qualls
Simon Poulson
Ralph Seiler
Alan Welch
Jim Thomas
DeEtta Fosbury
Emile Sawyer
Scott Brown
Jason Assam
Pam Willard
Lynell Qualls
Jodi Ericson
Jennifer Reisig
Tom Stewart

Table of Contents

Abstract.....	i
List of Tables.....	viii
List of Figures.....	ix
Chapter 1: Introduction.....	1
Project Significance.....	1
Background and previous work.....	4
1. Hydrogeologic setting.....	4
2. Groundwater recharge.....	5
2.1 Shallow alluvial aquifer.....	6
2.2 Intermediate alluvial aquifer.....	6
3. Arsenic occurrence.....	8
3.1 General.....	8
3.2 Sources of arsenic in the Lahontan Valley.....	9
Hypotheses.....	11
Chapter 2: Variation in Arsenic Concentrations.....	13
Abstract.....	13
Introduction.....	14
1. The intermediate-depth aquifer in the Lahontan Valley.....	15
2. Hypotheses.....	17
Methods.....	17
1. Water samples.....	18
2. Laboratory methods.....	19

3. Data analysis.....	20
3.1 Graphical methods.....	20
3.2 Statistical methods.....	22
Results.....	23
1. Water chemistry.....	23
1.1 Temporal variation.....	23
1.2 Spatial variation.....	23
Discussion.....	24
1. Temporal variation.....	24
1.1 Stable isotopes.....	24
1.2 Major ions.....	24
1.3 Other parameters.....	25
1.4 Arsenic.....	25
2. Spatial variation.....	26
2.1 Stable isotopes.....	26
2.2. Major ions.....	26
2.3 Other parameters.....	27
2.4 Arsenic.....	27
3. Arsenic and other correlations.....	28
Conclusions.....	29
Chapter 3: Arsenic enrichment mechanisms.....	52
Abstract.....	52
Introduction.....	53

1. Eh/pH controls on precipitation/dissolution	54
2. Adsorption.....	59
3. Exchange.....	63
4. Reaction rates.....	63
Hypotheses.....	64
Methods.....	64
1. NETPATH 2.0.....	67
2. Visual MINTEQ 2.3.....	68
Results.....	68
1. NETPATH Analysis.....	70
2. Visual MINTEQ Analysis.....	71
Discussion.....	73
Conclusions.....	77
Chapter 4 – Future Work.....	96
Literature cited.....	98
Appendices.....	102
Appendix A - Complete sample data.....	102
Appendix B - Ionic strength calculations.....	107
Appendix C - Eh-pH diagram calculations.....	108
Appendix D - Colorimetric iron analyses.....	111
Appendix E - complete NETPATH modeling results.....	121
Appendix F - Modeled ferrihydrite equilibrium with Fe ³⁺	123
Appendix G - Fe substrate determination for MINTEQ.....	124

List of Tables

Table 1 - Sampled parameters.....	32
Table 2 - Methods and detection limits used for analysis.....	33
Table 3 - Summaries of chemical and physical characteristics of wells A—E through time.....	34
Table 4 - Summary of statistical analyses to evaluate the existence of temporal trends for A _{ST}	35
Table 5 - Pearson's correlation coefficients (R) and probabilities (p) of Type II error (failure to reject the null hypothesis when the null hypothesis is false) for chemical and physical characteristics versus distance and well depth.....	36
Table 6 - Average parameter values for NETPATH input.....	81
Table 7 - Average parameter values for MINTEQ input.....	82
Table 8 - Iron activity associated with the five methods for measuring or estimating Eh	83
Table 9 - Selected NETPATH flow-path results using data from Table 6, colorimetric Fe(T), and field and MINTEQ-computed Eh values segment A-D and segment A-E.....	84
Table 10 - Saturation indices modeled by MINTEQ and NETPATH using colorimetric Fe(T), field and computed Eh values.....	85

List of Figures

Figure 1 - Lahontan Valley Hydrographic Region.....	12
Figure 2 - Well location map with general groundwater flow direction, including Whitney (1994) and Lico and Seiler (2004) wells	37
Figure 3 - Well depths along the flow path (Wells A—E) with ground surface elevations and measured depths to water.....	38
Figure 4 - $\delta^2\text{H}$ vs. $\delta^{18}\text{O}$ plot for study wells and data sets, showing results of previous analyses, this study (wells A—E), Fosbury (2008), Lico and Seiler (1994) and the Global Meteoric Water Line (Craig, 1981b).....	39
Figure 5 - Expanded view of $\delta^2\text{H}$ vs. $\delta^{18}\text{O}$ plot for wells A—E.....	40
Figure 6 - Time-series plots for major ions.....	41
Figure 7 - Time-series plots for As_T , $\text{As}(\text{III})$, pH, dissolved organic carbon (DOC), Eh, conductivity and dissolved oxygen (DO).....	42
Figure 8 - Major ions for A-E (Wells A-D, n=20; Well E, n=19). Upper, middle, and lower boundaries of the boxes represent the 75th, 50th, and 25th percentile of the data, respectively.....	43
Figure 9 - Summaries of sampling data for As_T , $\text{As}(\text{III})$, pH, DOC, Eh, conductivity and dissolved oxygen (DO) for wells A—E.....	44
Figure 10 - A time-series of As_T concentrations, with LOWESS smoothing to evaluate seasonal cycling.....	45
Figure 11 - Piper plots for flow-path well chemistry for major ions.....	46
Figure 12 – As_T vs distance for sampled wells.....	47

Figure 13 - Significant linear relationships between As_T and HCO_3^- , Na, SO_4^{2-} and Cl.....	48
Figure 14 - Relationships between As_T and pH, conductivity, dissolved organic carbon and total phosphorus, expressed with linear relationships developed by regression analysis.....	49
Figure 15 - Linear relationships between As_T and Eh, DO, and Fe.....	50
Figure 16 - $As(III)/As_T$ vs pH and P(T).....	51
Figure 17 - Eh/pH stability diagram for arsenic species (Nordstrom and Archer, 2003).....	86
Figure 18 - pH dependency on adsorption on ferrihydrite for $As(III)$ and $As(V)$ (Stollenwerk, 2003).....	87
Figure 19 - Arsenic adsorption with phosphate (Stollenwerk, 2003).....	88
Figure 20 - ICP-MS Fe(T) and colorimetric Fe(T) compared for Wells A-E.....	89
Figure 21 - $As(T)$ adsorption as a function of Eh at average pH for all wells (8.79).....	90
Figure 22 - Arsenate and arsenite adsorption as a function of Eh at average pH for all wells (pH=8.79).....	91
Figure 23 - MINTEQA2 modeled As adsorption as a function of pH at field-measured Eh values.....	92
Figure 24 - PO_4^{3-} and HCO_3^- adsorption on HFO as a function of pH at field-measured Eh.....	93
Figure 25 - Eh/pH stability field for selected redox couples at pH range of study.....	94

Figure 26 - Proposed reaction mechanisms associated with carbon sources, mediated by
microbial activity.....95

Chapter 1 - Introduction

Introduction

Dissolved arsenic is commonly found in two valence states: arsenate (As(V)) and arsenite (As(III)). These forms of arsenic occur as oxyacids and their conjugate bases as well as within several organic compounds. In January 2006, the Environmental Protection Agency (EPA) reduced the maximum contaminant level (MCL) for arsenic in public drinking water supplies from 50 µg/L to 10 µg/L (EPA 2008). Although the MCL does not distinguish between As(V) and As(III) for regulation purposes, As(III) has been cited as being more toxic than As(V) (Peters, McCurdy et al. 1996; Lepkowski 1998; Saranko, Halmes et al. 1998; ATSDR 2000). Sub-acute doses of arsenic can cause nausea, diarrhea, fatigue, skin lesions, and circulatory and peripheral nervous disorders. Long-term exposure to subacute doses of arsenic can cause organ failure and a variety of cancers, including those of the liver, bladder, kidneys, prostate, and lungs. The dose associated with these complications is less for As(III) than that for arsenate (As(V)) (ATSDR 2000). The 50% lethal dose (LD₅₀) for As(III) in rats is between 15 and 110 mg/kg, compared with As(V) at 110 to 175 mg/kg (ATSDR 2000).

Project significance

Approximately 60% of the 24,000 residents in the Lahontan Valley in Churchill County, Nevada, obtained their water from the City of Fallon municipal water system which operates a treatment facility that maintains arsenic levels at or below 10 µg/L. The remaining residents pumped household water from nearly 5000 domestic wells drilled in

the region. These residents are potentially the most affected by high concentrations of arsenic in groundwater (Lico and Seiler 1994; Thundiyil, Yuan et al. 2007).

Agricultural irrigation water accounts for the vast majority of surface recharge to regional aquifers in the Fallon area and is applied only during the growing season, which lasts approximately 216 days from early April to late October. Approximately 84% of surface water recharge in the Fallon area is due to the application of irrigation water, which may cause seasonal geochemical changes in the water table due to changes in salinity (Seiler and Allander 1993; Herrera, Seiler et al. 2000); associated changes in redox potential and/or pH could affect the proportion of total arsenic occurring as As(III). Arsenic concentrations can vary daily and seasonally in surface streams but remain fairly constant in groundwater (Seiler 2004; Steinmaus, Yuan et al. 2005). Several studies have observed seasonal change in total arsenic concentration (Frost, Frank et al. 1993; Steinmaus, Yuan et al. 2005; Thundiyil, Yuan et al. 2007). However, they did not examine the chemical or hydrological mechanisms associated with such changes.

Recent studies suggest that groundwater arsenic concentrations do not change with irrigation or rainfall (Thundiyil, Yuan et al. 2007). Of the 356 wells observed by Thundiyil et al (2007), a significant percentage (44%) of them had arsenic concentrations that differed by season. However, this proportion was not significant to conclude that arsenic concentrations varied from dry season to wet season. Steinmaus et al. (2005) came to a similar conclusion based on samples from 759 wells taken several years apart. Where arsenic concentrations changed, mechanisms for the fluctuation in arsenic concentration included dilution of groundwater by rainfall, redox changes due to changing pumping rates, movement of groundwater, and depth of water tables. However,

no data exist that constitute a time series for individual wells. Instead, the data represent single samples partitioned according to assumptions about hydrologic mechanisms on a relatively coarse time step.

This study has important implications for the residents of the Lahontan Valley. In private domestic wells arsenic concentrations have been observed from $<10 \mu\text{g/L}$ to over $3000 \mu\text{g/L}$, with elevated concentrations of many other chemical constituents (Lico and Seiler 1994; Thundiyil, Yuan et al. 2007). Although some of these domestic sources are equipped with a point-of-use (POU) treatment device such as a reverse osmosis (RO) unit at the kitchen tap, most domestic well water is untreated (Walker, Seiler et al. 2007). It has also been shown that elevated As(III) concentrations can significantly reduce the efficiency of treatment in the alkaline groundwater in the Lahontan Valley, especially because RO units are frequently poorly maintained or neglected (Walker, Seiler et al. 2007). An understanding of the seasonal and spatial occurrence of arsenic, including the proportion that occurs as As(III), would allow residents and public officials to take the necessary steps to limit exposure to arsenic.

Because the water balance for the valley includes significant irrigation water, it is possible that (1) total arsenic [As(T)] concentrations in groundwater may fluctuate seasonally; that (2) arsenic may occur as As(III) due to reducing conditions in the shallow and intermediate-depth aquifers; and (3) fluctuations in the water table may produce alternating oxic and anoxic zones in saturated aquifer sediments that change the [As(III)]/[As(T)], especially in aquifers close to the soil surface.

Background and Previous Work

1. Hydrogeologic setting

The Lahontan Valley is a closed basin within the Great Basin of west-central Nevada that receives discharge from the Carson River in the west, occasional overflow from the Humboldt River to the north, and numerous creeks, springs, and ephemeral runoff from surrounding mountain ranges (Figure 1). Four major aquifers (basalt, shallow, intermediate, and deep aquifers) have been identified within the basin. The city of Fallon obtains public drinking water from a basalt intrusion at the center of the alluvial basin (Glancy 1986). The shallow aquifer extends from the land surface to about 50 feet below the land surface. The intermediate aquifer lies between 50 and 500 feet below land surface. The deep aquifer lies from 500 to as much as 8,000 feet below land surface (Glancy 1986). The aquifers are not homogeneous units, but can be distinguished based on the hardness and pH of groundwater. Shallow groundwater is considerably harder (>70 mg/L CaCO_3) with a mean pH of 7.3 compared to that of intermediate water (<25 mg/L CaCO_3) with a mean pH of 8.3 (Seiler 2004). Shallow groundwater is also more enriched in the stable isotopes ^2H and ^{18}O (Lico and Seiler 1994). The deep aquifer is considerably more saline than both the shallow and intermediate aquifers.

The lithology of the shallow aquifer is an abruptly changing mix of fine sand, silt and clay derived from a variety of fluvial regimes including deltas, shorelines, lakeshores, river channels and sand dunes (Maurer, Johnson et al. 1996). The geochemistry of the groundwater reflects that of the recharge water and the sediments through which it flows. It is primarily alkaline and ranges from a slightly saline sodium-

calcium-bicarbonate-sulfate type (~1000 mg/L) to a very saline sodium-sulfate-bicarbonate type (~10,000 mg/L) (Lico, Welch et al. 1987).

The subsurface redox environment of the Lahontan Valley shallow aquifer has been shown to be strongly reducing, which may favor the presence of As(III) when arsenicals are present (Langmuir 1997; Seiler, Stollenwerk et al. 2005). In reducing environments groundwater contains little dissolved oxygen (DO) and is likely to have high concentrations of sulfides and ferrous iron due largely to anaerobic degradation of organic material by subsurface microbes. Palmer, et al (2006) reported that of 307 wells sampled in the Lahontan Valley 22% of the A_{ST} was in the form of As(III). Homogeneous solutions of humic and fulvic acids (DOC) were found to reduce arsenate to arsenite at higher pH values, and reduction was less likely at higher concentrations (Palmer, Freudenthal et al., 2006).

The vast majority of domestic wells drilled in the area pump from the shallow aquifer, although some irrigation and exploratory wells reach the intermediate and deep aquifers. Once entering the Lahontan Valley on the west by way of the Carson River and two irrigation canals, groundwater generally flows northeast toward the Stillwater Marsh and southeast toward Carson Lake (Maurer, Johnson et al. 1996).

2. Groundwater recharge

Recharge occurs in the Lahontan Valley by river channels, irrigation, canal leakage, and precipitation, with the major source being irrigation and canal leakage (Glancy 1986; Lico and Seiler 1994). Movement of groundwater appears to be downward from the shallow aquifer to the intermediate aquifer in the west, and upward in the east and south. The hydraulic gradient has been estimated at 7.5 ft/mi in the shallow aquifer

and 6.5 ft/mi in the intermediate aquifer. Specific capacities of up to 70 gal/min/ft have been estimated in the shallow aquifer and between 0.5 and 12 gal/min/ft in the shallow aquifer (Lico and Seiler 1994).

2.1 Shallow alluvial aquifer

Since the Newlands Project began diverting water for irrigation in the Lahontan Valley in 1905, the water level in the shallow alluvial aquifer has risen up to 15 feet in some areas (Lico, Welch et al. 1987). This is apparently in direct response to recharge from irrigation and leakage from unlined canals. Of the approximately 340,000 acre-ft/yr in net diversions from Lahontan Reservoir, about 170,000 acre-ft/yr is actually delivered to 56,600 acres, while an equal amount is lost from the diversion points to head-gates. Of the amount lost, about 100,000 acre-ft/yr of recharge is due to percolation and seepage in 340 miles of unlined canals. With the addition of 20,000 acre-ft/yr from precipitation to the 170,000 acre-ft/yr delivered and an on-farm loss of 10,000 acre-ft/yr, approximately 180,000 acre-ft/yr is available for consumptive use by crops (Maurer, Johnson et al. 1996; Newlands 2004). An estimated one-third of this amount (60,000 acre-ft/yr) recharges the aquifers (Chambers and Guitjens, 1995). Maurer et al. (1996) estimated that regional contributions to the shallow aquifer are 59% from applied irrigation water, 7% from precipitation, and 34% from leakage from canals.

2.2 Intermediate alluvial aquifer

The intermediate alluvial aquifer of the Lahontan Valley has been shown to be highly reducing and alkaline (Seiler, Stollenwerk et al. 2005) and is distinguished from the shallow aquifer by its aqueous chemistry and stable isotopes of oxygen and hydrogen (Glancy 1986). Stable isotopes of hydrogen (^2H , or deuterium) and oxygen

^{18}O) can be used to determine the provenance of groundwaters because meteorological processes change the proportion relative to the Standard Mean Ocean Water (SMOW) composition, producing an observable fractionation (Clark and Fritz 1997). Subsequent precipitation can further fractionate the isotopes, and infiltration can preserve a distinct isotopic signature. In particular, evaporation enriches the proportions of ^2H and ^{18}O relative to SMOW (Craig, 1961). Conversely, a preponderance of the lighter isotopes of hydrogen and oxygen (^1H and ^{16}O) indicates that source water may have existed in a cooler time period, since cooler weather tends to concentrate the lighter isotope. Water in aquifers is not subject to evaporation and the proportions of ^2H and ^{18}O are stable except in regions of hydrothermal influence or in areas of groundwater mixing (Fosbury 2007).

The lithology of the intermediate-depth aquifer is a sharply changing mix of fine sand, silt and clay derived from a variety of Pleistocene to Holocene fluvial regimes including deltas, shorelines, lakeshores, river channels and sand dunes. Intermediate-depth water consists primarily of dissolved calcium, sodium, sulfate, and bicarbonate with a mean pH of 8.3 (Seiler 2004). It is typically softer water than that in the shallow and deep aquifers and is less saline. The solution chemistry is the result of chemical reaction with feldspars, calcite, augite, CO_2 , montmorillonite, gypsum, silica, sodium chloride and pyrite. Model analyses indicate that clay minerals act as exchange sites, with Na substituting for Ca (Lico and Seiler 1994).

Lico and Seiler (1994) concluded that groundwater in the intermediate aquifer is isotopically lighter - containing a smaller proportion of the heavier isotopes - compared to present-day Carson and Truckee River water. Therefore, these rivers (and by association, irrigation water, seepage, or precipitation) are unlikely to be a source of

recharge for the intermediate aquifer. The heavier shallow aquifer water ($\delta^2\text{H} \approx -90 \text{‰}$) is enriched in ^2H by evaporation prior to infiltration. Intermediate water, however, is much lighter ($\delta^2\text{H} \approx -110 \text{‰}$) and must have come either directly from local mountain runoff affected little by evaporation, or ancient recharge during a cooler period when fractionation would have produced lighter precipitation. Carbon-14 data appears to support ancient recharge (even pre-Lake Lahontan) for this aquifer. Lico and Seiler (1994) have estimated ages of up to 7700 years for this water based on carbon-14 analyses of their estimated carbon sources of calcite, organic matter, and soil-zone CO_2 gas. Water became progressively older - from decades and centuries, to millenia in age - across the region from west to east.

3. Arsenic occurrence

3.1 General

Rock-forming minerals containing arsenic are usually found in granitic and volcanic rocks. These include realgar (As_4S_4), orpiment (As_2S_3), arsenopyrite (FeAsS), arsenolite (As_2O_3) and loellingite (FeAs_2) (Manning and Goldberg 1997; Magalhaes 2002). Arsenic is not commonly found in its elemental state because it oxidizes easily and combines with other elements to form oxides, sulfides, and organic arsenicals.

Exposure to water and air decomposes arsenic minerals, releasing aqueous acids and ions to surface and ground water systems. Aqueous arsenic species include both oxyacid and oxyanion forms of arsenate and arsenite, and their presence or absence depends upon the general oxidation/reduction state of the water (Welch and Stollenwerk 2003). Both of the common forms of arsenic (As(III) and As(V)) have high ionic potential (IP) - which is defined as the valence (Z) divided by its crystallographic radius,

which puts oxyanions of As in solution (Harvey and Beckie 2005). Oxygenated waters favor As(V) species, and due to the low equilibrium coefficients of arsenic acid (H_3AsO_4 ; $\text{pK}_{a1} = 2.3$, $\text{pK}_{a2} = 6.8$, $\text{pK}_{a3} = 11.6$) (Welch and Stollenwerk 2003) only the di- and mono-protonated oxyanions, H_2AsO_4^- and HAsO_4^{2-} , are found in oxygenated natural groundwaters. In contrast, reduced conditions favor As(III) species, and since the pKa of arsenious acid is fairly high (H_3AsO_3 ; $\text{pK}_{a1} = 9.2$, and $\text{pK}_{a2} = 12.7$) (Welch and Stollenwerk 2003), H_3AsO_3 and H_2AsO_3^- are the arsenite species found in most reduced groundwater systems (Pierce and Moore 1982; Manning and Goldberg 1997; Council 2000; Goyer 2000; Goldberg 2002). Neutral HAsO_2 molecules are also found up to pH 9 (Pierce and Moore 1980).

Processes that can contribute to the mobility of arsenic in groundwater include precipitation/dissolution, adsorption/desorption, exchange, oxidation/reduction, and microbial action (Welch and Lico, 1998). Arsenic speciation has been studied by many researchers, though not as a function of time. In the study of acidic mine-workings of an Idaho lead-zinc mine the seasonal $[\text{As(V)}]/[\text{As(III)}]$ correlated positively with metals concentrations (Zn and Fe) at low pH (Mok et al. 1988). High concentrations of both As and metals were found during spring run-off presumably due to leaching of acid reaction products.

3.2 Sources of arsenic in the Lahontan Valley

The granitic and volcanic uplands that surround the Lahontan Valley and within the Carson River Hydrographic Region may be important sources of arsenic in groundwater. Lahontan Valley sediments and tephra containing volcanic-lithic fragments

also are potential sources (Welch and Lico 1998). According to Welch and Lico (1998), arsenic concentration in the Lahontan Valley is comparatively high due to evaporative concentration of Carson River water, which is the main source of recharge to the region. Anthropogenic sources of arsenic such as those from wood preservatives, arsenical fertilizers, and cattle-dipping vats containing arsenic pesticides are possible sources, primarily historical and likely to be very localized (Welch, Westjohn et al. 2000).

Although irrigation water below the Lahontan Diversion Dam has total arsenic concentrations between 9 and 13 $\mu\text{g/L}$ (Lico, Welch et al. 1987), and rainwater concentrations are negligible, arsenic is frequently found in concentrations exceeding the MCL and can exceed 1000 $\mu\text{g/L}$ in groundwater (Welch and Lico 1998; Fitzgerald 2003; Walker, Benson et al. 2003; Walker and Fosbury 2003; Seiler 2005). Some authors have suggested that As(III) should dominate due to reducing conditions, and that the As(III)/As(T) ratio could change due to changing redox conditions in the saturated zone (Seiler and Allander 1993; Seiler, Stollenwerk et al. 2005). Concentrations of the most common aqueous arsenic species are small enough to be controlled by pH and redox conditions (Harvey and Beckie 2005).

Mechanisms for As mobility and enrichment include: 1) dissolution of As-bearing minerals, including oxides and sulfide; 2) reductive dissolution of arsenic-bearing solids, including oxyhydroxides of Fe, Mn, and Al (Stollenwerk 2003); 3) desorption of As ligands from these oxides under alkaline conditions due to increase in negative surface charge (Stollenwerk 2003); and 4) displacement from surfaces by competition with other ligands (Smedley and Kinniburgh 2002). Oxyhydroxides are especially important due to their large surface area and number of charged sorption sites per unit area. Since the

intermediate-depth aquifer of the Lahontan Valley is both reducing and alkaline with a high ionic strength, all three mechanisms may lead to elevated As concentrations. In addition, evaporative concentration has been suggested as a mechanism for arsenic enrichment in shallow sediments of semi-arid regions (Smedley and Kinniburgh 2002), and in the shallow aquifer of the Lahontan Valley, in particular (Lico, Welch et al. 1987).

Hypotheses

This study of arsenic in groundwater of the Lahontan Valley sought to determine (1) if there is temporal stability of arsenic and other chemical constituents in groundwater in the intermediate aquifer (>50 ft and <500 ft); (2) if there is a gradient in arsenic concentration along the west-southeast trending groundwater flow-path in the intermediate aquifer; and (3) whether the chemical mechanisms that are commonly associated with arsenic mobility (dissolution of arsenic oxides and sulfides, desorption, and reductive dissolution of ferric oxides) are responsible for spatial trends in arsenic concentration in the intermediate aquifer of Lahontan Valley.

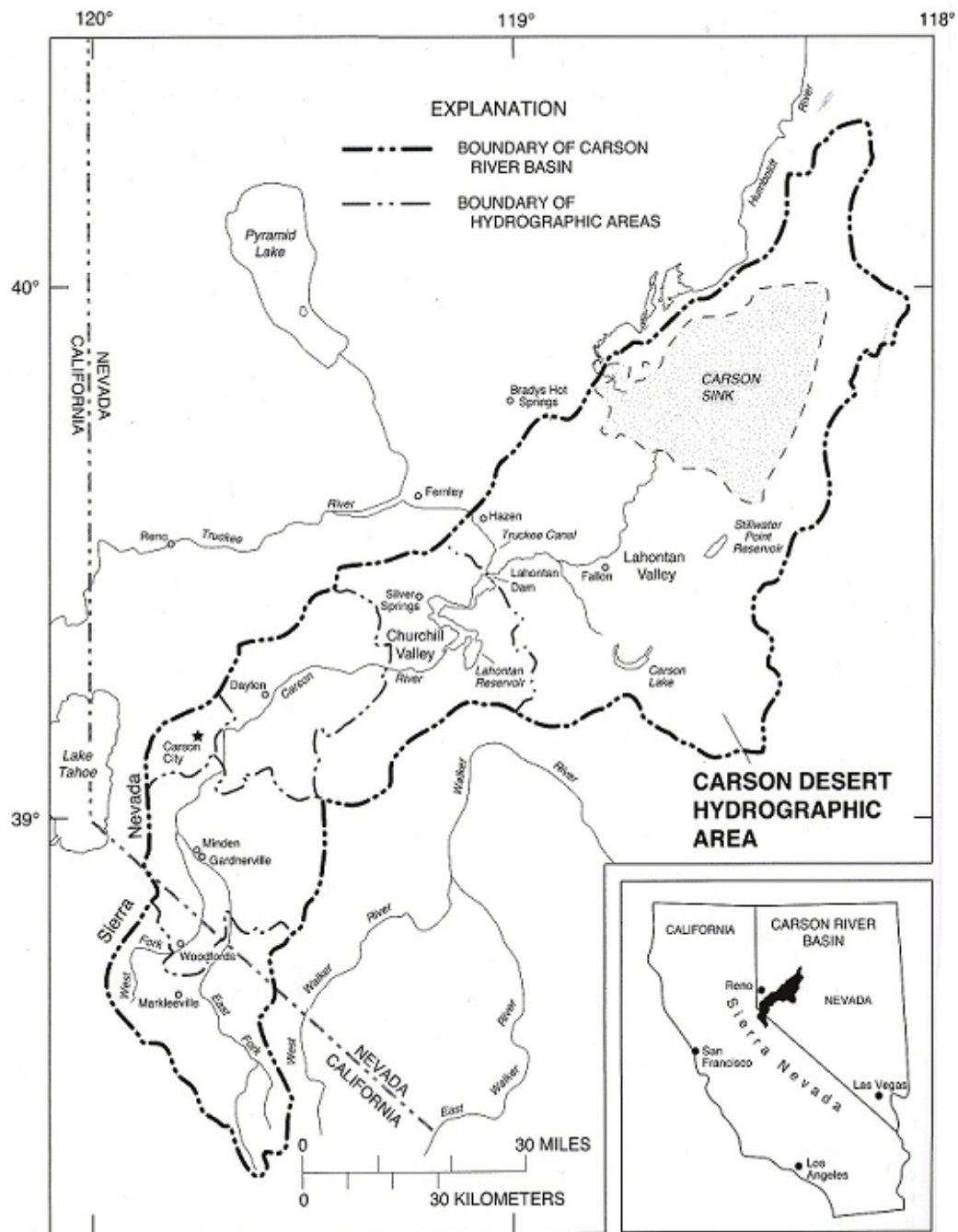


Figure 1 - Lahontan Valley Hydrographic Region (Maurer and Welch, 2001)

Chapter 2 - Variation in Arsenic Concentrations

Abstract

A study was conducted in the intermediate-depth alluvial aquifer (50-500 ft) of Lahontan Valley, Nevada to examine the temporal and spatial stability of dissolved arsenic concentrations. Five wells previously observed to have substantial concentrations of both As(V) and As(III) were chosen to represent a groundwater flow-path and were sampled over an 18-month period (February, 2004 to August, 2005) for a variety of physical parameters and chemical constituents. Arsenic concentrations were observed to be statistically stable for the sampling period at each well, as were the majority of chemical constituents and physical parameters. Spatially, total arsenic As_T concentrations increased significantly - nearly seven-fold along the flow-path. The ratio of $[As(III)]/[As_T]$ decreased. As_T correlated well with dissolved organic carbon DOC, HCO_3^- , total phosphorus (P_T) and distance along flow-path and not as well with pH. However, the data suggest that pH is a potentially controlling factor that could explain increases in the concentration of As_T along the flow-path.

Introduction

This research examined aqueous arsenic concentrations over time and space from west to east within the intermediate regional alluvial aquifer of the Lahontan Valley of western Nevada. The objective was to identify (a) significant chemical and physical changes along a flow-path in an aquifer of intermediate-depth (50-500 ft) and (b) the significance of relationships between changes in arsenic concentrations and other physical and chemical characteristics. The study sought to establish that chemical concentrations and physical characteristics of water remained stable through time, which would indicate that chemical processes along a flow-path were separate from the overlying shallow aquifer. The study also sought to establish that even though chemical and physical characteristics were stable at each point in the flow-path, there was an overall gradient in arsenic concentrations from west to east. The study examined data collected statistically, to determine which factors might be used to explain changes in concentration using models that account for interactions between chemicals and ambient physical conditions.

The intermediate aquifer and the shallow aquifer (from the land surface to 50 feet in depth) provide drinking water to approximately 5000 domestic wells in the Lahontan Valley. Of these, less than half tap the intermediate aquifer (Fitzgerald 2003). The intermediate depth aquifer has been described as being a highly reducing environment (Seiler and Allander 1993; Seiler, Stollenwerk et al. 2005). Typically, water in the intermediate aquifer contains little dissolved oxygen due largely to anaerobic degradation of organic material by subsurface microbes. It also contains high concentrations of sulfides and ferrous iron. Chemical mechanisms that can increase arsenic mobility may

be operate in this environment. Since arsenic has been shown to cause a variety of disorders (including diarrhea, circulatory disorders, and cancer), and the toxic effect increases with concentration, understanding the occurrence of arsenic is important for public health protection.

The Intermediate Depth Aquifer in the Lahontan Valley: Previous Studies

The intermediate aquifer is an abruptly changing mix of fine sand, silt and clay derived from a variety of Pleistocene to Holocene fluvial regimes including deltas, shorelines, lakeshores, river channels and sand dunes (Maurer, Johnson et al. 1996). Intermediate-depth water is distinguished by its aqueous chemistry and stable isotopes of oxygen and hydrogen (Glancy 1986). It is composed primarily of calcium, sodium, sulfate, and bicarbonate with a mean pH of 8.3 (Seiler 2004). It is typically softer and less saline water than that in the shallow and deep aquifers. Lico and Seiler (1994) have suggested that the solution chemistry is the result of chemical reaction with feldspars, calcite, augite, CO₂, montmorillonite, gypsum, silica, sodium chloride and pyrite. Model analyses (BALANCE; reported by Parkhurst, 1982) indicated that clay minerals act as exchange sites, with Na substituting for Ca.

Lico and Seiler (1994) concluded that the intermediate aquifer is not hydraulically connected to the present-day Carson and Truckee rivers, based on isotopes of hydrogen (²H) and oxygen (¹⁸O). This suggests that wells in the intermediate aquifer along water table gradient could be considered as sampling points for a flow path, with each point presumably being hydraulically connected with all other points. It also suggests that flow traverses the region without significant recharge or loss (Maurer, Johnson et al. 1996).

Three intermediate-depth wells sampled by Lico and Seiler (1994) close to the wells used in the conceptual flow-path of this study were found to contain stable isotope values for $\delta^2\text{H}$ of -114‰ and $\delta^{18}\text{O}$ values between -14.4 to 14.7‰ . Lico and Seiler (1994) suggested any that changes in $\delta^2\text{H}$ and $\delta^{18}\text{O}$ occurred by mixing with different water sources and/or water-rock interaction since water in the intermediate aquifer is not subject to evaporation. By comparison, the Carson and Truckee rivers (and by association, irrigation water, seepage, or precipitation) have been shown to be enriched, likely by evaporation (up to -76‰ of $\delta^2\text{H}$ and -8.2‰ of $\delta^{18}\text{O}$) (Lico, Welch et al. 1987; Lico and Seiler 1994) and are, therefore, unlikely to be a source of recharge for the intermediate aquifer. Lico and Seiler (1994) estimated ages of up to 7700 years for this water based on carbon-14 analyses of their carbon sources of calcite, organic matter, and soil-zone CO_2 gas, with the water becoming progressively older along the flow-path from west to east.

Concentrations of naturally occurring salts and metals often exceed the maximum contaminant level (MCL) for many metals in the intermediate aquifer. Arsenic is frequently found in concentrations exceeding the MCL of $10\text{ }\mu\text{g/L}$ in some areas by more than two orders of magnitude (Welch and Lico 1998; Fitzgerald 2003; Walker, Benson et al. 2003; Walker and Fosbury 2003; Seiler 2005).

Arsenic concentrations have been demonstrated to remain constant through time (Seiler 2004; Steinmaus, Yuan et al. 2005; Thundiyil, Yuan et al. 2007). Recent studies of non-mountainous regions of western Nevada counties (Douglas, Churchill, Storey, Mineral, Lyon, and Carson City) suggested that seasonal variation in groundwater arsenic concentration is not dependent upon irrigation patterns or rainfall when these are

dominant sources of recharge (Thundiyil, Yuan et al. 2007). However, of the 356 wells they tested, 44% had arsenic concentrations that varied by season. Steinmaus, Yuan et al. (2005) came to a similar conclusion based on samples from 759 wells taken several years apart. In addition, where arsenic concentrations were observed to have changed, mechanisms proposed included dilution of groundwater by rainfall, redox changes due to changing pumping rates, movement of groundwater, and seasonally changing depth of water tables (Steinmaus et al., 2005). However, Thundiyil et al. (2007) observed no relationship between seasonal arsenic concentration and well depth.

Fitzgerald (2003) attempted to characterize the distribution of arsenic in the Lahontan Valley using inverse distance weighting (IDW) and kriging analysis and depicted a general trend of arsenic concentration increasing from west to east with significant local variation. Other authors have noted this spatial trend as well (Lico, Welch et al. 1987; Walker, Benson et al. 2003).

Hypotheses

The hypotheses, stated in the null form, that guided data collection were:

- 1) Arsenic concentrations do not fluctuate over time in the intermediate aquifer, and
- 2) There is no change in arsenic concentrations along a conceptual flow-path in the intermediate aquifer.

Methods

The study area was within the Lahontan Valley of Churchill County, western Nevada. The five wells (wells A-E) along the flow-path were located south of the Carson River, which had an assigned origin at UTM Zone 11S (NAD 83) northing 4237238; easting 11S 337643, trending 120° for approximately 5 miles as described in the

following section. Five intermediate-depth wells, designated as A—E, that were previously identified as having a high proportion of $[\text{As(III)}]/[\text{As}_T]$ (Benson 2003) were sampled monthly for 18-months from February 2004—August 2005 (Figure 2).

1. Water samples

Table 1 lists all sampled chemical constituents and physical properties. These were included based on their potential to influence thermodynamics of chemical reaction, physical changes of the aquifer, changes in redox potential and changes in subsurface chemistry. Chemical constituents included major and minor cations and anions to assess the charge balance and ionic strength of the sample as well as that of anthropogenic influences (for example, nitrogen occurring as nitrate).

Before sampling, the water level was measured in each well using an electric sounding tape. The depths obtained did not represent static water levels since homeowners were not asked to restrict water use.

Water samples were obtained in polyethylene bottles provided by the Nevada State Health Laboratory (NSHL - a certified drinking water analysis laboratory) by passing water through a flow-through cell attached to a YSI 556MPS multimeter. In this way, a constant water flow was maintained across YSI membranes and probes. The cell was attached to the well through a faucet or standpipe closest to the wellhead, before storage in a pressure tank, and before any filtration or treatment was applied. The well was purged by pumping until the temperature, conductivity, and pH had stabilized (with the range of fluctuations of no more than 20% from an observed central value). This usually occurred within 20 minutes of the beginning of pumping.

As per the NSHL sample handling protocols, unfiltered metal samples were preserved in 1% nitric acid, and total phosphorous and nitrate samples were preserved in 1% sulfuric acid. Additional arsenic samples were obtained and preserved in 0.125 M EDTA to sequester both arsenic species, then passed through 3 mL Supelclean LC-SAX anion-exchange cartridges (Garbarino, Bednar et al. 2002) from which As(III) was eluted with nitric acid for atomic absorption analysis. Samples for other chemical species were unpreserved. All samples except DOC were stored at 34° F until analyzed.

Samples for both ^2H and ^{18}O were obtained in 16 mL glass vials with inverted poly-seal lined caps and sealed with Parafilm to prevent contact with the atmosphere. Samples for dissolved organic carbon (DOC) were filtered with Fisher GF/F 0.45 μm glass microfiber filters into polyethylene bottles and kept frozen until analyzed.

Hydrogen sulfide concentrations were determined in the field using a Hach Model HS WR hydrogen sulfide field test kit.

To determine the concentration of Fe(II), water samples were passed through a 0.45 μm Millex-HA syringe-driven filter unit to remove particulates and then delivered to 30 mL HDPE bottles with 1.5 mL 0.2% 2,2'-bipyridine solution to preserve Fe(II) for later colorimetric analysis.

2. Laboratory Methods

All chemical constituents except DOC, H_2S , ^2H , and ^{18}O were analyzed at the Nevada State Health Laboratory (NSHL) on the campus of the University of Nevada, Reno (UNR). Analytic methods used by the NSHL and reporting limits are shown in Table 2 (APHA 1989; EPA 2009).

In addition to NSHL analysis, samples preserved for arsenic speciation were analyzed in the Natural Resource and Environmental Science (NRES) laboratory of Dr. Mae Gustin at UNR using graphite-furnace atomic absorption spectrometry with a Varian 220 AA Spectrometer for As(III) and As_T. A 50 µg/L standard was used at the beginning of each sample run, and was successively diluted and analyzed to 15, 30, and 45 µg/L to produce a calibration curve. Each series of 10 samples analyzed was followed by one of a succession of arsenic standards of 50, 100, and 500 µg/L. In addition, one duplicate and/or one blank per 10 samples was analyzed. NSHL arsenic results were then compared with those obtained in the NRES lab for consistency. For the latter half of the study, As(III) was analyzed at NSHL.

The stable isotope analysis was carried out by the Stable Isotope Laboratory at UNR. DOC samples were analyzed using high temperature combustion at UNR (Shimadzu TOC 5050 organic carbon analyzer) as per Standard Method 5210 B (APHA 1989). H₂S samples were analyzed in the field using a Hach Kit for sulfide detection using the methylene blue method (Hydrogen Sulfide test kit, #223801, Hach, Inc., Loveland, CO).

3. Data analysis

3.1 Graphical methods

A southeast-trending flow-path (bearing ~120°) in the intermediate aquifer was identified that coincided with the general groundwater flow pattern suggested by Maurer, Johnson et al. (1996). The flow-path considered began in the western portion of the Lahontan Valley south of the Carson River (Figure 2). A previously sampled well about 4 miles northwest of Well A served as the datum for the flow-path. Distances along the

flow path were expressed relative to the datum and orthogonal from a line trending from the datum at 120°. Well profiles from logs obtained from the Nevada State Engineer's office, of the Nevada Division of Water Resources (<http://water.nv.gov/>, last accessed 07/2009) were used to determine well depths, perforated well-casing intervals, and lithologies for water-bearing units. Figure 3 illustrates average depths to water from the land surface during the sampling period, and may not represent static waters, as previously noted. Water obtained from these wells may represent very different chemical environments that are linked by a common flow system. However, the wells are unlikely to offer the opportunity to carry out synoptic sampling, because of the extended periods of time estimated for water movement between wells. Maurer, Johnson et al (1996) estimated that hydraulic conductivities in the intermediate aquifer were from 45-79 ft/day and provided specific discharges of 0.063-0.11 ft/day using Darcy's Law ($q = K dh/dl$). Average linear velocities ($v = q/\Phi$), calculated using an average porosity (Φ) of 0.3 (Lico and Welch 1998), were estimated to be between 0.21-0.37 ft/day and not sufficiently rapid for water to traverse the approximately 5-mile distance between the wells during the sampling period. Even at the highest rate, travel time from well A to wells B, C, D, and E was estimated to be 70, 140, 190, and 200 years, respectively. Accordingly, the flow-path analysis likely represents long-term localized equilibria at each point.

A comparative time-series plot was created for all measured parameters for each well in Microsoft EXCEL. These plots were inspected to identify temporal and spatial variation in $[As_T]$ and $[As(III)]/[As_T]$ and other parameters for each well. USGS GW Chart software was used to create Piper diagrams illustrating the balance of major ions.

Stable isotope data for ^2H and ^{18}O for each sample were plotted for each well against the Global Mean Water Line (GMWL) (Craig, 1961) and the other data sets (Lico and Seiler, 1994; Seiler 2004; Fosbury 2007) for comparison, and to see if mixing of waters was occurring.

3.2 Statistical methods

To characterize the temporal and spatial variability of parameter values for each well, several approaches were taken including graphical depiction of time series data and statistical analyses of concentrations over time.

Linear regression was used in combination with LOWESS smoothing (Cleveland 1988) with temporal data to determine if a trend in $[\text{As}_T]$ or other chemical constituents occurred over time. Using regression of $[\text{As}_T]$ against time, a slope near 0 would indicate no trend. In addition, regression analysis was performed for all combinations of parameters to determine if arsenic concentrations were correlated with chemical or physical conditions within the aquifer..

Coefficients of variation ($\text{CV} = s/m$, with s representing the sample standard deviation and m representing the sample mean) compared the sample standard deviations to sample means. In this way, the variation of a given parameter value could be compared from well to well when population means differed. A small CV value indicated less fluctuation for a parameter than a larger value.

The Mann-Kendall Test compared the change in a parameter over successive months in each of two "seasons" - in this case, the first and second halves of the sampling period (Jan-Dec 2004 and Jan-Aug 2005). The seasons did not represent seasons of the year because stable isotope data indicate surficial influence to be negligible within the

intermediate aquifer. The Seasonal Kendall Test then compared the data pairs for the same month between seasons to create a Z statistic to evaluate the null hypothesis (H_0) that no trend existed (Helsel and Hirsch 1992), using a p -value ≤ 0.05 as a criterion to reject H_0 .

To test spatial variation, an analysis of variance (ANOVA) test was performed to determine whether As_T values were significantly different from each other along the flow-path. ANOVA evaluated the null hypothesis, $H_0 (\mu_A = \mu_B = \mu_C = \mu_D = \mu_E)$, using $p \leq 0.05$ as the criterion to reject H_0 (DeVore 2004). The mean square error (MSE) obtained from ANOVA was used to find the Least Significant Difference by applying Tukey's Procedure (DeVore 2004).

Results

1. Water chemistry

Figures 4 and 5 display the stable isotopes of δ^2H vs. $\delta^{18}O$ in general and in detail.

1.1 Temporal variation

Time-series plots for major ions are displayed in Figure 6. Time-series graphs for other chemical and physical parameters are displayed in Figure 7. Due to equipment malfunction, DO results for the first half of the sampling period were discarded as well as the samplings from 6/6/2004—10/6/2004 for pH. DOC results were collected only for the latter third of the sampling period. A time-series summary is shown in Table 3.

1.2 Spatial variation

Major ion concentrations (sodium, calcium, bicarbonate, sulfate, potassium, magnesium, carbonate, chloride) for Wells A-E are presented in box and whisker format

in Figure 8. The complete data sets for As_T , $As(III)$, pH, DOC, Eh, conductivity and dissolved oxygen (DO) are included in Figure 9 for each well.

Discussion

1. Temporal variation

1.1 Stable isotopes

All flow-path waters plotted below the Global Meteoric Water Line, GMWL ($\delta^2H = 8 * \delta^{18}O + 10$) of Craig (1961) for the stable isotopes, δ^2H and $\delta^{18}O$ indicating that intermediate waters have been enriched by evaporation. They were found to be extremely stable throughout the sampling period with coefficients of variation <0.006 for all wells. These data correspond to stable isotope data of Lico and Seiler (1994) for intermediate aquifer waters (Figure 5). Samples for this study grouped tightly in a region bounded by δ^2H values between ~ 108 ‰ and 113 ‰; and $\delta^{18}O$ values between ~ 14.35 ‰ and 14.75 ‰. Variation about means was possibly due to local mixing or analytical variation in stable isotope analysis of $\sigma = 1$ ‰ for δ^2H and $\sigma = 0.1$ ‰ for $\delta^{18}O$ (Poulson 2008). The only significant deviation from this grouping was found in Well A (Figure 6) in which waters were slightly more enriched - possibly due to greater mixing from the shallow aquifer or from other sources, such as geothermal. Well A was the shallowest of the sampled wells (65 ft).

1.2 Major ions

Time-series plots and coefficients of variation (CV) suggest that little variation occurred for the major ions (Na, Ca, Mg, K, HCO_3 , SO_4 , and Cl) during the sampling period. Most CV values for the major ions were below 0.01 and all were below 0.25

(Table 3). Parameters with large coefficients of variation (> 0.25) include Eh and DO. However, measurements of Eh may have been of limited usefulness because the variety of redox couples in sampled waters may have made Eh measurements using the platinum electrode of the YSI unreliable (Kehew 2001). In addition, DO values were only reliable for the latter half of the sampling period because of equipment malfunction.

1.3 Other parameters

Conductivity and pH fluctuated very little during the sampling period with CV values of ~ 0.09 ; and ~ 0.02 , respectively (Table 3), however, an unexplained reduction in conductivity was observed for the 13th and subsequent samplings, perhaps due to meter malfunction or errors in calibration. DOC had greater fluctuation with CV values between 0.10 for Well D and 0.23 for Well A. DO concentrations fluctuated with CV values between 0.75 and 0.96 while Eh values were very inconsistent with CV values between 1.5 and 10.7.

1.4 Arsenic

Coefficients of variation for As_T were below 0.08 for all wells suggesting very little fluctuation in concentration over time. As indicated by LOWESS smoothing (Figure 10), each time-series and regression analysis (concentration vs. time) indicated slopes of approximately ~ 0.001 for As_T concentration vs. time for wells A and B, and ~ 0.05 for wells C, D, and E. No annual cycle was apparent.

The seasonal Kendall's test produced $p \sim 0.5$ for the test statistic for all wells. Therefore the null hypothesis that seasonal trends existed (indicated as H_0 for two seasons (irrigation (f) (from April through October) and non-irrigation (i) (November

through March): $\text{prob}[Y_{\hat{t}} > Y_i] = 0.5$, where time $T_{\hat{t}} > T_i$) was not rejected. Table 4 summarizes the statistical results for analysis of temporal variation.

As(III) concentrations fluctuated little over the sampling period for Wells A and B (CV = 0.09 and 0.06), but had large variation for Wells C, D, and E, which had CV values of 0.40, 0.56, 0.51, respectively (Table 3). As(III) concentrations decreased over time for down-gradient wells. The ratio $[\text{As(III)}]/[\text{As}_T]$ likewise varied little for Wells A and B, and widely for Wells C, D, and E.

2. Spatial variation

2.1 Stable isotopes

Flow-path results for the stable isotopes, $\delta^2\text{H}$ and $\delta^{18}\text{O}$, indicated that with the exception of Well A, provenance of the groundwater was very similar from well to well (Figure 5, Table 3). Isotopically, the value for $\delta^2\text{H}$ was between -109 and -113‰, and for $\delta^{18}\text{O}$ between 14.25 and 14.75‰. The only significant change occurred between Wells A and the remaining wells, where the water became slightly more depleted (by $\sim 1.5\text{‰}$ in $\delta^2\text{H}$, and by $\sim 0.50\text{‰}$ in $\delta^{18}\text{O}$). Except for Well A, all down-gradient wells grouped closely, suggesting that recharge from other sources that might significantly affect chemical composition was unlikely. The isotope values were consistent with intermediate wells sampled in other studies (Lico and Seiler 1994).

2.2 Major ions

Time-series plots and Piper plots indicate that water chemistry became increasingly sodium and bicarbonate-rich along the flow-path during the sampling period (Figures 6 and 11). Pearson's correlation coefficients (R) further illustrate this trend (Table 5). Distance along flow-path was positively correlated with $[\text{Na}]$ and $[\text{HCO}_3]$

($R=0.87$ and 0.89 , respectively), negatively correlated with $[\text{SO}_4]$ ($R=-0.70$). Weaker correlations were observed for $[\text{Cl}]$. $[\text{Ca}]$, $[\text{Mg}]$, $[\text{K}]$, and $[\text{CO}_3]$ were not significantly correlated with distance along the flow path, nor were major ions concentrations and physical characteristics significantly correlated with depth.

2.3 Other parameters

Pearson's correlation coefficients indicate correlations between distance along flow-path and pH ($R=0.91$), conductivity ($R=0.83$), NO_3 ($R=0.86$), PO_4 ($R=0.95$), and DOC ($R=0.86$) (Table 5). Well depth was correlated significantly correlated with pH ($R=0.91$), silica ($R=0.91$), $[\text{As(III)}]/[\text{As}_T]$ ($R=-.090$) and SO_4 ($R=0.86$).

2.4 Arsenic

As_T concentration increased with distance along the flow-path (Figure 12), and followed a trend previously suggested by three wells along the flow-path from two other studies (Whitney, 1994; Seiler 2004).

Analysis of variation (ANOVA) verified that As_T concentrations were significantly different at each point. The null hypothesis ($H_0: \mu_A = \mu_B = \mu_C = \mu_D = \mu_E$) for mean As_T concentrations) was rejected at $p = 0.05$. Tukey's Method indicated minimum significant differences in As concentrations of at least $7.1 \mu\text{g/L}$ between wells, which was the case for all wells on the flow-path. This statistic suggests that arsenic enrichment occurs along the flow-path.

It should be noted that well depth coincidentally increased with distance. As a result, correlations with depth may not be independent of correlations with distance along the flow-path.

3. Arsenic and other correlations

Regression analysis revealed that As_T was correlated with Na and HCO_3 , but not with SO_4 and Cl (Figure 13). Processes that increase the concentration of conservative ions in solution may likewise affect As_T concentrations. These processes include possible dissolution and exchange of Na for Ca to produce Na, and $CaCO_3$ dissolution in the presence of CO_2 to produce HCO_3 .

Several other parameters correlated with As_T including pH, conductivity, DOC, and total phosphorus (P_T) (Figure 14). The positive correlation between DOC and As_T may indicate the formation a DOC-As complex . The strong correlation between As_T and P_T may indicate some causative relationship, although Stollenwerk (2003) demonstrated the preference of phosphates over both species of arsenic on sorbing surfaces at pH ranges of the study.

Parameters that may indicate reducing conditions (low Eh, low DO, and the presence of H_2S) were not correlated with increasing As_T (Figure 15). Nevertheless, reducing conditions are suggested by decreasing SO_4 along the flow-path (as sulfur is reduced to S^{2-}). Reducing conditions may dissolve iron oxyhydroxides (HFO) with sorbed As when Fe(III) reduces to Fe(II), releasing both Fe and As, though Fe was not significantly correlated with distance along the flow-path (Table 5).

The proportion $[As(III)]/[As_T]$ showed negative correlation with pH and P_T as shown in Figure 16. Since As(III) was observed to increase along the flow-path, only a greater increase in As(V) could produce a smaller $[As(III)]/[As_T]$ proportion. An increasing pH, therefore, correlates with increasing As(V), and, consequently increasing P_T .

Conclusions

Five intermediate-depth wells that approximate a groundwater flow-path were chosen to evaluate the evolution of chemical characteristics of water, with an emphasis on arsenic, in the Lahontan Valley of western Nevada. Samples were taken monthly for 18 months to identify and quantify temporal and spatial changes in arsenic concentrations and the proportion of As occurring in the reduced arsenic (As(III)) form. The primary purpose for identifying trends, especially spatial trends, was twofold. First, several authors have noted that concentrations of arsenic appear to increase from west to east, corresponding with general trends in groundwater flow. However, interaction between the intermediate aquifer and potential recharge sources from the shallow aquifer and other sources could confound identification of such a trend, especially if such interactions were seasonal (for example, related to application of irrigation water). Second, if significant relationships along the flow-path could be identified, such relationships could be the foundation for hypotheses to be tested about potential chemical processes that could explain why such trends existed.

Statistical analyses for temporal trends, including linear regression, coefficients of variation, and the Seasonal Kendall test, indicated that As_T concentrations did not vary significantly at each sampling point during the study period. Linear regression of As_T vs. time showed slopes ≤ 0.05 , and CV values for As_T were less than 0.075 for all wells, indicating stable total arsenic concentrations regardless of location along the flow-path. Accordingly, the null hypothesis that As_T did not fluctuate over time was not rejected.

As(III) concentrations were stable for Wells A and B, but fluctuated considerably for Wells C, D, and E. $[As(III)]/[As_T]$ was similarly stable for Wells A and B, and not

stable for C, D, and E. Fluctuating redox conditions in the intermediate aquifer over time may be responsible for the instability in Wells C, D, and E. These conditions were observed in Eh, DO, and H₂S, which had large CV values (Table 3). However, pH was stable for all wells. Fe concentrations, which may also be indicative of redox condition had significant fluctuation as well.

The concentration of the major ions, Na, Ca, Mg, K, HCO₃, CO₃, SO₄, and Cl remained stable at each well (CV < 0.10) during the sampling period.

ANOVA, time-series analysis, and linear regression for spatial stability indicated that As_T concentrations increased considerably along the flow-path from ~60 µg/L to >400 µg/L, behaving much like the conservative ions Na and HCO₃, which correlated well with As_T. The hypothesis that As_T was not enriched along the flow-path was rejected in favor of the alternative hypothesis that there was a significant difference in arsenic concentrations between wells. Using Tukey's Least Significant Difference method, the concentrations of As_T in all wells were significantly different from one another. Correlation analyses also indicated a strong relationship between As_T and DOC, conductivity, and P_T. Although As_T did not correlate as well with pH, both increased with distance along the flow-path. The correlations shown in Table 5 suggest that chemical mechanisms that concentrated major ions may be the same as those that concentrated arsenic.

Although As(III) increased along the flow-path, its negative correlation with [As(III)]/[As_T] and significant positive correlation with As_T suggest that As(V) increased to a greater extent than As(III) with distance and with depth. As(V) may be reduced to As(III) in reducing conditions. However, an increase in pH with no corresponding

decrease in Eh may leave As(V) oxidized, and even oxidize As(III). Suspected mechanisms for increased A_{S_T} include dissolution of arsenic salts, reduction of ferric iron in hydrous ferri-oxides (HFO) that may release arsenic to solution, desorption of arsenic from HFO and DOC due to increasing pH.

While waters along the flow-path became increasingly alkaline, arsenic-rich, sulfate-, chloride-, and silica-poor, and increasingly of the sodium bicarbonate-type, the ratio As(III)/ A_{S_T} decreased. Of the key redox indicators that would suggest increasingly reduced conditions along the flow-path (H_2S , As(III)), none were correlated with distance. Reasons for this observation could be incomplete data, erroneous field measurement or laboratory analysis, and inconsistency in sulfide concentrations.

The significant difference in A_{S_T} concentrations between wells, and correlations between A_{S_T} and HCO_3^- , DOC, and P_T , in particular, suggest mechanisms for arsenic enrichment that include dissolution of arsenic salts, reductive dissolution of HFO (to which As may be complexed), desorption of As from HFO, and competitive ligand replacement. These mechanisms may be examined using geochemical models, which is the subject of the next chapter.

physical property	unit	chemical constituent	unit
water depth	ft	Na, Ca, Mg, K	mg/L
temperature	°C	HCO ₃ , CO ₃ , SO ₄ , Cl	mg/L
pH		P _{total} , PO ₄ , Fe, Mn, Si, DOC, NO ₃	mg/L
conductivity	mS/cm	total dissolved solids (TDS)	mg/L
dissolved oxygen (DO)	% saturation	total arsenic (As _{total})	μg/L
redox potential (Eh)	mV	arsenite (As ³⁺)	μg/L
		δ ¹⁸ O	‰
		δ ² H	‰

Table 1 - Sampled parameters

test	method		reporting limit (mg/L)
alkalinity	SM 2320 B	titration	20
As	EPA 200.8	ICP-MS	3 µg/L
HCO ₃	SM 2320 B	titration	-
Ca	EPA 200.7	ICP-AES	5
CO ₃	SM 2320 B	titration	-
Cl	EPA 300.0	ion chromatography	25
OH	SM 2320 B	titration	-
Fe	EPA 200.7	ICP-AES	0.05
Mg	EPA 200.7	ICP-AES	5
NO ₃	EPA 300.0	ion chromatography	0.5
K	EPA 200.7	ICP-AES	5
Si	EPA 200.7	ICP-AES	1
Na	EPA 200.7	ICP-AES	5
SO ₄	EPA 300.0	ion chromatography	25
P _T	SM 4500 PE	ascorbic acid	0.01
PO ₄	SM 4500 PE	ascorbic acid	0.01
Mn	EPA 200.7	ICP-AES	0.02

Table 2 - Methods and detection limits used for analysis. “EPA” refers to an analytic method published by the U.S. Environmental Protection Agency. “SM” refers to a method published in “Standard Methods for the Examination of Water and Wastewater, 20th ed. (Clesceri, L., Greenberg, A., Eaton, A. (eds). 1998).” Reporting limits represent the results of quality control/quality assurance procedures performed by the Nevada State Health laboratory (a certified drinking water analysis facility). The symbol “-“ indicates that reporting limits were not determined for these methods.

	Well A			Well B			Well C			Well D			Well E		
	mean	SD	CV	mean	SD	CV	mean	SD	CV	mean	SD	CV	mean	SD	CV
pH	8.28	0.25	0.03	8.37	0.22	0.03	9.15	0.17	0.02	9.11	0.18	0.02	9.05	0.21	0.02
conductivity	0.47	0.04	0.09	0.38	0.03	0.09	0.53	0.05	0.09	0.71	0.06	0.09	0.82	0.07	0.08
temperature	15.73	0.31	0.02	17.12	0.07	0.00	15.81	0.11	0.01	16.07	0.05	0.00	16.93	0.54	0.03
Eh	-4.75	50.72	-10.68	4.91	42.75	8.72	36.96	53.90	1.46	-13.66	52.98	-3.88	53.03	78.36	1.48
DO	1.36	1.02	0.75	1.28	1.13	0.88	1.49	1.33	0.89	1.24	1.19	0.96	1.12	1.04	0.93
TDS	0.32	0.02	0.05	0.26	0.01	0.05	0.37	0.02	0.04	0.50	0.02	0.04	0.57	0.02	0.04
H₂S	0.15	0.07	0.48	0.12	0.04	0.38	0.16	0.04	0.23	1.35	0.29	0.21	0.01	0.01	2.40
Na	95.80	2.61	0.03	73.50	2.46	0.03	128.00	5.23	0.04	173.50	5.87	0.03	197.89	6.31	0.03
K	6.90	0.72	0.10	7.90	0.55	0.07	4.85	0.67	0.14	4.85	0.67	0.14	5.00	0.00	0.00
Ca	4.90	0.45	0.09	5.85	0.67	0.11	4.75	1.12	0.24	4.75	1.12	0.24	5.00	0.00	0.00
Mg	4.60	1.23	0.27	4.35	1.60	0.37	4.50	1.53	0.34	4.75	1.12	0.24	5.00	0.00	0.00
SO₄	68.30	1.59	0.02	43.25	2.27	0.05	37.95	1.57	0.04	33.80	1.77	0.05	38.53	1.31	0.03
Cl	18.10	1.12	0.06	7.60	0.68	0.09	6.25	0.44	0.07	6.60	0.50	0.08	10.00	0.47	0.05
HCO₃	148.85	3.27	0.02	150.15	3.62	0.02	197.65	12.25	0.06	300.30	18.19	0.06	352.53	18.88	0.05
CO₃	4.25	2.86	0.67	4.65	2.85	0.61	37.55	5.11	0.14	48.95	7.60	0.16	50.11	8.03	0.16
NO₃	0.46	0.14	0.31	0.46	0.14	0.31	0.48	0.11	0.24	0.48	0.11	0.24	0.50	0.00	0.00
Fe_T	0.27	0.47	1.73	0.06	0.02	0.29	0.22	0.06	0.27	0.44	0.16	0.37	0.42	0.13	0.31
Mn	0.07	0.01	0.16	0.02	0.01	0.37	0.05	0.00	0.10	0.02	0.00	0.11	0.04	0.01	0.27
Si	49.95	1.36	0.03	47.65	1.23	0.03	34.10	0.79	0.02	39.65	1.63	0.04	37.05	1.65	0.04
P_T	0.24	0.01	0.04	0.27	0.03	0.12	1.21	0.07	0.06	1.93	0.06	0.03	1.76	0.29	0.17
DOC	1.31	0.30	0.23	1.12	0.16	0.14	2.07	0.36	0.18	3.47	0.35	0.10	2.95	0.36	0.12
As(III)	52.64	4.51	0.09	49.28	3.20	0.06	43.78	17.41	0.40	62.42	34.97	0.56	111.80	57.37	0.51
As(T)	59.90	4.42	0.07	68.00	3.78	0.06	241.90	14.96	0.06	309.00	19.44	0.06	412.63	19.68	0.05
As(III)/As(T)	0.90	0.08	0.09	0.73	0.05	0.07	0.17	0.08	0.47	0.20	0.11	0.54	0.27	0.15	0.54
δ¹⁸O	-14.39	0.03	0.00	-14.67	0.04	0.00	-14.69	0.04	0.00	-14.65	0.04	0.00	-14.61	0.04	0.00
δ²H	-110.19	0.59	-0.01	-111.41	0.61	-0.01	-111.30	0.47	0.00	-111.41	0.54	0.00	-111.34	0.57	-0.01

Table 3 – Summaries of chemical and physical characteristics of wells A—E through time.

	regression w/ LOWESS smoothing (m, slope)	coefficient of variation (CV) (s/m)	Seasonal Kendall ($H_0: P[Y_i > Y_j] =$ (p)
well			
A	-0.001	0.074	0.47
B	0.010	0.056	0.52
C	0.050	0.062	0.51
D	0.043	0.063	0.51
E	0.051	0.048	0.52

Table 4 - Summary of statistical analyses to evaluate the existence of temporal trends for AS_T

	distance		well depth	
	R	p	R	p
pH	0.91	0.03	0.91	0.03
temp	0.24	0.70	0.23	0.71
Eh	0.45	0.45	0.72	0.17
cond	0.83	0.08	0.67	0.21
Na	0.87	0.05	0.73	0.16
K	-0.81	0.10	-0.77	0.12
Ca	-0.34	0.57	-0.29	0.64
Mg	0.30	0.26	0.47	0.43
SO ₄	-0.89	0.04	-0.86	0.06
Cl	-0.70	0.18	-0.73	0.16
HCO ₃	0.89	0.04	0.72	0.16
H ₂ S	0.40	0.50	0.06	0.93
NO ₃	0.86	0.07	0.85	0.07
Fe	0.62	0.26	0.38	0.55
Mn	-0.68	0.21	-0.59	0.30
Si	-0.85	0.07	-0.95	0.01
P _{total}	0.95	0.01	0.80	0.10
PO ₄	0.95	0.01	0.80	0.10
DOC	0.89	0.04	0.67	0.22
As _T	0.94	0.02	0.87	0.06
As(III)	0.57	0.31	0.49	0.41
As(III)/As _T	-0.91	0.03	-0.90	0.03

Table 5 - Pearson's correlation coefficients (R) and probabilities (p) of Type II error (failure to reject the [null hypothesis](#) when the null hypothesis is false) for chemical and physical characteristics versus distance and well depth. From this analysis, distance along the flow path was significantly correlated well ($p < 0.05$) with pH, sodium, sulfate, phosphate, DOC, concentration of total arsenic and the ratio of trivalent arsenic to total arsenic.

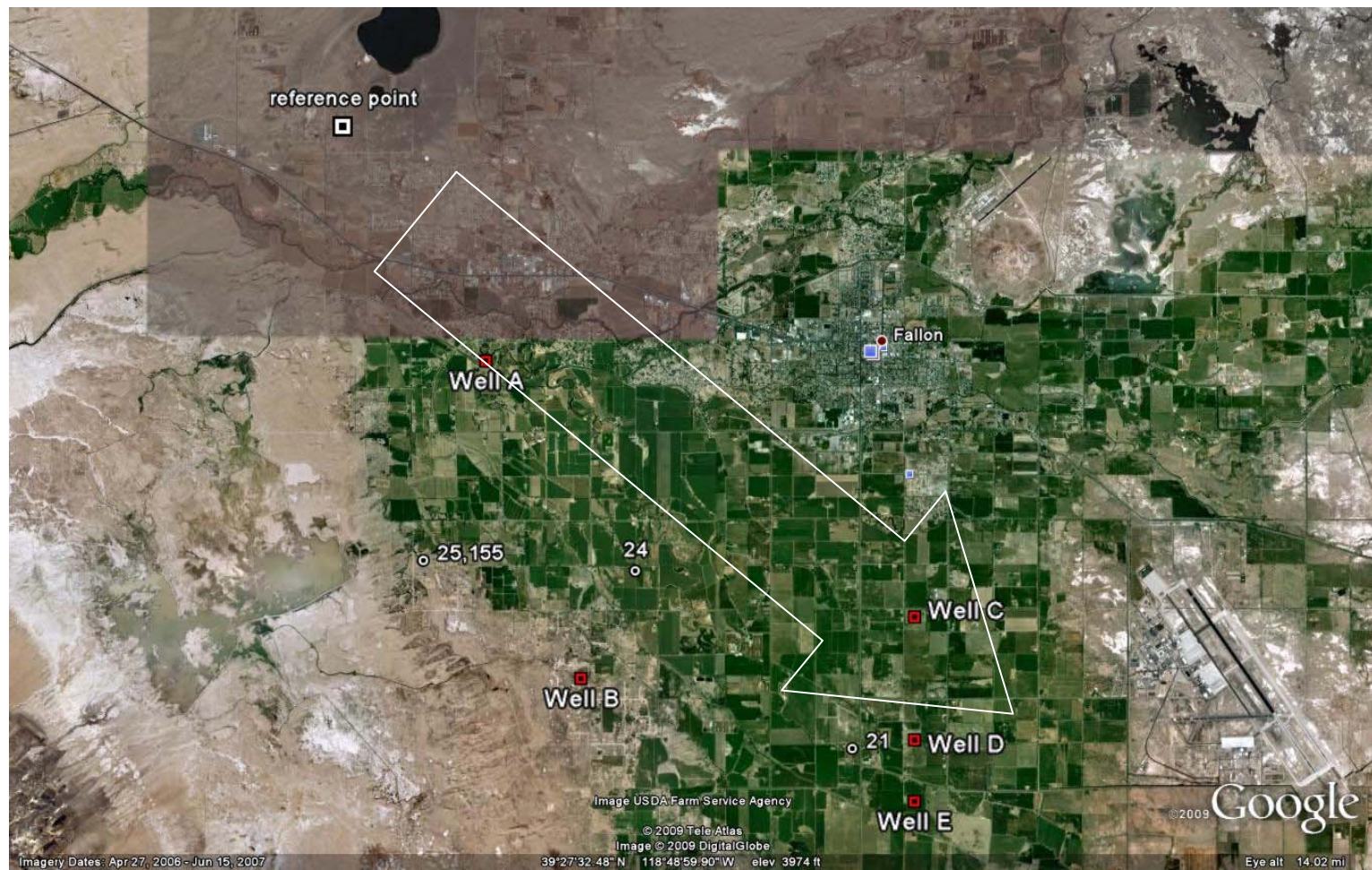


Figure 2 - Well location map with general groundwater flow direction, including Whitney (1994) and Lico and Seiler (2004) wells.

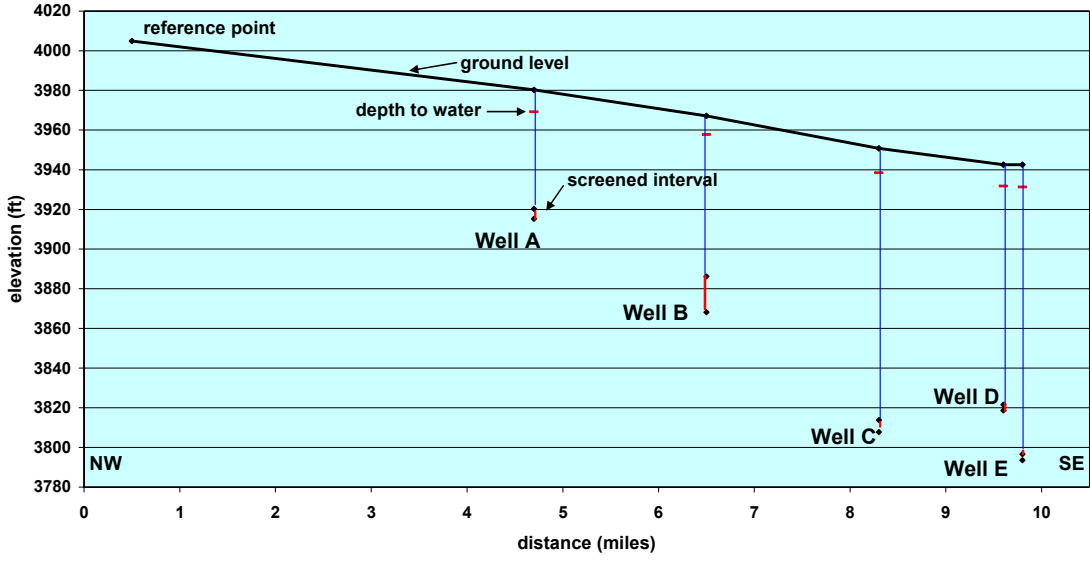


Figure 3 - Well depths along the flow path (Wells A—E) with ground surface elevations and measured depths to water.

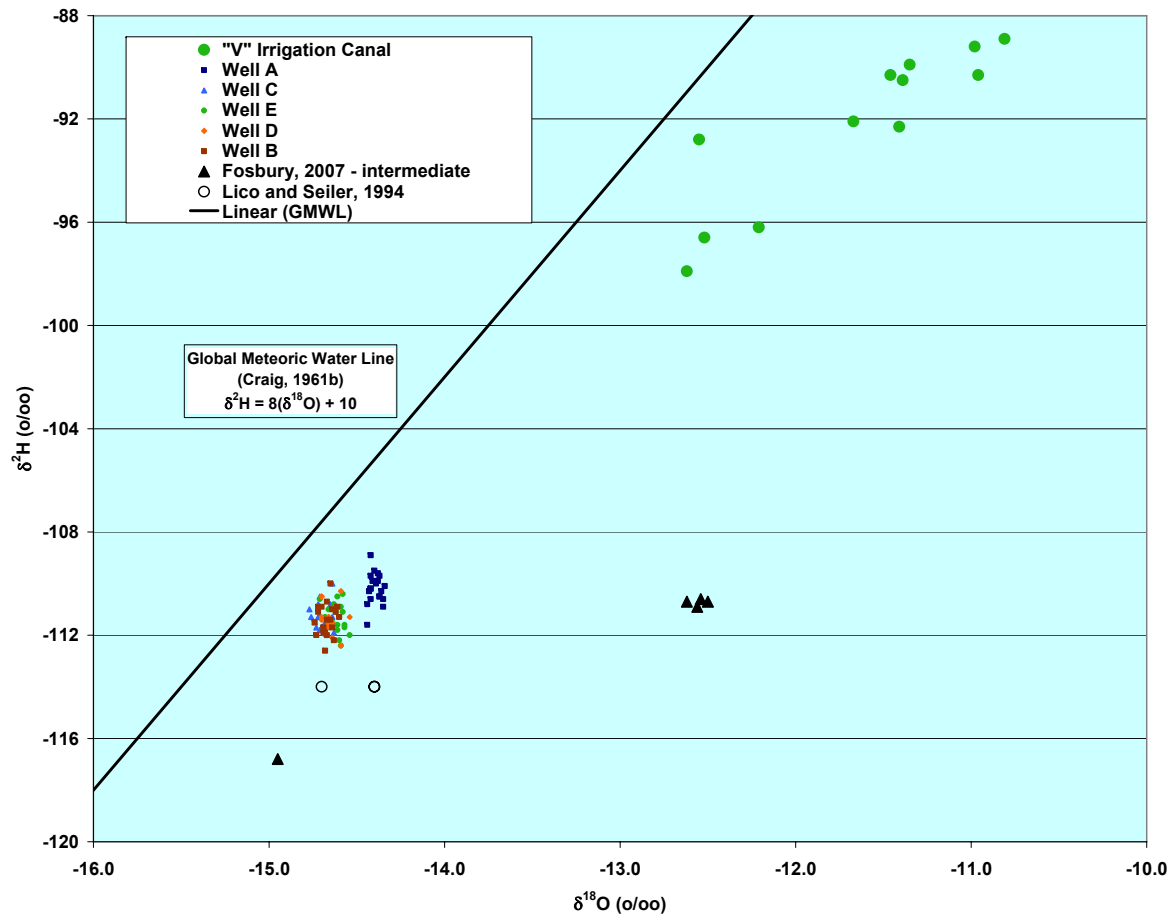


Figure 4 - $\delta^2\text{H}$ vs. $\delta^{18}\text{O}$ plot for study wells and data sets, showing results of previous analyses, this study (wells A—E), Fosbury (2007), Lico and Seiler (1994) and the Global Meteoric Water Line (Craig, 1981b).

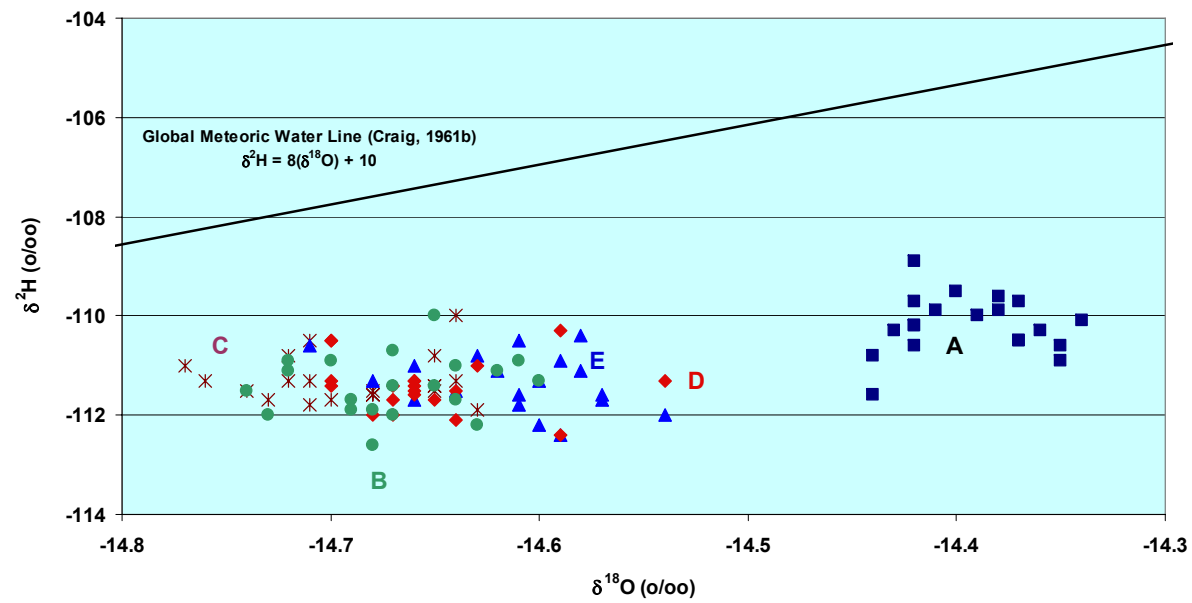


Figure 5 – Expanded view of $\delta^2\text{H}$ vs. $\delta^{18}\text{O}$ plot for wells A—E.

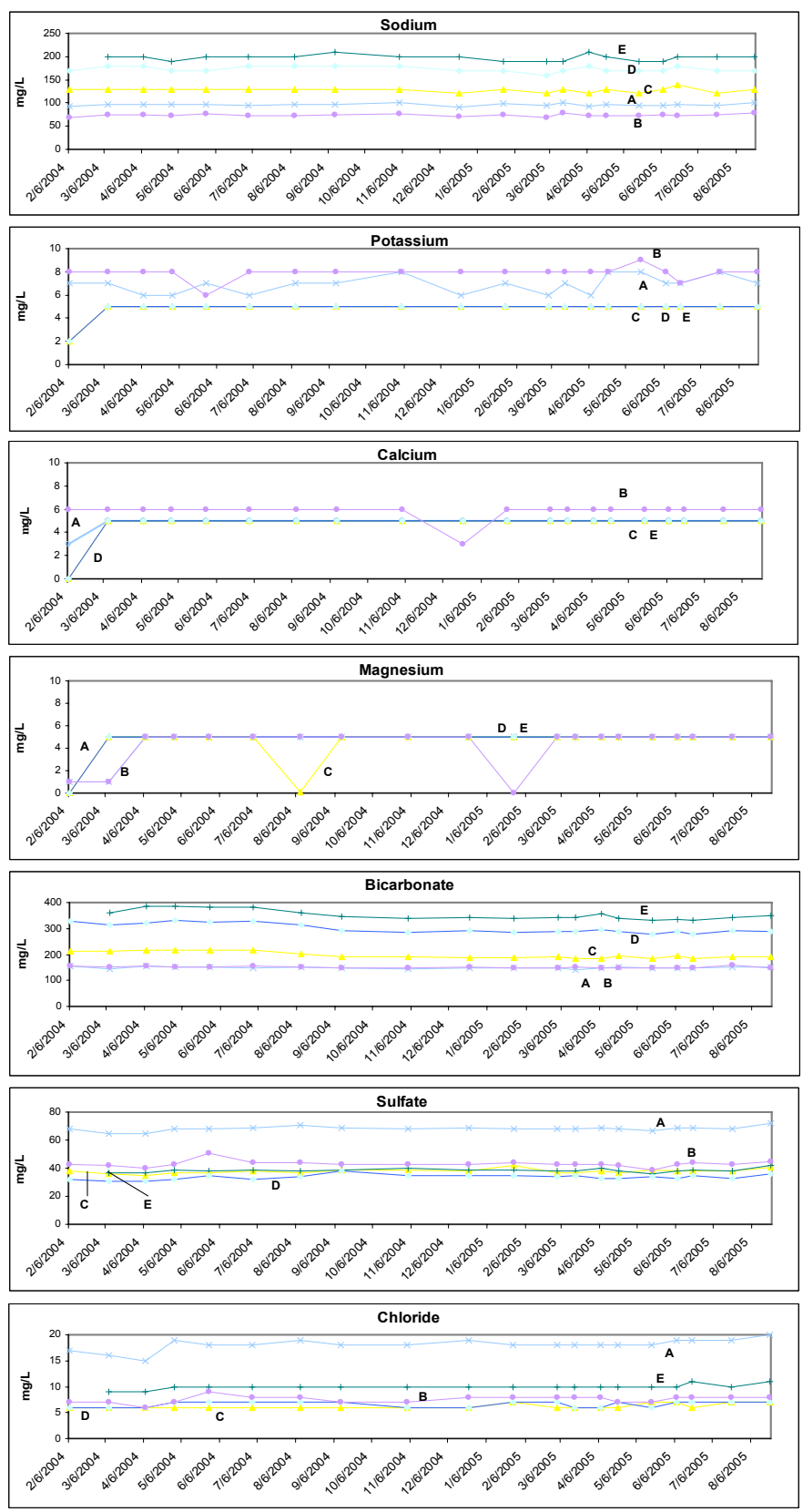


Figure 6 - Time-series plots for major ions, wells A—E.

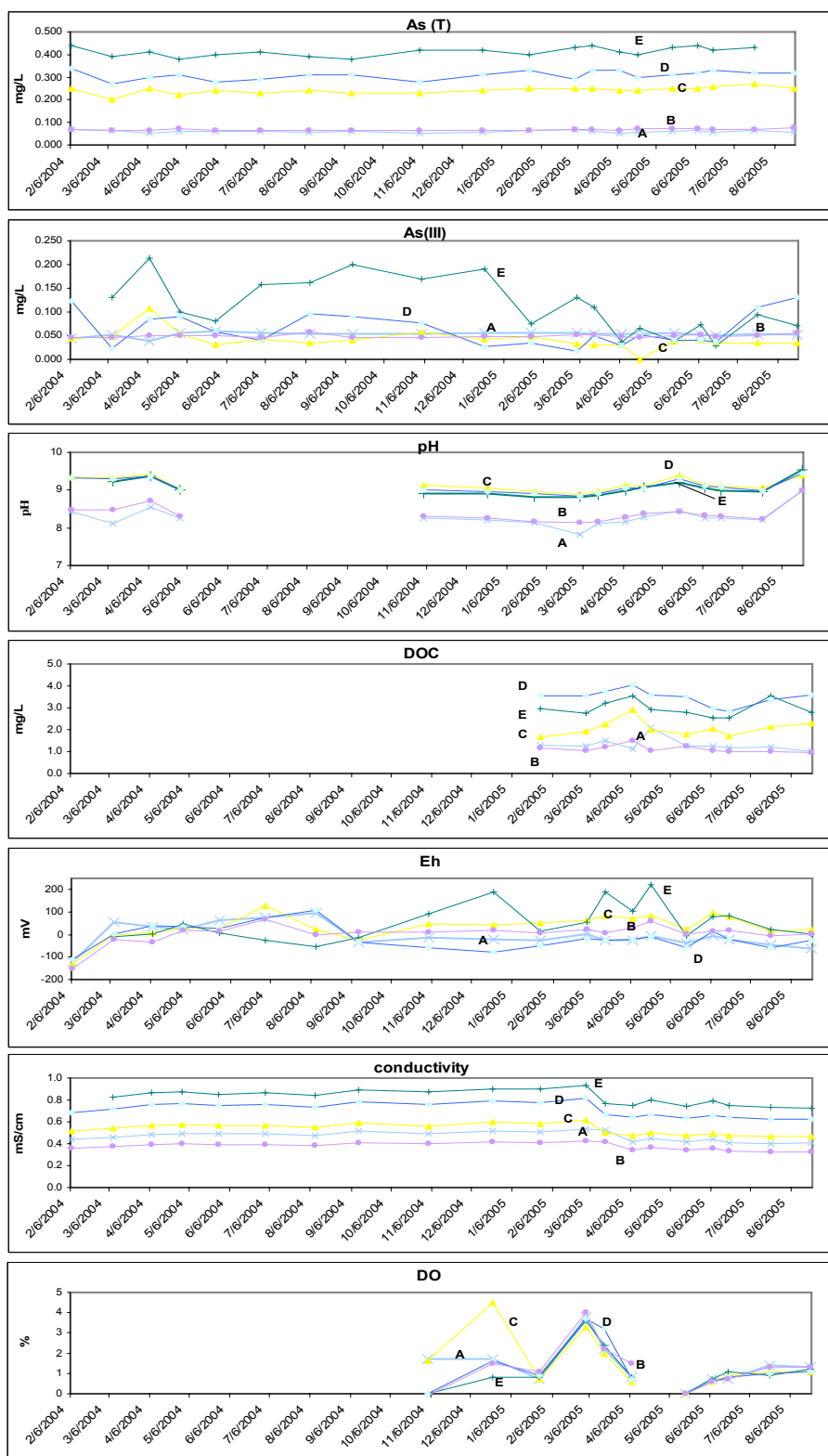


Figure 7 - Time-series plots for As_T , $As(III)$, pH, dissolved organic carbon (DOC), Eh, conductivity and dissolved oxygen (DO).

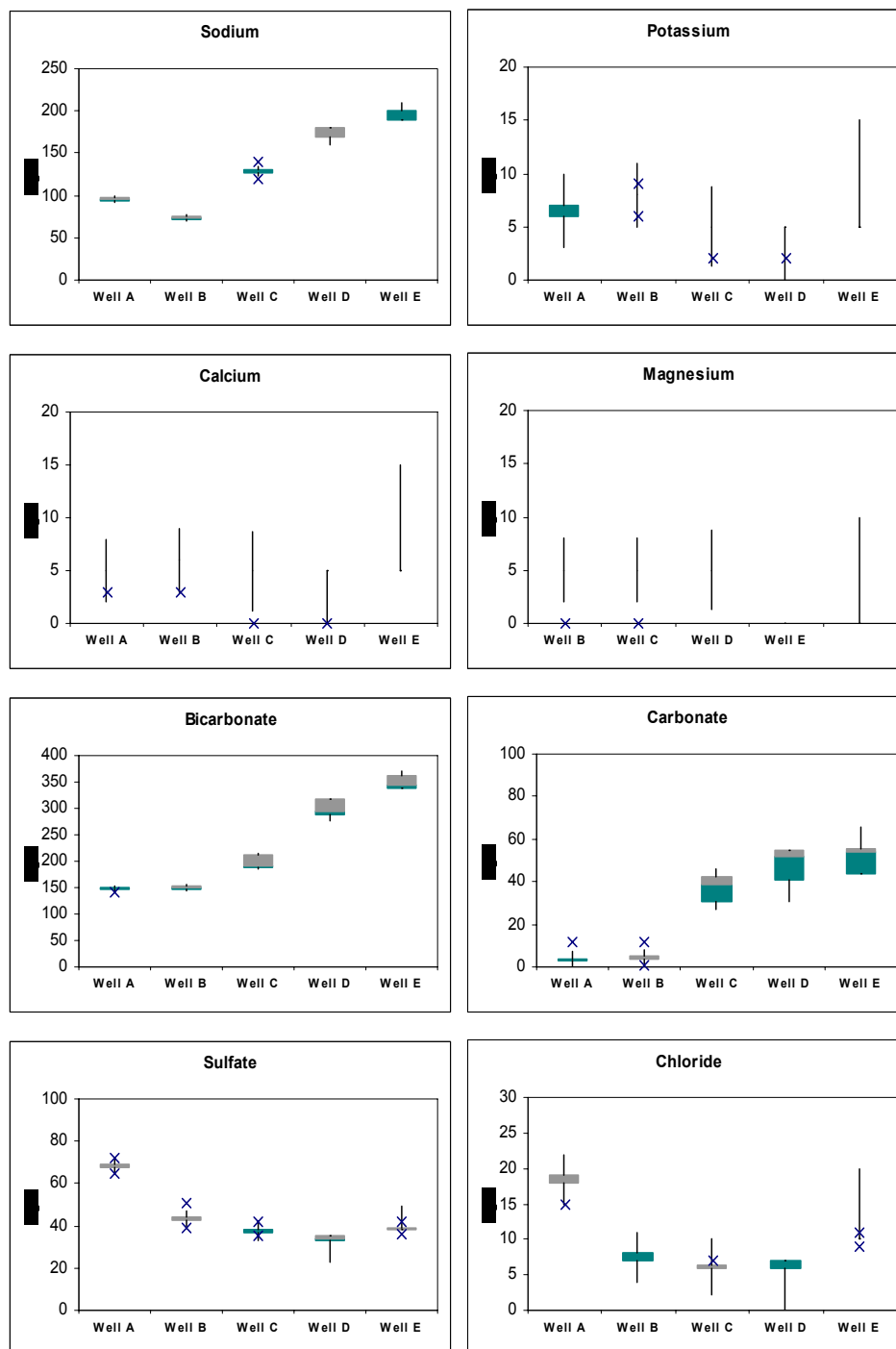


Figure 8 - Major ions for A-E (Wells A-D, n=20; Well E, n=19). Upper, middle, and lower boundaries of the boxes represent the 75th, 50th, and 25th percentile of the data, respectively. Each "whisker" connects the box to the outlier while "x" represents an extreme outlier which is 3 standard deviations or more from the mean.

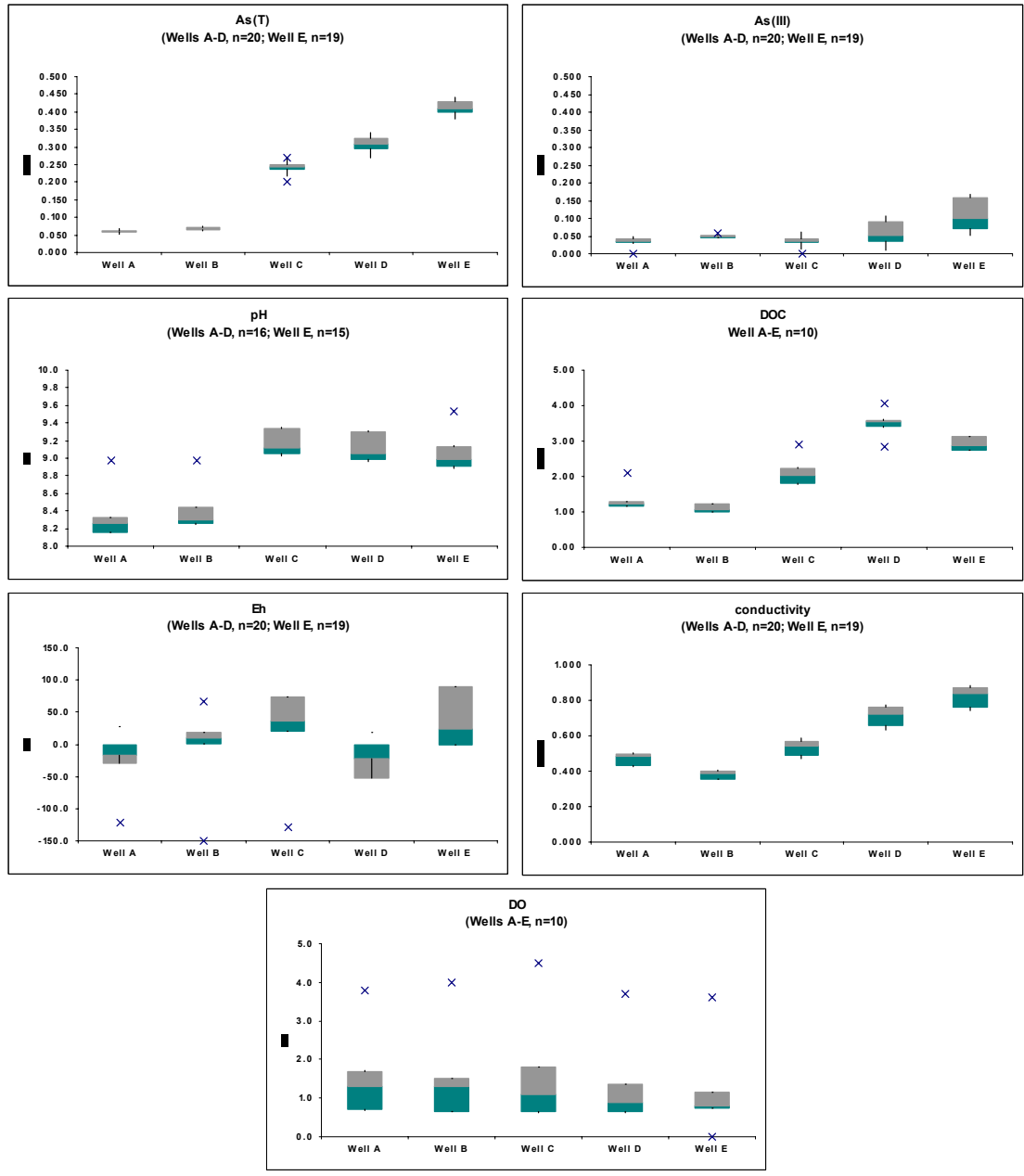


Figure 9 – Summaries of sampling data for As_T, As(III), pH, DOC, Eh, conductivity and dissolved oxygen (DO) for wells A–E.

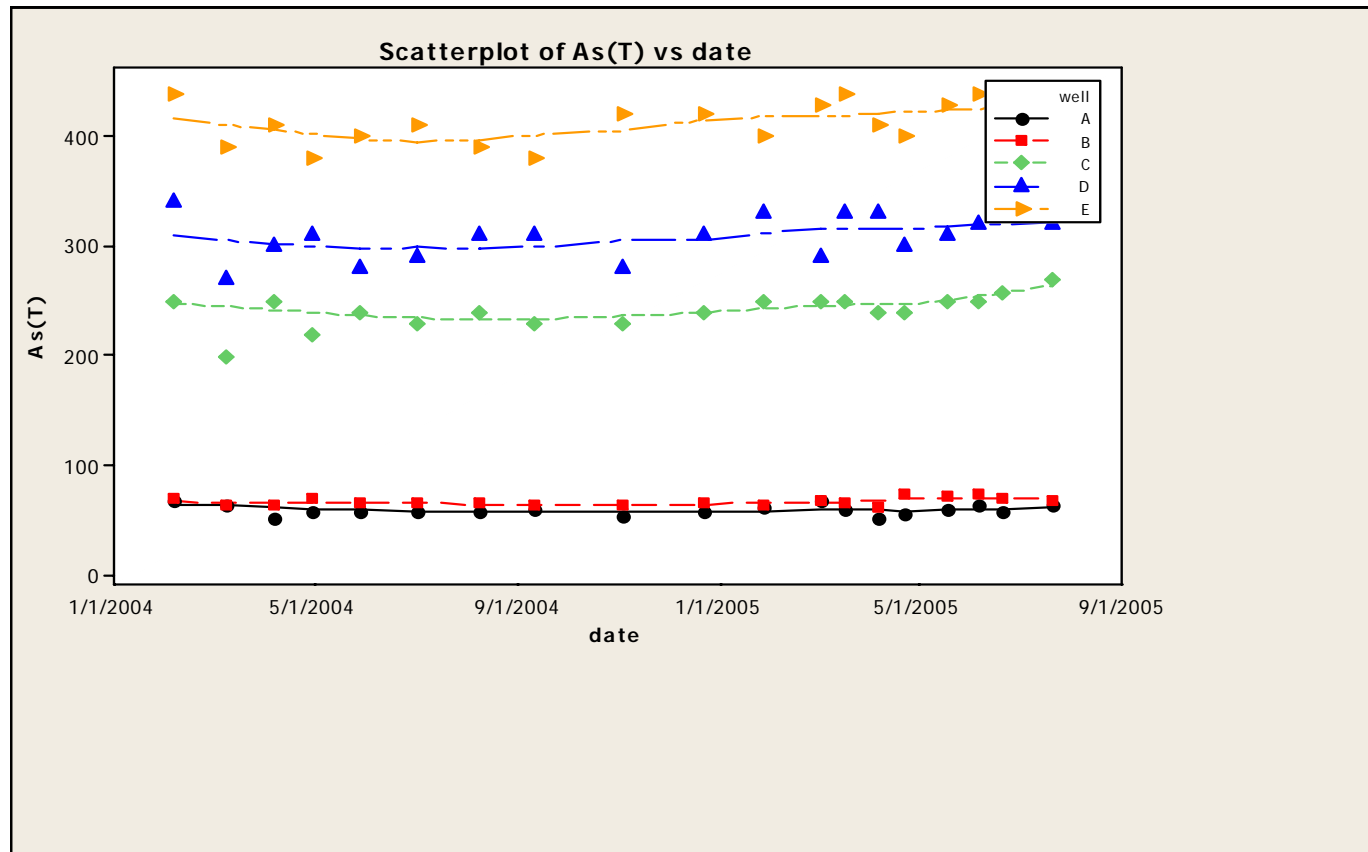


Figure 10 – A time-series of As_T concentrations, with LOWESS smoothing to evaluate seasonal cycling.

EXPLANATION

- Well A
- Well B
- △ Well C
- ▽ Well D
- ★ Well E

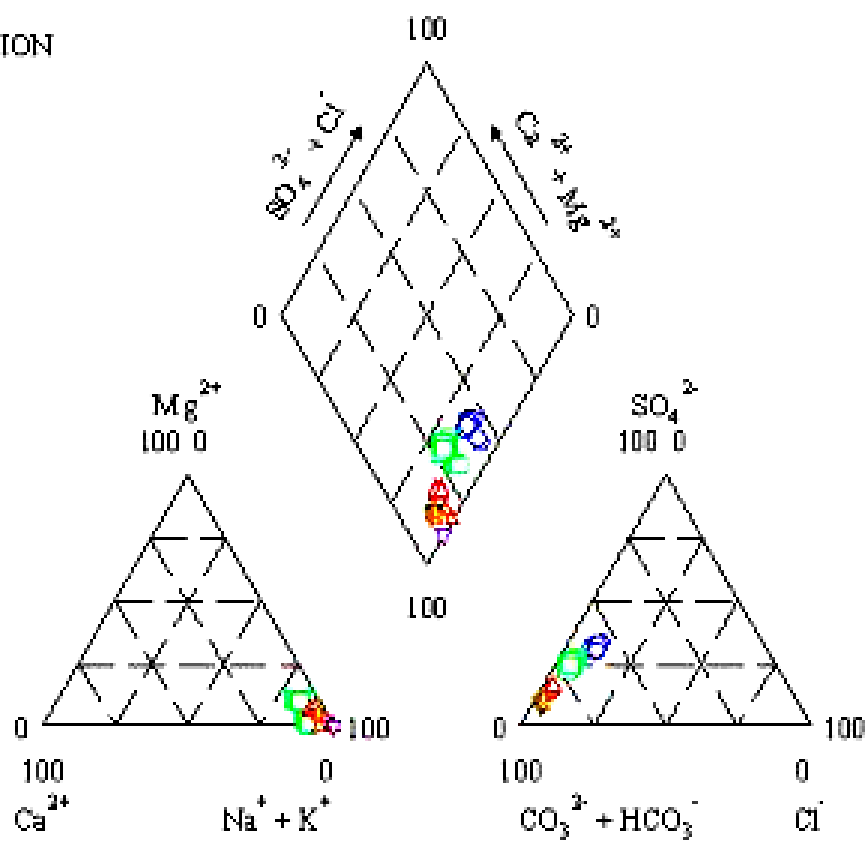


Figure 11 - Piper plots for flow-path well chemistry for major ions

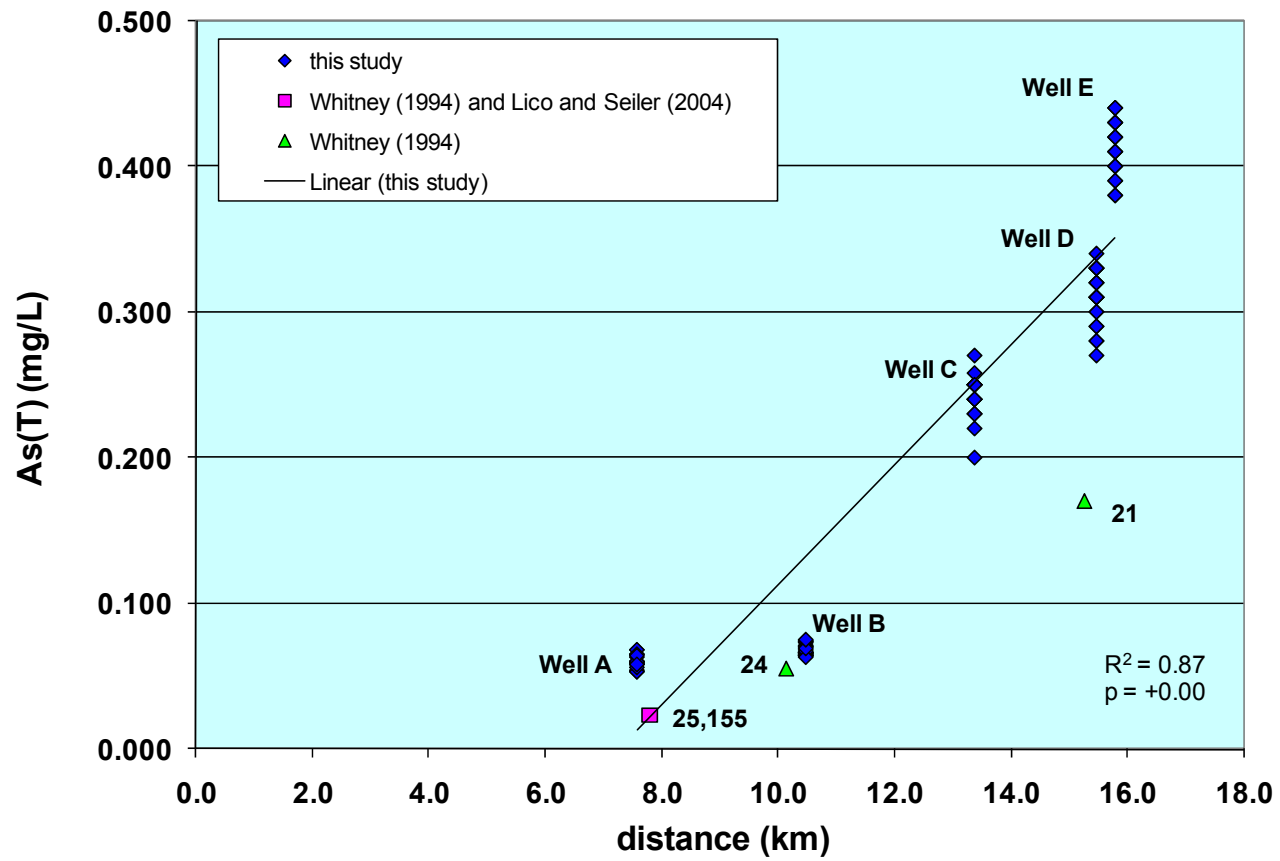


Figure 12 - As_T vs distance for sampled wells

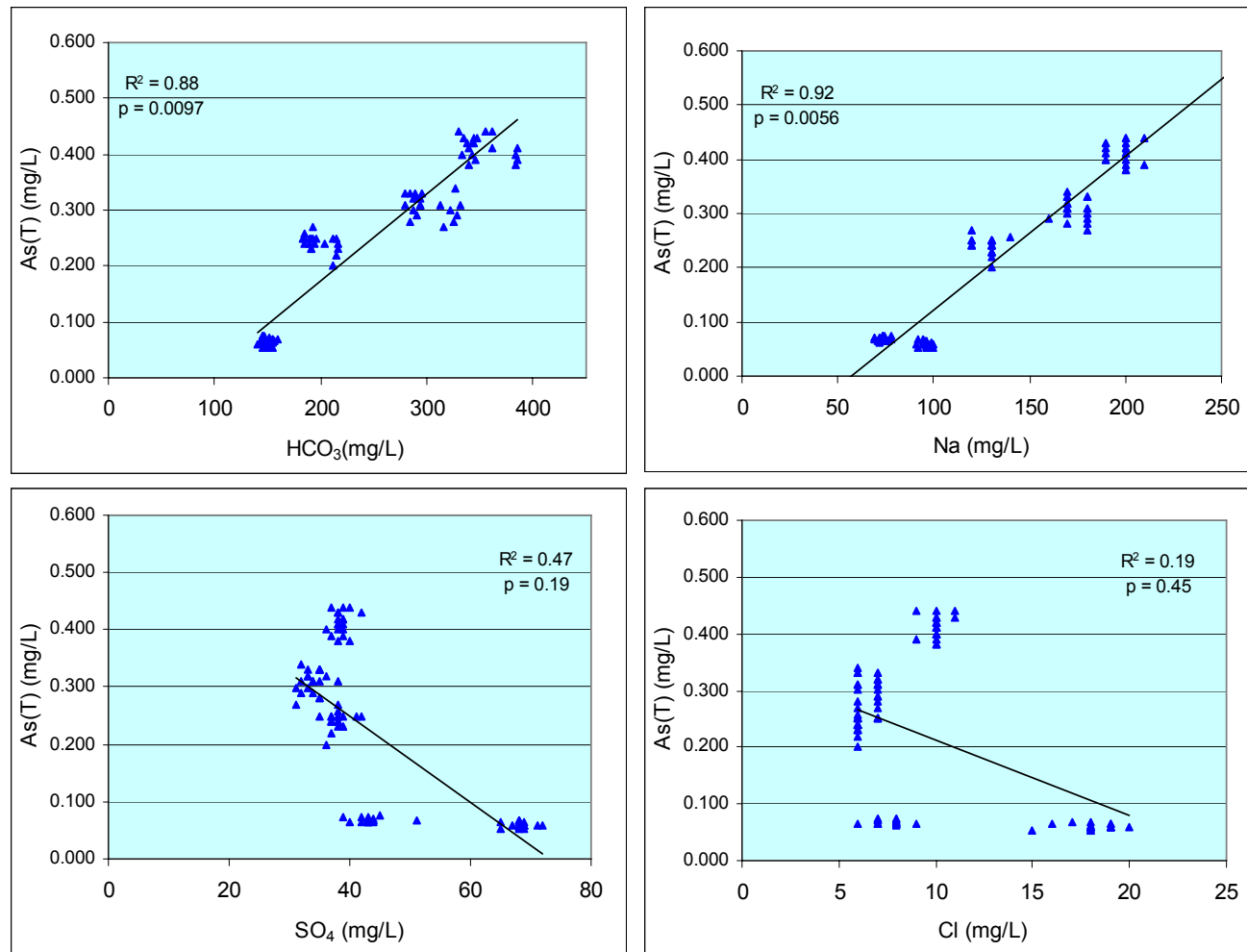


Figure 13 - Significant linear relationships between As_T and HCO_3 , Na, SO_4 and Cl.

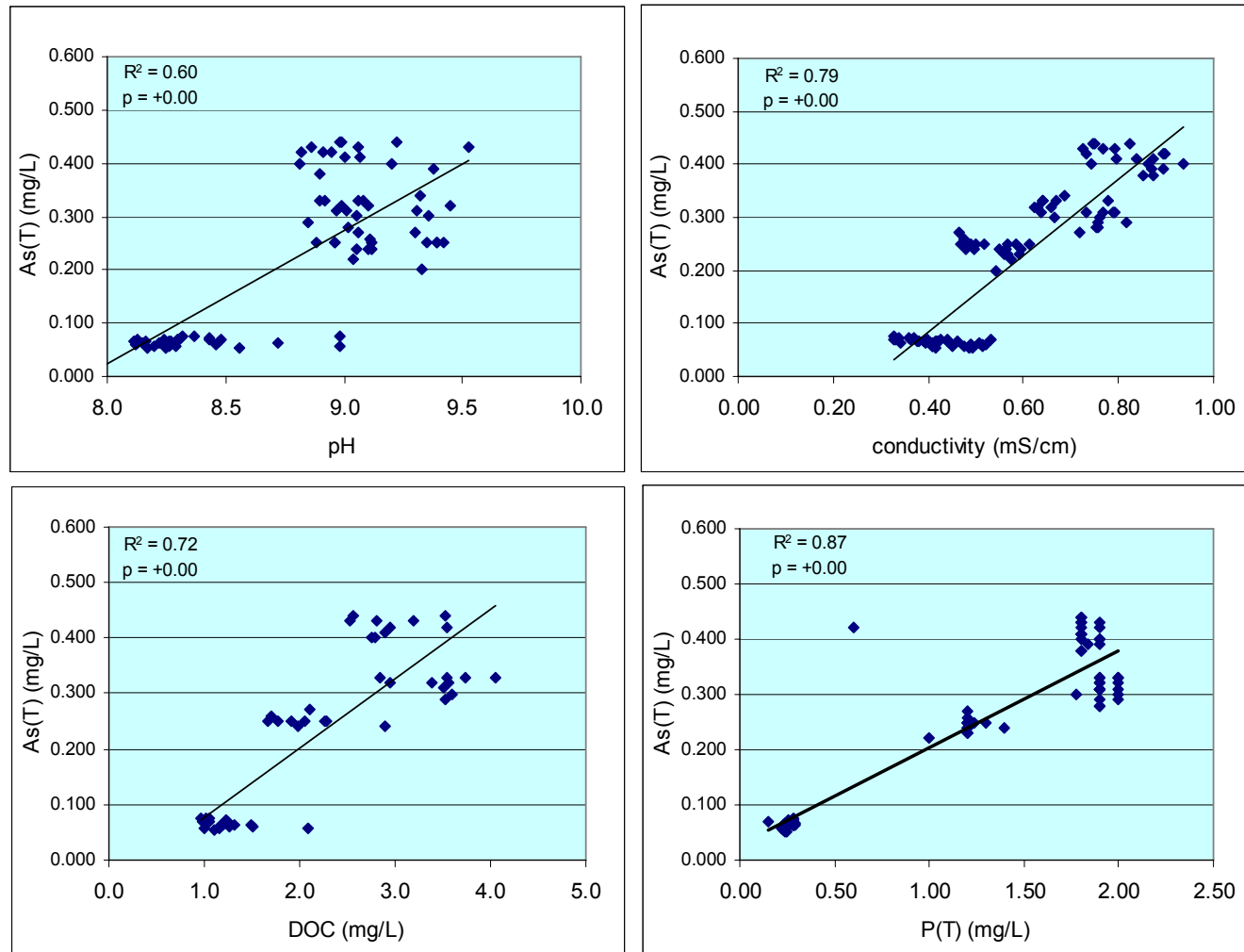


Figure 14 – Relationships between As(T) and pH, conductivity, dissolved organic carbon and total phosphorus, expressed with linear relationships developed by regression analysis.

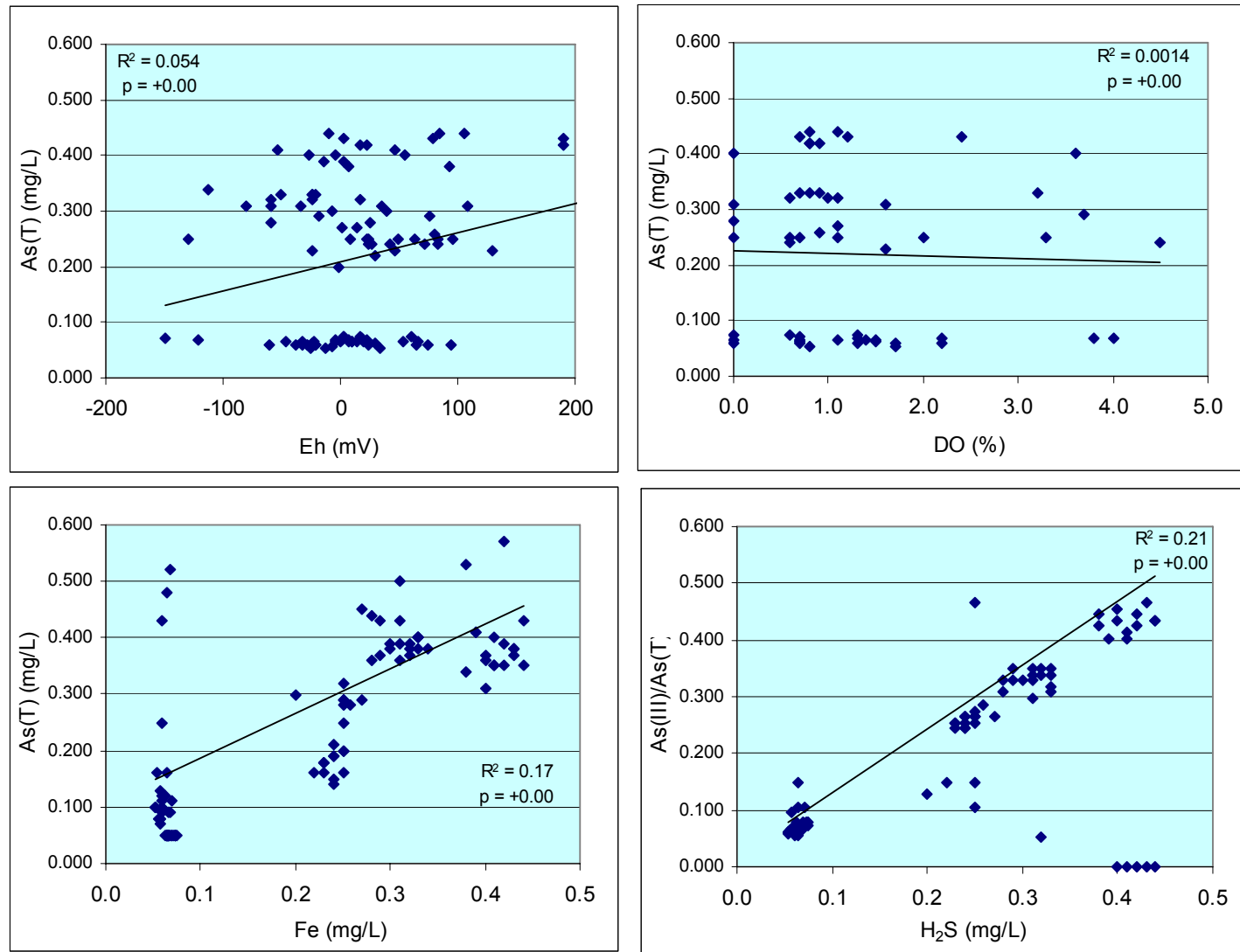
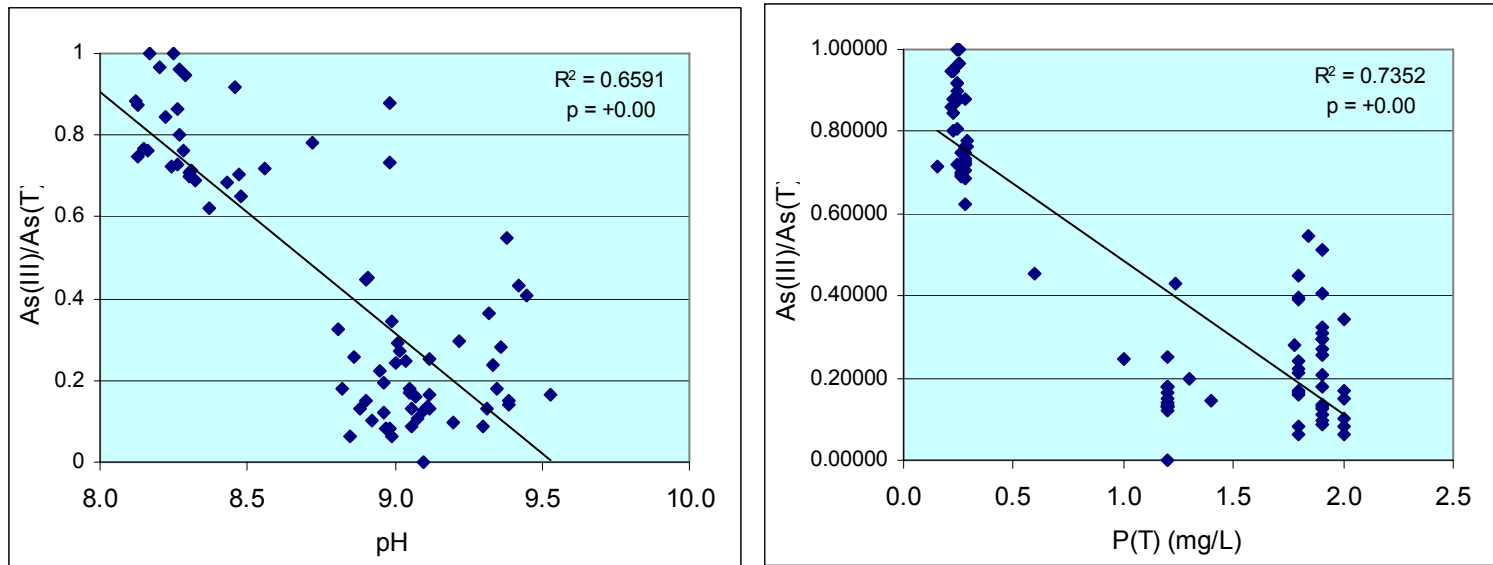


Figure 15 – Linear relationships between As(T) and Eh, DO, and Fe

Figure 16 - $As(III)/As_T$ vs pH and P_T

Chapter 3 – Arsenic enrichment mechanisms

Abstract

A study was conducted in the intermediate-depth alluvial aquifer (50-500 ft) of Lahontan Valley, Nevada to examine potential mechanisms for dissolved arsenic enrichment along a likely groundwater flow path. Five wells previously observed to have substantial concentrations of both As(V) and As(III) were chosen to represent a groundwater flow-path and were sampled over an 18-month period (February 2004—August 2005) for a variety of physical parameters and chemical constituents. NETPATH 2.0 and Visual MINTEQ 2.3 geochemical models were employed to model geochemical reactions potentially controlling arsenic release to the aquifer. Field-measured and MINTEQ-computed values for electric potential (Eh) were used in the models. Models indicated minor arsenic desorption along the flow path from hydrous ferric oxides (HFO) - primarily for As(V) - and less so with increasing pH. Competition with arsenate and arsenite for sorption sites from other ligands also occurred – particularly that of PO₄. Reductive dissolution of HFO may have accounted for arsenic enrichment but only at the low Eh values estimated by MINTEQ. However, neither arsenic desorption nor reductive dissolution of HFO appeared to be sufficient to account for the arsenic gradient observed along the flow path. Other chemical processes, including the role of dissolved organic carbon as an electron source, could be explored with an enhanced field investigation to explain the As_T gradient in the intermediate-depth alluvial aquifer of the Lahontan Valley.

Introduction

This research examined mechanisms that may cause enrichment of aqueous arsenic within the intermediate-depth regional aquifer of the Lahontan Valley of western Nevada. The objective was to produce a conceptual model that would identify (a) possible chemical and physical mechanisms along a flow-path in an aquifer of intermediate-depth (50-500 ft) and (b) how those changes may affect arsenic concentrations. A flow-path comparison for intermediate-depth wells was appropriate since water at this depth has minimal influence from the surface and can be expected to traverse the length of the flow-path without significant recharge or loss (Maurer, Johnson et al. 1996).

The intermediate-depth aquifer and the shallow aquifer (from the land surface to 50 feet in depth) provide drinking water through approximately 5000 domestic wells in the Lahontan Valley. Of these, less than half exploit the intermediate-depth aquifer (Fitzgerald 2003). The intermediate-depth aquifer has been described as being a highly reducing environment (Seiler and Allander 1993; Seiler, Stollenwerk et al. 2005). Typically, water in the intermediate-depth aquifer contains little dissolved oxygen and contains high concentrations of sulfides and ferrous iron due largely to anaerobic degradation of organic material by subsurface microbes. Chemical mechanisms that can increase arsenic mobility may be enhanced in this environment, especially, reductive dissolution of iron oxyhydroxides and desorption of arsenic oxyanions at elevated pH. Since arsenic has been shown to cause a variety of disorders (including diarrhea, circulatory disorders, and cancer), and the toxic effect increases with concentration,

understanding the occurrence of arsenic is important for public health protection, especially because of the observed trends along the groundwater flow path.

1. Eh/pH controls on precipitation/dissolution

Precipitation/dissolution reactions are highly dependent upon the solution chemistry of the minerals involved, and the degree of saturation. Reactions are also dependent upon the redox condition of the groundwater, which determines if the groundwater is sufficiently reducing to lower the valence of metal cations, which may increase solubility. In very reducing environments, pyrite (FeS_2) and orpiment (As_2S_3) can incorporate arsenic where sulfate reduces to sulfide (Sracek 2004). At $\text{pH} > 7.0$, Ca, Mg, and Fe(III) arsenates in the presence of carbon dioxide can produce carbonates as the stable phase and releasing arsenic to groundwater. Arsenic is mobilized at $\text{pH} > 7.0$ if Ca and CO_3 are present (Magalhaes 2002). The latter condition is common in the Lahontan Valley.

Geochemical models analyses with WATEQ4F (a program that models species distribution, ion activities and saturation indices) in Lahontan Valley groundwater suggest that arsenic minerals are undersaturated, which precludes precipitation as a sink for arsenic (Ball and Nordstrom 1991). Although equilibrium constants for various arsenic minerals suggest a high propensity for precipitation under local groundwater conditions (Nordstrom and Archer 2003), samples collected by Welch and Lico (1998) did not indicate precipitation of arsenic minerals.

Thermodynamically favorable reductive dissolution of Fe-oxides that contain arsenic could contribute arsenic to groundwater in the southern Lahontan Valley. The hydrous ferric oxides (HFO) most often mentioned in the literature are goethite (α -

FeOOH) and ferrihydrite ($5\text{Fe}_2\text{O}_3 \cdot 9\text{H}_2\text{O}$, or more simply $\text{Fe}(\text{OH})_3$). Petrographic examination and extractions of Lahontan Valley sediments indicated Fe-oxide concentrations ranging from 180 to 2600 mg/kg (Welch and Lico 1998) and much of the Fe-oxide contained arsenic. However, increased aqueous Fe and Mn concentrations did not correlate to increased arsenic concentration (Welch and Lico 1998). This was explained by secondary carbonate mineral coprecipitation with calcite. Saturation indices suggested saturation or oversaturation with respect to calcite for 96% of southern Lahontan Valley samples. However, saturation indices for rhodochrosite (MnCO_3) and siderite (FeCO_3) indicated undersaturation for the lateral-flow region in the shallow aquifer (Welch and Lico 1998).

Ahmed et al. (2004) found reductive dissolution of iron oxyhydroxides to be the main release mechanism for arsenic in alluvial aquifers of Bangladesh. The aquifers are analogous to the intermediate aquifer of the Lahontan Valley in that they are generally fine-grained Holocene sediments, with elevated As concentrations within ~20-50 m of the land surface, moderate to strongly reducing conditions and circumneutral pH. Ahmed et al (2004) also observed dissolved sulfides, indicating reduction of SO_4 .

Depending upon the oxidation state, the redox condition of the groundwater can determine solubility, mobility, toxicity and bioavailability (Deuel and Swoboda 1972; Penrose 1974). Manning and Goldberg (1997) concluded that distribution between dissolved As(III) and As(V) is dependent upon redox potential (Eh). Arsenate predominates in oxygenated soils but can be converted to arsenite under even mildly reducing Eh conditions (0—100 mV) (Masscheleyn et al. 1991b, Ferguson and Gavis 1972; Sadiq et al. 1983). At Eh from 200-500 mV, arsenic solubility is low, and As(V) as

the major species in solution (Masscheleyn, Delaune et al. 1991). Masscheleyn, et al (1991b) also determined that the concentration of arsenic was controlled by dissolution of iron oxyhydroxides, when Eh values ranged from 0-100 mV, and As(III) was the dominant form. With Eh values at -200 mV, solubility increased ~13 fold. Magalhaes (2002) reported that iron and arsenic reduction promoted ferric arsenate dissolution even more so than calcium arsenates when redox potentials were negative. Since Lahontan Valley groundwater is considered highly reducing (Seiler and Allander 1993; Seiler, Stollenwerk et al. 2005) and reductive dissolution may be an important mechanism determinant of concentration, As(III) may be the more dominant species.

The phase stability diagram in Figure 17 illustrates oxidation-reduction and pH dependence of the predominant mineral species for arsenic under equilibrium conditions for most aquifers (Nordstrom and Archer 2003). Conditions that lead to occurrence of As(III) are not found in most groundwater systems because As(V) predominates at the pH of the study area and most values of Eh. With high pH (7.5-9.5; median 9.1; Lico and Seiler 2004) and reducing conditions (Seiler and Allander 1993; Seiler, Stollenwerk et al. 2005), Lahontan Valley groundwater closely straddles the redox boundary between As(III) and As(V) species.

Increased pH alone can lead to the oxidation of As(III) to As(V), especially at sorption sites on illite and kaolinite clays (Manning and Goldberg 1997). Nevertheless, the main mechanism for As(III) mobility appears to be the onset of reducing conditions in sediments where particles have sorbed arsenic (Korte 1991; Masscheleyn, Delaune et al. 1991; Lombi, Wenzel et al. 1999).

Oxidation-reduction (redox) is largely controlled by the availability of electron donors and acceptors. The single largest source of electron-donors within Lahontan Valley groundwater is likely to be sedimentary organic carbon (SOC), derived primarily from plant material in the Fallon Formation, the youngest member of the Lahontan Valley Group (Maurer, Johnson et al. 1996). This formation consists of eolian, alluvial, deltaic, and shallow lacustrine sediments that at one time supported significant plant growth (Maurer, Johnson et al. 1996). It is the dissolved portion of this organic carbon (dissolved organic carbon, or DOC) that affects groundwater chemistry. Groundwater typically contains less than 1 to 2 mg-C/L. However, in certain environments, recharge with much higher DOC concentrations can flush significant quantities of DOC to the saturated zone particularly in agricultural areas, or in the spring when soil microbial activity is low (Wassenaar, Aravena et al. 1990a). Additional carbon can provide electrons for the reduction of chemical species that may include As(V), Fe(III) and SO_4^{2-} . In the process DOC is oxidized to CO_2 . High concentrations of sulfides in the Lahontan Valley have been attributed to the reduction of sulfates (Seiler, Stollenwerk et al. 2005). Seiler et al. (2005) note that high concentrations of Fe, Mn, and inorganic C content in groundwater indicate reduction of the metal oxides while oxidizing organic matter.

Seiler and Stollenwerk (2005) describe Lahontan Valley groundwater as being strongly reducing and that tungsten concentrations mirror those of arsenic where these conditions exist. These concentrations are partly due to pH-controlled desorption of these metals, and the dissolution of HFO under these reducing conditions. Sracek (2004) and Kirk et al., (2004) drew similar conclusions and suggest that where SO_4 reduction occurs, sulfides may remove arsenic in the form of arsenic sulfides. Reducing conditions

are enhanced where organic matter is introduced into sulfur and iron-rich systems and authigenic pyrite can precipitate (Harvey and Beckie 2005). Kirk, et al., (2004) suggested that the presence (or lack) of sulfate-reducing bacteria directly affects As concentration. They observed high arsenic concentrations where sulfate reduction was at a minimum (low or absent sulfate-reducing bacteria), and low concentrations of As where sulfate reduction was active. Reductive dissolution of oxyhydroxide coatings on sand grains and mica – especially during excess pumping - was implicated in As enrichment (especially that of As(III)) in the reducing conditions of Holocene sediments in Bangladesh (Ahmed, Bhattacharya et al. 2004). Small grain size and depth to water from the land surface (20-50m) were also a factor in that study. High pH (>8.5) in arid to semi-arid alluvial basins where sulfates are low (<1 mg/L) and slow rates of groundwater flow have also been linked to high As concentrations (Welch and Lico 1998; Smedley and Kinniburgh 2002). Strongly reducing conditions, ground-water age, and depth have been implicated in elevated arsenic concentrations in glacial aquifers (Thomas 2007).

In a study conducted in Bangladesh, dissolved arsenic concentrations were determined to be unrelated to reductive dissolution of HFO because the oxide was not observed in aquifer materials (Polizzotto, Harvey et al. 2006). However, As concentrations were drastically different in wells separated by as little as 100 meters. They suggest instead that As is released from surface and shallow aquifer sediments where redox conditions fluctuate and then is transported deeper.

Sequestration of arsenic in sulfides may reduce arsenic concentrations in groundwater (Kirk, Holm et al. 2004), although that may be offset by the release of arsenic from the dissolution of HFO (Harvey and Beckie 2005).

2. Adsorption

Adsorption reactions are important mechanisms for retention and release of arsenic (Stollenwerk 2003). These reactions are a function of the nature of the adsorbing surfaces present, the pH and ionic strength of the solution, and the valence state of the arsenic species involved. Comparing adsorption to precipitation, Livesey and Huang (1981) concluded that concentration of arsenic in solution was controlled by adsorption reactions in soils rather than precipitation of arsenate compounds. Welch and Lico (1998) drew similar conclusions for arsenic in the Lahontan Valley. The potential sorbents most commonly described that can adsorb aqueous arsenic species include clay, silt, and sand with mineral compositions that include oxides of Fe, Mn and Al (Stollenwerk 2003). Magalhães (2002) lists the following substances in order of their adsorption ability: aluminum hydroxide > synthetic iron (III) oxyhydroxide > goethite > clay. Clays can be important in the adsorption of arsenic due to their surface charge and large specific area (Masscheleyn, Delaune et al. 1991; Magalhaes 2002). Oxide coatings can develop because of oxidizing conditions and elevated pH, producing insoluble metallic oxides that precipitate onto sediment surfaces. Coordination shells of oxygen around the metals are completed by the addition of hydroxyl functional groups in the presence of water, which form surface sites such as $\equiv\text{SOH}_2^+$, $\equiv\text{SOH}$, or $\equiv\text{SO}^-$ by hydrolysis (Stollenwerk 2003). The formation of these groups is largely dependent upon pH, which, in turn, determines the adsorption properties at the surface. At higher solution pH, where surface protons are not abundant, a negative charge can develop on particle surfaces. At lower solution pH, protons are attracted to the surface creating a positive surface charge. Since the predominant arsenate (As(V)) species are charged oxyanions (H_2AsO_4^- and HAsO_4^{2-}),

arsenate adsorption is enhanced in acidic aqueous solution and arsenate desorption is enhanced in basic solution (Carillo and Drever 1998; Stollenwerk 2003). Others have also observed maximum arsenate adsorption at acidic pH ranges, decreasing with pH above 9, 7, and 5 for Al oxides, Fe oxides and clays, respectively (Goldberg 2002). Other studies also show that arsenate is preferentially adsorbed at low pH (Pierce and Moore 1982; Lombi, Wenzel et al. 1999; Stollenwerk 2003) (Figure 18).

The predominant As(III) species in aqueous solution is a neutral molecule of arsenious acid (H_3AsO_3) and sorption is not enhanced at any pH. However, As(III) exhibited parabolic behavior with ferrihydrite according to both Stollenwerk (2003) and Goldberg (2002) with maximum arsenite adsorption at neutral pH, and pH = 8.5, respectively. Separate adsorption experiments showed that both As(V) and As(III) exhibited minimal adsorption at high pH (Stollenwerk 2003) (Figure 18). The parabolic adsorption behavior may be due to the dominance of chemical binding energy over electrostatics (Dzombak and Morel 1990; Stollenwerk 2003). Seiler, et al (2005) suggest that desorption of arsenic from iron oxyhydroxides brings arsenic into solution in the Lahontan Valley.

Amorphous hydrated oxides such as goethite and ferrihydrite may provide the dominant adsorption sites involved in arsenate sorption processes (Pierce and Moore 1982; Welch and Lico 1998). Comparison between experimental and modeled results (using the MICROQL and MINTEQA2) suggested that As is sorbed mostly by oxyhydroxide surfaces in the natural environment (Carillo and Drever 1998). Subsurface minerals with Fe oxide surfaces in the pH ranges found in the southern Lahontan Valley may have high As(V) retention capacity (Welch and Lico 1998). Pierce and Moore

(1982) saw continuous adsorption of arsenate even at the highest As concentrations studied (1000 $\mu\text{g/L}$), which suggests that the surface of the amorphous goethite (FeOOH) is a loose, hydrated structure with heterogeneous surface sites that allow oxyanions to be incorporated within the porous surface layer as well as on the surface. In addition, the surface charge of oxides decreases with increasing pH, which leads to As(V) desorption. These surfaces sorb arsenic primarily by inner-sphere complexation, which is considered a "specific adsorption" in which ligands such as arsenite and arsenate coordinate directly with metal centers of the oxide surface. The coordination complex has been shown to be independent of the ionic strength of the solution (Stollenwerk 2003). This may be due to the dominance of direct bonding energies ($\Delta G_{\text{intrinsic}}$) over that of electrostatics ($\Delta G_{\text{coulombic}}$) in the overall free energy of reaction (Dzombak and Morel 1990).

Competition among adsorbing ions can play a significant role in the mobility of arsenic species. Ions that compete for adsorption sites with As(V) include SiO_3^{2-} , VO_4^{3-} , and PO_4^{3-} . Exclusion of any of these from adsorption models, especially SiO_3^{2-} , affected the predicted amount of As sorbed (Welch and Lico 1998). The exclusion of SO_4^{2-} and F^- from adsorption models did not significantly change the predicted amount of As adsorbed. SO_4^{2-} , HCO_3^- , WO_4^{2-} may also have a role in sorption, in addition to DOC (Stollenwerk 2003; Harvey and Beckie 2005).

Although spectroscopic studies have shown respective surface complexes for PO_4^{3-} and AsO_4^{3-} to be identical (Stollenwerk 2003), experiments have shown that the surface complexation of AsO_4^{3-} on goethite decreases significantly when in competition for adsorption sites with PO_4^{3-} in 0.7 M NaCl solution; and the decrease is proportional to concentration of phosphate (Gao and Mucci 2001) (Figure 19). This may be due to

increases in surface charge at greater ionic strength at any given pH, resulting in less affinity of AsO_4^{3-} on mineral surfaces (Dzombak and Morel 1990; Gao and Mucci 2001).

Conversely, phosphate is less affected by the presence of arsenate. In short, if phosphate is already sorbed, arsenate is not likely to replace it. Conversely, if arsenate is sorbed, phosphate is likely to replace it. In either case, arsenate is the more mobile species.

Similarly, silicic acid, H_4SiO_4 , has been shown to effectively compete for adsorption sites with both arsenate and arsenite on goethite, and can result in as much as 60% reduction in arsenic uptake for both arsenate and arsenite (Waltham and Eick 2002).

Sulfate should not affect adsorption of arsenic species due to its apparent electrostatic attraction for surfaces as an outer-sphere complex (Stollenwerk 2003). In fact, sulfates have been shown to be inconsequential to the adsorption of As(V) at all pH ranges, though they decrease As(III) adsorption at $\text{pH} < 7$ (Stollenwerk 2003).

There is limited research on competitive adsorption of carbonates with arsenate. Complexation has been assumed to be outer-sphere by most researchers. However, its ubiquitous nature in many groundwaters may influence competitive adsorption in ways not yet understood (Stollenwerk 2003). Bicarbonate, too, as a direct product of DOC oxidation, has been implicated as competing for As sites.

The presence of DOC has been shown to decrease the adsorption of both arsenate and arsenite on ferrihydrite, especially that of As(III) (Grafe, Eick et al. 2002). In particular, citric acid decreased adsorption of As(V), and citric and fulvic acids decreased the adsorption of As(III). Direct complexation of As and Fe(III) to DOC (and particulate organic carbon from which it is derived) has been observed to affect the mobility and

subsequent coprecipitation of metals by complexation (Langmuir 1997). Both humic and fulvic acids (two forms of DOC) are soluble at alkaline pH (Langmuir 1997).

Phosphates were shown to out-compete arsenate as adsorbates on goethite in proportion to their concentration (Waychunas, Fuller et al. 1993; Gao and Mucci 2001), thus mobilizing arsenate. Further research suggested that arsenic could be extracted by 0.1 M PO_4 at "ambient pH" to determine the amount of As(V) available to be released to solution (Gao, Fujii et al. 2004).

Finally, the introduction of DOC into groundwater systems as the catalyst for reductive dissolution of HFO has been suggested as a key factor in arsenic mobilization (Harvey and Beckie 2005).

3. Exchange

In exchange reactions divalent calcium may be taken up by negatively charged surfaces (such as clay), releasing sodium. These reactions appear to be common in Lahontan Valley groundwater and may contribute to high Na concentrations (Lico, Welch et al. 1987; Lico and Seiler 1994; Seiler, Stollenwerk et al. 2005).

4. Reaction rates

Arsenic reaction rates in the literature focus on redox transformations, though research results are inconsistent. Masscheleyn (1991) characterized redox transformations as slow, such that both oxidation states of arsenic are found in soils regardless of redox conditions. However, other research suggests that the redox state of arsenic in groundwater is useful as an indicator of redox condition in groundwater because arsenic occurs in small concentrations, and the transfer of only a small number of electrons allow it to attain equilibrium rapidly (Cherry, Shaikh et al. 1979). Other research suggests that

equilibrium is seldom attained with arsenite/arsenate redox couples (Welch, Westjohn et al. 2000) .

Gulens et al. (1979) observed that adsorption of As on amorphous iron hydroxide occurred within 24 hours. Pierce and Moore (1982) found that 90% of the As(III) adsorbed onto amorphous iron hydroxide within 2 hours, and As(V) completely adsorbed within 4 hours.

Hypotheses

The hypotheses that were tested with modeling arose from the geochemical trends identified statistically in Chapter 2. They were:

- 1) Desorption of arsenic species from iron oxyhydroxides is a principle mechanism for arsenic enrichment, and
- 2) Reductive dissolution of iron oxyhydroxides is a principle mechanism for arsenic enrichment.

Methods

Geochemical models were used to simulate the groundwater conditions observed from field sampling in the intermediate-depth aquifer of the Lahontan Valley, and in particular, to compare observed and modeled arsenic concentrations. NETPATH 2.0 (Plummer, Prestemon et al. 1994) is a geochemical modeling program that calculates water-mineral interactions along a flow-path with an emphasis on the cation/anion balance of the major ions. NETPATH provides dissolution/precipitation models based on the chosen phases that can account for the final solution chemistry. Visual MINTEQ 2.3 (Gustafsson 2006) is a geochemical equilibrium speciation model that calculates chemical equilibria for solid, aqueous, gas, and adsorbed phases. Output is in the form of

species concentration/activities, species distribution, mass distribution, and saturation index.

Eh values for modeling were critical to both the NETPATH and MINTEQ analyses. Field-measured Eh values were erratic (Table 3, Chapter 2) and four additional methods were used to estimate Eh values. The five methods (including field measurements) were:

1) Field-measured Eh values were obtained from the platinum electrode of the YSI 556 MPS and averaged over the sampling period for each well;

2) Activities for the iron couple, Fe(II) and Fe(III), were obtained from colorimetric analysis and Eh was calculated using these values in the Nernst Equation;

3) Fe(II) activity obtained from colorimetric analysis was used with modeled Fe(III) activities from ferrihydrite equilibrium, $\text{Fe}(\text{OH})_3 (\text{s}) \leftrightarrow \text{Fe}(\text{III}) (\text{aq})$, using ferrihydrite as an "infinite solid" in MINTEQ over the pH range for each well. Fe(III) was then chosen at the average pH for that well (Appendix F). Eh was then calculated from the Nernst equation;

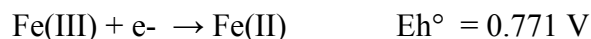
4) Fe(II) activity obtained from colorimetric analysis was used with the minimum Fe(III) activity of 10^{-16} for ferrihydrite accepted by MINTEQ. Eh was then calculated from the Nernst equation; and

5) Fe(II) activity obtained from colorimetric analysis. MINTEQ computed Eh values based on three redox couples for which data was available from the study and whose reactions are included in the MINTEQ thermodynamic database: $\text{Fe}^{3+}/\text{Fe}^{2+}$, $\text{SO}_4^{2-}/\text{HS}^-$, and $\text{AsO}_4^{3-}/\text{H}_3\text{AsO}_3$. When each member of the couple was assigned an activity, the ratio of the two members of the couple were compared to their standard reduction

potential (E_h°) for their respective redox reaction to conform to the Nernst Equation.

MINTEQA then computed a composite E_h value.

Colorimetric analysis using the 2,2'-bipyridine-Fe(II) complex method for Fe(II) and reactive Fe(II+III) was utilized to obtain values for the iron couple (Baedecker and Cozzarelli 1992) for four consecutive filtered (<0.45 μm) samplings. Iron standards of 0.1, 0.2, 0.6, 1.0, 2.0, and 4.0 mg/L were prepared with 10 mL 1:2 (by volume) 0.2% 2,2'-bipyridine solution and 10% $\text{NH}_2\text{OH}\cdot\text{HCl}$ added to each blank and standard. Each 10 mL preserved Fe(II) field sample, standard, and blank was treated with 1 mL 4.3 M sodium acetate buffer and all standards, blanks and samples were measured for absorbance. For total Fe analysis, 10% $\text{NH}_2\text{OH}\cdot\text{HCl}$ was added to samples (in addition to blanks and standards) to reduce Fe(III) to Fe(II). One mL 4.3 M sodium acetate buffer was added. The $[\text{Fe}(\text{bipy})_3]^{2+}$ complex formed is a red solution whose concentration is determined by light absorbance in the spectrometer. All tubes were measured for absorbance at 520 nm. A plot of average absorbance versus concentration for standards was produced, and Fe(II) and Fe(II+III) values determined. Fe(III) activities were determined by subtraction from Fe(II+III). Fe(II) and Fe(III) activities were then used to calculate E_h with the standard reduction potential for Fe(III) (Schuylenborgh, 1966) and the Nernst Equation (Brown, LeMay et al. 2000):



$$E_h = E_h^\circ - (2.303RT/nF) \cdot \log Q$$

in which V represents Volts (electrical potential), R is the universal gas constant (8.3144 Joules/(K mol), T is temperature (K), n is the number of electrons transferred in the half-

reaction, F is the Faraday constant 96450 Coulombs/mol e^-) and Q is the reaction quotient, specific to the reaction involved.

1. NETPATH 2.0 model

Major ion contributions to intermediate-depth groundwater were modeled by NETPATH version 2.0. Phases included in the model were calcite, gypsum, albite, iron sulfides, exchange complexes, dissolved organic carbon (DOC), goethite and montmorillonite. Phases were chosen based upon the available sample data (Chapter 2), and because each has been discussed in the literature as a possible mineral source or sink or process observed in the Lahontan Valley groundwater system (Lico and Seiler 1994). Chemical concentrations (referred to as "constraints" in NETPATH) included C, Ca, S, Na, Fe, Al, Mg in mg/l and Eh (V). Constraints were chosen to optimize the quality of the models produced by NETPATH. NETPATH uses an iterative approach to produce values for phase concentration changes (the output) that are consistent with the input at each well. Aluminum was not sampled. However, inclusion in model analyses allowed for greater flexibility by allowing inclusion of albite. Values for most parameters were previously shown to be statistically stable (Chapter 2) due to their minimal fluctuation during the sampling period; therefore, physical and chemical parameters entered into NETPATH reflected average values obtained during the 18-month sampling period. A flow-path model was produced for the Well A-D segment and Well A-E segment. The two endpoints were chosen because they were less than $\frac{1}{2}$ mile apart, but differed markedly in H_2S concentration. Models were run using Fe(T) values from ICP-MS analysis, and field-measured Eh values. Parameters and average values that were used for NETPATH modeling are shown in Table 6.

2. Visual MINTEQ 2.3 Model

Average values for well chemistry for the sampling period were used to model arsenic adsorption and speciation using Visual MINTEQ to compare results with observed concentrations from each well, with respect to arsenic concentrations and species distribution, saturation indices and mass distribution of other chemical components. MINTEQ input included average values for pH, alkalinity, the partial pressure of CO₂ (pCO₂ from NETPATH), temperature, and ionic strength. For surface complexation modeling in MINTEQ, the data base for hydrous ferric oxide double layer model (HFO with double layer model, DLM) was chosen (Dzombak and Morel 1990). Three redox couples were chosen to represent oxidation-reduction reactions in the system: Fe³⁺/Fe²⁺, SO₄²⁻/HS⁻, and AsO₄³⁻/H₃AsO₃. No attempt was made to limit the adsorption reactions to a single species since a more realistic estimation of As surface complexation was possible using complete solution chemistry. Default values for site density and specific surface area were 2.312 sites/nm² and 600 m²/g, respectively. The extracted iron substrate of 7.15 g/L of sediment was obtained from the extracted iron data of Welch and Lico (1998) and Assam (2007) for wells in the Lahontan Valley. Ferrihydrite was chosen as an "infinite solid" in all models except for the calculation of ferrihydrite saturation indices. Average parameter data used in MINTEQ models are shown in Table 7.

Results

A summary of Eh values for the assumptions described above are shown in Table 8. Colorimetric iron calculations are shown in Appendix D, and modeled Fe(III) activities for ferrihydrite equilibrium (assumption 3) are shown in Appendix F.

Field values for Eh (assumption 1) had large standards of deviation and coefficients of variation over the sampling period. However, all the values were below about 200 mV which is considered "moderately reducing" by Seiler (2005).

Assumption (2) returned values in the 700 mV range which approaches H₂O-O₂ equilibrium for the pH range of the study and is considered unreasonable. Fe(III) values for this assumption may have been too high due to the inclusion of unfiltered colloidal and/or complexed Fe(III) in addition to the labile Fe(III) fraction necessary for Eh calculation in the Nernst Equation. Fe(III) complexation with DOC and particulate organic carbon (POC) has been shown to occur (Langmuir 1997). The additional Fe(III) would have produced higher than expected values for the colorimetric Fe(II)+Fe(III) value, and, consequently, higher Eh values. Also oxidation of Fe(II) prior to analysis may have occurred.

Assumption (3) had Eh values average about 500 mV, which are not considered sufficiently reducing to have produced H₂S, observed in most wells. Also, an Eh in the 0.150-0.310 V range is presumed necessary for sulfate reduction (Denker, 2004; Langmuir, 1997).

Assumption (4) Eh values (average 210 mV) are consistent with Langmuir (1997), Denker (2004), and Seiler (2005). However, the minimum Fe(III) value accepted by MINTEQ was not consistent with the assumption of ferrihydrite equilibrium (Appendix F).

The MINTEQ option to calculate Eh values based well chemistry (assumption 5) provided Eh values of -284 mV and -339 mV for Wells B and D, respectively. These

values correspond favorably to the Eh-pH diagram produced for equilibria under study conditions and is discussed later (Figure 25).

For the reasons outlined above, both NETPATH and MINTEQ models were run using field-measured Eh values and those computed by MINTEQ for comparison.

In addition, the colorimetric Fe(T) analysis provided a comparison to that of ICP-MS Fe(T) analysis and the latter was found to be several times larger for all wells except Well B (Figure 20) in addition to having a large standard deviation for all wells (Table 3). The unfiltered ICP-MS Fe(T) samples likely included colloidal Fe that could have interfered with model reactions, or Fe(III) complexed with DOC. For these reasons the colorimetric Fe(T) value was used for all models (Tables 6 and 7).

1. NETPATH analysis

Table 9 displays the favored models produced in NETPATH for flow-path segments A-D and A-E. All other models are presented in Appendix E. The (+) and (-) sign listed beside a phase indicates that the phase was forced by the program to be added to the system (+) by dissolution, or removed from the system (-) by precipitation in the model. No sign allowed either dissolution or precipitation to occur. Positive and negative values for a segment (ie., flow-path A-D) indicate millimoles of that phase added to (+) or removed from (-) the system per kilogram of solution along that segment of the flow-path.

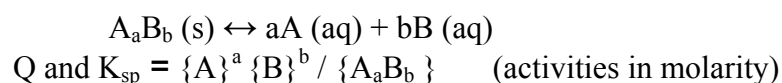
Only models showing the dissolution (reduction) of CH_2O were retained since DOC was presumed to be the electron donor in the system. Pyrite was oversaturated at all wells in NETPATH (Table 10), so models in which pyrite precipitation occurred were retained. Appendix E gives the results for all models. The use of field-measured Eh and

MINTEQ-computed Eh produced the same flow-path results in NETPATH (Appendix E), although their saturation indices were different for some of the minerals. NETPATH provided fewer minerals in its SI calculations.

2. Visual MINTEQ Analysis

Output for MINTEQ models was in the form of concentration and activity of aqueous inorganic species including Fe surface-complexes, percent distribution among these same species, mass distribution between dissolved and sorbed phases, and saturation index.

Saturation index (SI) is a measure of the tendency for a forward or reverse hydrolysis reaction to occur (that is, dissolve or precipitate). For the reaction



which relates the reaction quotient (Q) of the solution, to the solubility product constant (K_{sp}):

$$SI = \log (Q/K_{sp})$$

From these data, qualitative assessments for arsenic mineral dissolution, reductive dissolution of HFO, and arsenic desorption from HFO were made.

Estimated saturation indices for relevant minerals using colorimetric Fe(T) and both field-measured Eh and MINTEQ- computed Eh were modeled in MINTEQ for Wells A and D and are summarized in Table 10. The table was limited to these two wells because they are representative of the general solution chemistry at the flow-path endpoints, and a the limited scope provided brevity and clarity. Table 10 also includes estimates of saturation indices produced by NETPATH.

Fe(III) and sulfide minerals were most sensitive to field and MINTEQ-computed Eh values in the MINTEQ models. Equilibrium (SI = 0) was not established for most minerals, although calcite, siderite, and strengite were close. All arsenic-containing minerals were shown to be undersaturated regardless of the Eh, although field-measured Eh values produced the most negative values. Most Fe(III) minerals were oversaturated at all wells at field-measured Eh, but became undersaturated under computed Eh conditions. This includes ferrihydrite. NETPATH values for the available minerals compared much better for the computed Eh values than for the field values.

Figures 21 and 22 display total arsenic adsorption, and arsenate and arsenite adsorption on ferrihydrite as modeled by MINTEQ for an Eh range of -400 to 400 mV at the average pH of each well. The thermodynamic dataset for HFO with DLM (Dzombak and Morel 1990) was used with average well pH, well chemistry, and ionic strength (Table 7). Ionic strength was calculated separately and calculations are shown in Appendix B. Calculation of the extracted iron substrate of value of 7.15 g/L of sediment (Welch and Lico 1998; Assam 2007) is shown in Appendix G. All models used colorimetric Fe(T) values as input. Surface complexes included in the MINTEQ model were those provided in the database: $\equiv\text{FeAsO}_4^{2-}$, $\equiv\text{FeH}_2\text{AsO}_3$, $\equiv\text{FeH}_2\text{AsO}_4$, $\equiv\text{FeHAsO}_3^-$, $\equiv\text{FeAsO}_4^-$, $\equiv\text{FeOHAsO}_4^{3-}$.

As_T adsorption was greatest for Wells C, E, and D (Figure 21). Arsenate was sorbed to a greater degree than arsenite for wells above Eh values of about -150 mV, -150 mV, -250 mV -250 mV and -150 mV respectively (Figure 22).

Arsenic adsorption on ferrihydrite was also modeled for the pH range of the study (8.0 to 9.4) using average field-measured Eh values (Figure 23). Both arsenate and

arsenite were adsorbed to ferrihydrite to a lesser degree along the flow-path according to the model.

According to MINTEQ modeling, AsO_4^{3-} is the dominant sorbed arsenic species on ferrihydrite at all pH values. Increasing pH resulted in a slight increase in adsorption for AsO_4^{3-} for Wells A and B and no increase for Wells C-E. A decrease in adsorption by several orders of magnitude occurred for H_3AsO_3 for all wells. Overall, a larger amount of AsO_4^{3-} desorbed from ferrihydrite along the flow-path than H_3AsO_3 .

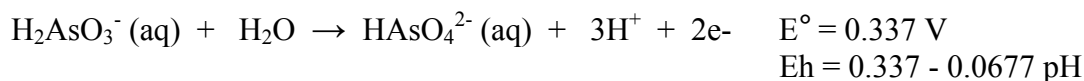
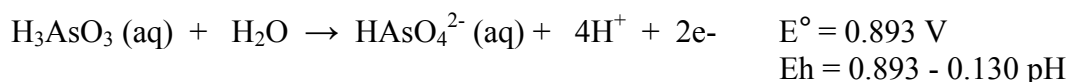
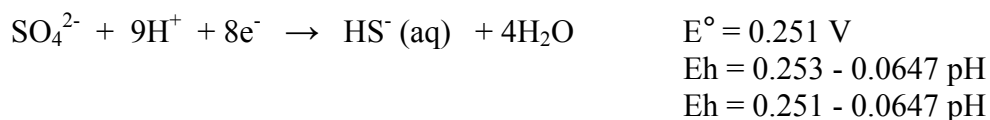
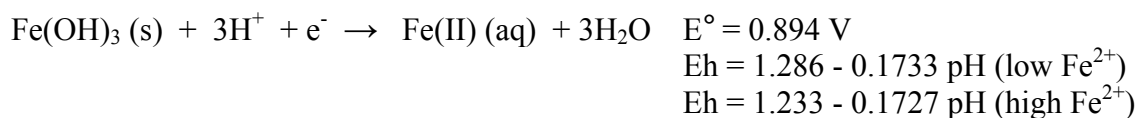
Figure 24 indicates PO_4 and HCO_3 adsorption on ferrihydrite for the same range of pH and field-measured Eh as that shown in Figure 22. PO_4 adsorbed to a lesser degree as pH increased for any given well. However, greater adsorption occurred overall for Wells C-E, and therefore, along the flow-path. Bicarbonate showed lesser adsorption on ferrihydrite with increasing pH, and from well-to-well.

Discussion

Eh values were of considerable interest because model results were heavily influenced by the values selected to represent ambient conditions. Eh values measured in the field and MINTEQ-computed Eh appeared to reflect likely groundwater conditions and agreed with previously measured values (<200 mV Seiler (2005)) and the MINTEQ value was based on the complete results of water sample analyses.

To further test the validity of Eh values, an Eh/pH diagram (Figure 25) was produced for the equilibria of ferrihydrite ($\text{Fe}(\text{OH})_3/\text{Fe}^{2+}$), sulfate ($\text{SO}_4^{2-}/\text{HS}^-$), and arsenic (As(III)/As(V)) for the range of pH under study conditions. Equations for both high and low (Fe^{2+}) values from colorimetric analysis were calculated for ferrihydrite, as well as

extreme values for SO_4/HS^- . The slope-intercept equations are as follows, and complete calculations are shown in Appendix C.



The diagram is consistent with redox ladders of half-reaction couples, in that ferrihydrite reduces at a higher Eh than sulfate. Since H_2S was detected at most wells, sulfate reduction was likely to be occurring, and at these pH and Eh values it is likely that ferrihydrite reduction was also occurring. The diagram suggests that Eh values for the sampled wells in the intermediate alluvial aquifer are in the -250 to -350 mV range. The MINTEQ-computed values further suggest this is so for Wells A, B and D. However, it is unclear why field-measured Eh values differed so markedly from MINTEQ-computed Eh values. Since the computed value is based upon concentrations provided to the model for three redox couples from the extensive database the difference could be the result of redox couples that were unaccounted for in the well chemistry, as well as abundant DOC, a potentially inexhaustible electron-donor. Sampling errors may also have occurred. It is also unclear why $\text{SO}_4^{2-}/\text{HS}^-$ equilibrium differed from the Eh value of 0.150-0.310 V

described by Denker (1998) and Langmuir (1997) above. Field values for hydrogen sulfide may have been erroneous.

NETPATH models were identical for both field-measured Eh and MINTEQ-computed Eh (Table 9). However, saturation indices changed considerably for the Fe(III) minerals and pyrite at computed Eh values (Table 10). No form of the model completely described the conditions. However, both flow-path models indicated dissolution of albite and calcite (although calcite was near equilibrium according to its SI value) and approximately account for the concentration of Na and Ca found in solution. Further exchange of dissolved Ca for Na at clay surfaces may account for the significant increase in Na concentration between the wells while showing a negligible change in Ca concentration (Figure 8). CH_2O reduction (indicated as dissolution in NETPATH) is a possible source of HCO_3^- observed in the samples. Goethite (FeOOH) is the ferric oxyhydroxide provided in NETPATH and was not indicated as dissolved or precipitated in the models. However, it was oversaturated at both Eh values. Ferrihydrite was undersaturated in both models, suggesting that it dissolves under both Eh conditions and could be a source for arsenic enrichment. Amorphous Fe(II) sulfides (FeS in the model) were shown to dissolve. The apparent dissolution of pyrite in both segments may provide additional sulfide for H_2S production and Fe for goethite and amorphous Fe-S precipitation. Formation of montmorillonite may account for loss of silica. The model did not account for the decrease in Cl.

Both NETPATH and MINTEQ produced consistent saturation indices for their common minerals, especially using computed Eh results. The extreme undersaturation of all arsenic minerals suggests that As minerals are not present. Sulfide minerals were

undersaturated at both field-measured Eh and computed Eh values when supplied to MINTEQA2, suggesting dissolution in both cases. NETPATH shows FeS to be increasingly oversaturated along the flow-path, which may be interpreted as dissolution from Well A to D. The large H₂S concentration at Well D suggests little precipitation of sulfides. Fe(III) was over- or undersaturated depending upon Eh, so it is unclear whether dissolution occurred.

The decreased adsorption of As_T (and especially that of AsO₄³⁻) as indicated in Figures 21 and 22 below Eh ~ -100 mV (Wells A and B) and below Eh ~ -200 mV (Wells C-E) may be due to: 1) the reduction and subsequent dissolution of ferrihydrite; or 2) the direct reduction of AsO₄³⁻ (Figure 25), and therefore, less AsO₄³⁻ available for adsorption; The problem with the latter explanation is that although H₃AsO₃ is observed to increase from well to well, [As(III)]/[As_T] decreases, indicating that AsO₄³⁻ must increase to a greater extent. Hence, dissolution of ferrihydrite is the preferred explanation. A third explanation may be that an increase in pH with no reduction in Eh could oxidize H₃AsO₃ directly as suggested by Manning and Goldberg (1997). Nevertheless, increased reducing conditions along the flow-path are suggested by the high H₂S concentration at Well D and the computed Eh.

Although H₃AsO₃ at an individual well desorbed with increased pH at field-measured Eh values as expected (Stollenwerk 2003; Seiler, Stollenwerk et al. 2005), it is uncertain why AsO₄³⁻ adsorption was little affected by the same increase (Figure 23). Increasingly negative surface charges on ferrihydrite at increasingly alkaline pH was expected to promote desorption of both arsenic species as they were deprotonated at higher pH. Nevertheless, decreased adsorption from well-to-well at average pH is

indicated for both species. Adsorbed AsO_4^{3-} amounts are considerably greater than those of H_3AsO_3 at all pH so desorption of AsO_4^{3-} would have produced greater aqueous concentration from well-to-well. This may be observed in the average $[\text{As(III)}]/[\text{As}_T]$, which decreased along the flow-path (Table 3) in part because reducing conditions may have transformed As(V) to As(III). However, this hypothesized reaction is not observed in the samples. In fact, the desorption of AsO_4^{3-} appears to dominate. It was assumed that since adsorption of As_T was shown to decrease with decreasing Eh at average pH for each well (Figure 21), the modeling of adsorption vs pH for computed Eh values was unnecessary. Greater desorption of both As species is suspected under those conditions.

Additionally, decreased adsorption of both arsenic species may be enhanced by competitive ligand replacement of phosphate on ferrihydrite ($\equiv\text{FeH}_2\text{PO}_4$ and $\equiv\text{FeHPO}_4^-$, and $\equiv\text{FePO}_4^{2-}$). Although modeling indicated that total phosphate adsorption decreased for any given well with increased pH, there is an increase in adsorption from well-to-well at average pH (Figure 24). In addition, adsorption of HCO_3^- on ferrihydrite ($\equiv\text{FeCO}_3\text{H}$ and $\equiv\text{FeCO}_3^-$) decreased considerably from well-to-well, perhaps responding to the same negative surface charges that may have desorbed arsenic. This was expected based on the correlations noted in Chapter 2.

Conclusions

The processes suggested by modeling are consistent with those described in the literature: chemical reactions of feldspars, calcite, CO_2 , montmorillonite, gypsum, silica, and pyrite are occurring in sodium-calcium-bicarbonate-sulfate groundwater (Lico and Seiler 1994). Saturation indices indicate dissolution of calcite and albite in conjunction with exchange reactions may further increase Na concentrations. The reduction of DOC

likely accounts for the large and increasing HCO_3^- concentrations along the flow-path. As an electron-donor DOC facilitates reduction of both Fe(III) compounds, which forms more soluble Fe(II) compounds, and the reduction of SO_4^{2-} , which forms sulfides. NETPATH showed that FeS compounds dissolved along the flow-path and H_2S was produced. MINTEQA2 analyses indicated that remaining sulfides were undersaturated, which implies that sulfides would be dissolved. Furthermore, the abundance of H_2S in Well D and virtual lack of it in Well E may indicate the abundance and lack (respectively) of sulfate-reducing microbes, though the presence of sulfate- or iron-reducing bacteria was beyond the scope of this study. High As concentrations at both wells (and increasing from Well D to E) suggest little or no As precipitation with sulfides at either well. The models are in agreement because all sulfides are undersaturated in the models. Production of As seems independent of sulfate reduction in these two wells

Saturation indices between the two models were generally in agreement especially for computed Eh values. The reductive dissolution of ferrihydrite may have occurred although its saturation state depended upon Eh, being undersaturated only at the lower computed Eh values. These low Eh values were supported by the Eh-pH diagram produced from the well chemistry of the study (Figure 25). NETPATH would interpret the increasing SI values under both Eh conditions to be dissolution of the mineral.

The increased average pH of wells along the flow-path showed decreasing As adsorption onto ferrihydrite, thus, increasing As_T concentrations in the aquifer. Competitive ligand replacement with phosphate may have enhanced As desorption. Desorption of AsO_4^{3-} in particular appears to be a dominant source of arsenic enrichment

as its increased concentration and decreased $[\text{As(III)}]/[\text{As}_T]$ suggest. Since pH generally increased with distance, AsO_4^{3-} enrichment likely occurred along the flow-path.

Increasing concentrations of DOC make the molecule an inexhaustible electron-donor reservoir in the intermediate aquifer (O_2 was an unlikely electron-acceptor due to low levels of DO observed), oxidizing to CO_2 in the presence of electron-acceptors SO_4 and Fe(OH)_3 . DOC reduction ultimately forms HCO_3^- and contributes to CaCO_3 dissolution. No carbon isotope data were taken to distinguish between DOC and resultant inorganic carbon to prove that they are similar in age. However, strong correlation of arsenic with both HCO_3^- and DOC (Chapter 2; $p = 0.0097$, and 0.039 , respectively) suggests that DOC reduction could release complexed Fe and As. Although the presence of DOC has been shown to inhibit HFO-As complexation, DOC modeling with Fe and As was not performed. A summary of the reactions that could be involved is presented as a flow-diagram in Figure 26.

Changing redox condition of the groundwater has not been demonstrated as a causal effect for the increase in As_T concentration or the decrease in $[\text{As(III)}]/[\text{As}_T]$. None of the Eh values from field measurements, by colorimetric iron analyses, or by MINTEQA2 satisfactorily demonstrated a strong connection. However, reductive dissolution of ferrihydrite was suggested by the model at lower Eh values, the presence of H_2S in well water, and by the Eh-pH diagram produced for the well chemistry of the study.

Although observed geochemical trends in the intermediate aquifer of the Lahontan Valley produced a conceptual basis for arsenic enrichment and a decrease in $[\text{As(III)}]/[\text{As}_T]$, only pH-mediated desorption of AsO_4^{3-} was clear. However, as described

above, reliable Eh values were not established. Nevertheless, some useful relationships have been established that will benefit future As research in the intermediate aquifer of the Lahontan Valley.

It was not established that the five wells chosen in the study represent a true flow-path. Average linear velocity of groundwater flow in the intermediate aquifer was too slow to assume that a given parcel of groundwater was subsequently sampled down-gradient during the sampling period. However, equilibrium was not established in the wells according to modeling and sampling data. Elevated and increasing arsenic concentrations observed in the groundwater, then, are likely the result of disequilibrium reactions in the vicinity of each well and/or the accumulation of this labile fraction down-gradient over time and space.

parameter	Well A	Well B	Well C	Well D	Well E
pH	8.28	8.37	9.15	9.11	9.05
temp (°C)	15.73	17.12	15.81	16.07	16.93
avg field Eh (mV)	-4.75	4.91	37.0	-13.7	53.0
modeled Eh (mV)	-	-274	-	-339	-
(mmol/kg)					
Ca	0.123	0.146	0.119	0.119	0.125
Mg	0.189	0.179	0.185	0.195	0.206
Na	4.165	3.196	5.565	7.543	8.604
K	0.176	0.202	0.124	0.124	0.128
Cl	0.511	0.214	0.176	0.186	0.282
SO₄	0.711	0.451	0.395	0.352	0.401
HCO₃	2.440	2.461	3.240	4.923	5.779
Fe_T (ICP-MS)	0.003	0.0010	0.0040	0.0078	0.0075
Fe_T (colorimetric)	0.0013	0.00049	0.00114	0.00246	0.00135
Mn	0.001	0.0004	0.0009	0.0004	0.0007
Si	1.778	1.696	1.214	1.411	1.319
NO₄	0.007	0.007	0.008	0.008	0.008
P (total)	0.003	0.003	0.013	0.020	0.019
O₂ (aq) (%)	0.057	0.053	0.062	0.050	0.050
H₂S	0.004	0.003	0.005	0.040	0.0003
DOC (mg/L)	1.310	1.120	2.065	3.470	2.950

Table 6 - Average parameter values for NETPATH input

parameter	Well A	Well B	Well C	Well D	Well E
pH	8.28	8.37	9.15	9.11	9.05
temp (°C)	15.7	17.1	15.8	16.1	16.9
field Eh (mV)	-4.75	4.91	37.0	-13.7	53.0
modeled Eh (mV)	-	-274	-	-339	-
pCO₂	0.00067	0.00056	0.00011	0.00018	0.00024
ionic strength	0.0155	0.0147	0.0206	0.0181	0.0123
all in mg/L					
Na	95.8	73.5	128	174	198
K	6.90	7.90	4.85	4.85	5.00
Ca	4.90	5.85	4.75	4.75	5.00
Mg	4.60	4.35	4.50	4.75	5.00
SO₄	68.3	43.3	38.0	33.8	38.5
Cl	18.1	7.60	6.25	6.60	10.0
HCO₃	149	150	198	300	353
CO₃	4.25	4.65	37.55	48.95	50.11
NO₃	0.46	0.46	0.48	0.48	0.50
Fe_T(ICP-MS)	0.27	0.06	0.22	0.44	0.42
Fe_T(colorimetric)	0.0715	0.0275	0.0634	0.1376	0.0753
Mn	0.07	0.02	0.05	0.02	0.04
Si	50.0	47.7	34.1	39.7	37.1
P_T	0.24	0.27	1.21	1.93	1.76
DOC	1.31	1.12	2.07	3.47	2.95
HS	0.149	0.117	0.157	1.351	0.006
HAsO₃³⁻	0.053	0.049	0.044	0.062	0.112
AsO₄³⁻	0.0073	0.0187	0.198	0.247	0.301

Table 7 - Average parameter values for MINTEQ input.

		Fe(II) {M}	Fe(III) {M}	avg Eh (V)
1) field values for Eh	Well A	-	-	-0.0050 ± 0.040
	Well B	-	-	0.0050 ± 0.054
	Well C	-	-	0.037 ± 0.078
	Well D	-	-	-0.014 ± 0.053
	Well E	-	-	0.053 ± 0.043
colorimetric {Fe(II)} used for the remaining Eh determinations				calculated Eh (V)
2) colorimetric Fe(II) and Fe(III)	Well A	6.51E-07	9.16E-08	0.722
	Well B	1.76E-07	8.28E-08	0.752
	Well C	4.65E-07	1.21E-07	0.737
	Well D	1.32E-06	1.07E-07	0.708
	Well E	7.45E-07	8.59E-08	0.717
3) MINTEQ modeled Fe(III)	Well A	6.51E-07	1.31E-11	0.502
	Well B	1.76E-07	1.13E-11	0.529
	Well C	4.65E-07	1.05E-11	0.505
	Well D	1.32E-06	9.78E-12	0.477
	Well E	7.45E-07	9.16E-12	0.488
4) MINTEQ minimum Fe(III)	Well A	6.51E-07	1.00E-16	0.208
	Well B	1.76E-07	1.00E-16	0.238
	Well C	4.65E-07	1.00E-16	0.217
	Well D	1.32E-06	1.00E-16	0.190
	Well E	7.45E-07	1.00E-16	0.202
5) MINTEQ computed Eh	Well A	6.51E-07	-	-0.284
	Well B	1.76E-07	-	-0.275
	Well C	-	-	-
	Well D	1.32E-06	-	-0.338
	Well E	-	-	-

Table 8 - Iron activity associated with the five methods for measuring or estimating Eh

constraints: C, Ca, S, Na, Fe, redox, Al, K					
phase	components	field Eh	MINTEQ	field Eh	MINTEQ
		A-D	computed Eh A-D	A-E	computed Eh A-E
calcite	Ca,CO ₃	1.33	1.33	1.89	1.89
gypsum	Ca,SO ₄				
albite (+)	Na,K,Al,SiO ₃	0.80	0.80	0.74	0.74
exchange	Ca/Na	1.29	1.29	1.85	1.85
CH ₂ O (+)	DOC	1.02	1.02	1.24	1.24
goethite	FeOOH				
Fe-S	Fe,S	0.08	0.08	0.08	0.08
montmorillonite	Ca,K,Mg,Fe,Al,Si	-0.40	-0.40	-0.37	-0.37
H ₂ S	H, S	-1.72	-1.72	-2.25	-2.25
pyrite	Fe,S	-0.04	-0.04	-0.04	-0.04
all values in mmol/kg					
field Eh _A , Eh _D , Eh _E = -4.75 mV, -31.7 mV, and 53 mV, respectively					
computed Eh _A , Eh _D , Eh _E = -275 mV, -339 mV, and -340 mV, respectively					

Table 9 - Selected NETPATH flow-path results using data from Table 6, colorimetric Fe(T), and field and MINTEQ-computed Eh values segment A-D and segment A-E.

mineral	constituents			MINTEQ model				NETPATH model			
				avg field Eh (mV)		Eh computed (mV)		avg field Eh (mV)		Eh computed (mV)	
				4.9 Well A	-13.7 Well D	-284 Well A	-339 Well D	4.9 Well A	-13.7 Well D	-284 Well A	-339 Well D
Calcite	Ca+2	CO3-2		-0.4	0.9	-0.4	0.9	-0.5	0.52	-0.2	0.5
Arsenolite As2O3 (cubic)	H3AsO3	H2O		-21.3	-29.4	-11.2	-14.7	-	-	-	-
As2O5	AsO4-3	H+1	H2O	-35.6	-42.2	-45.5	-50.2	-	-	-	-
Ca3(AsO4)2·4H2O	Ca+2	AsO4-3	H2O	-13.4	-16.6	-23.3	-24.6	-	-	-	-
FeAsO4·2H2O	Fe+3	AsO4-3	H2O	-9.5	-10.4	-19.7	-21.0	-	-	-	-
Mn3(AsO4)2·8H2O	Mn+2	AsO4-3	H2O	-11.9	-17.6	-22.1	-25.8	-	-	-	-
Claudetite	H3AsO3	H2O		-21.3	-29.4	-11.2	-14.8	-	-	-	-
As2S3(am)	H3AsO3	HS-1	H+1	-138.7	-161.3	-8.4	-10.8	-	-	-	-
Realgar As4S4	H3AsO3	HS-1	H+1	-53.3	-62.5	-3.2	-4.3	-	-	-	-
Orpiment As2S3	H3AsO3	HS-1	H+1	-137.2	-159.8	-6.9	-9.3	-	-	-	-
CaS	Ca+2	HS-1	H+1	-52.5	-56.2	-12.4	-11.0	-	-	-	-
MnS (grn)	Mn+2	HS-1	H+1	-44.3	-48.8	-4.3	-3.6	-	-	-	-
MnS (pnk)	Mn+2	HS-1	H+1	-47.1	-51.6	-7.1	-6.4	-	-	-	-
FeS (ppt)	Fe+2	HS-1	H+1	-40.9	-43.8	-1.1	0.7	0.6	1.7	0.2	2.1
MgS	Mn+2	HS-1	H+1	-58.9	-62.4	-18.8	-17.1	-	-	-	-
Gypsum	Ca+2	SO4-2	H2O	-3.0	-3.4	-3.0	-3.5	-2.8	-3.2	-2.9	-3.2
Thenardite	Na+1	SO4-2		-9.0	-8.4	-9.0	-8.4	-	-	-	-
Melanterite	Fe+2	SO4-2	H2O	-7.8	-7.4	-8.1	-8.2	-7.2	-8.17	-7.8	-7.8
Pyrite FeS2	H+1	Fe+2	HS-1	-62.2	-69.0	7.7	9.4	18.2	20.8	8.0	9.8
Fe(OH)2·7Cl.3	H+1	Fe+3	Cl-1	4.8	7.0	-0.4	0.5	-	-	-	-
Ferrihydrite	Fe+3	H2O	H+1	1.7	4.1	-3.5	-2.4	-	-	-	-
Ferrihydrite (aged)	Fe+3	H+1	H2O	2.2	4.6	-3.0	-1.9	0.4	2.1	-4.6	-3.2
Goethite	Fe+3	H2O	H+1	4.6	7.0	-0.6	0.5	6.6	8.3	1.6	3.0
Hematite	Fe+3	H2O	H+1	11.6	16.3	1.1	3.3	13.8	17.3	4.0	6.6
K-Jarosite	K+1	Fe+3	SO4-2	-9.3	-4.7	-25.0	-24.3	-10.9	-9.1	-26.3	-25.0
Lepidocrocite	H+1	Fe+3	H2O	4.0	6.4	-1.2	-0.1	-	-	-	-
Maghemite	H+1	Fe+3	H2O	4.4	9.2	-6.1	-3.8	-	-	-	-
Magnesioferrite	H+1	Mg+2	Fe+3	5.4	11.4	-5.1	-1.6	-	-	-	-
Magnetite	H+1	Fe+3	Fe+2	16.6	23.3	5.9	9.4	-	-	-	-
Na-Jarosite	Na+1	Fe+3	SO4-2	-13.9	-8.8	-29.7	-28.4	-	-	-	-
Strengite	Fe+3	PO4-3	H2O	-3.2	-1.5	-8.5	-8.0	-	-	-	-
Fe3(OH)8	H+1	Fe+3	Fe+2	0.8	7.6	-10.0	-6.3	-	-	-	-
Siderite	Fe+2	CO3-2		-0.7	1.4	-1.0	0.6	-0.2	0.3	-0.5	0.6
Vivianite	Fe+2	PO4-3	H2O	-1.7	3.1	-2.4	0.6	-1.6	-0.2	-2.6	0.9
Fe(OH)2 (am)	Fe+2	H2O	H+1	-3.7	-1.8	-4.0	-2.6	-	-	-	-
Halite	Na+1	Cl-1		-7.8	-7.5	-7.8	-7.5	-	-	-	-

key: arsenic sulfur Fe(III) Fe(II)

Table 10 - Saturation indices modeled by MINTEQ and NETPATH using colorimetric Fe(T), field and computed Eh values

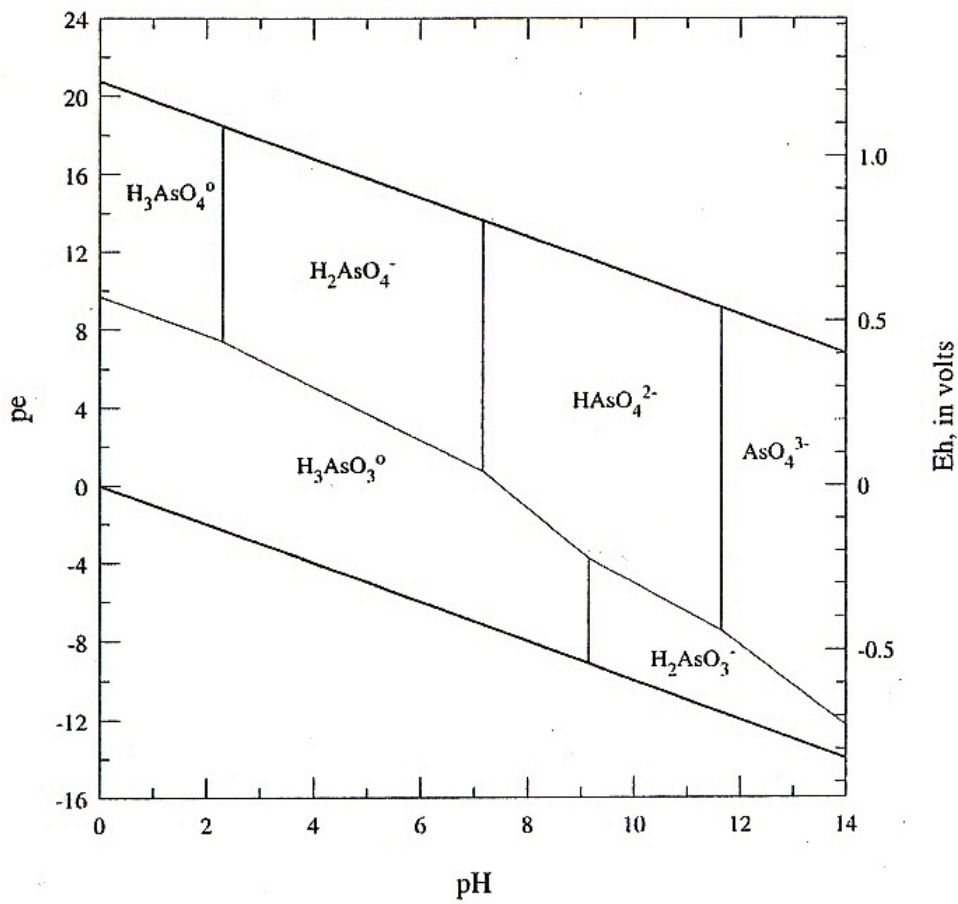


Figure 17 – Eh/pH stability diagram for arsenic species (Nordstrom and Archer, 2003)

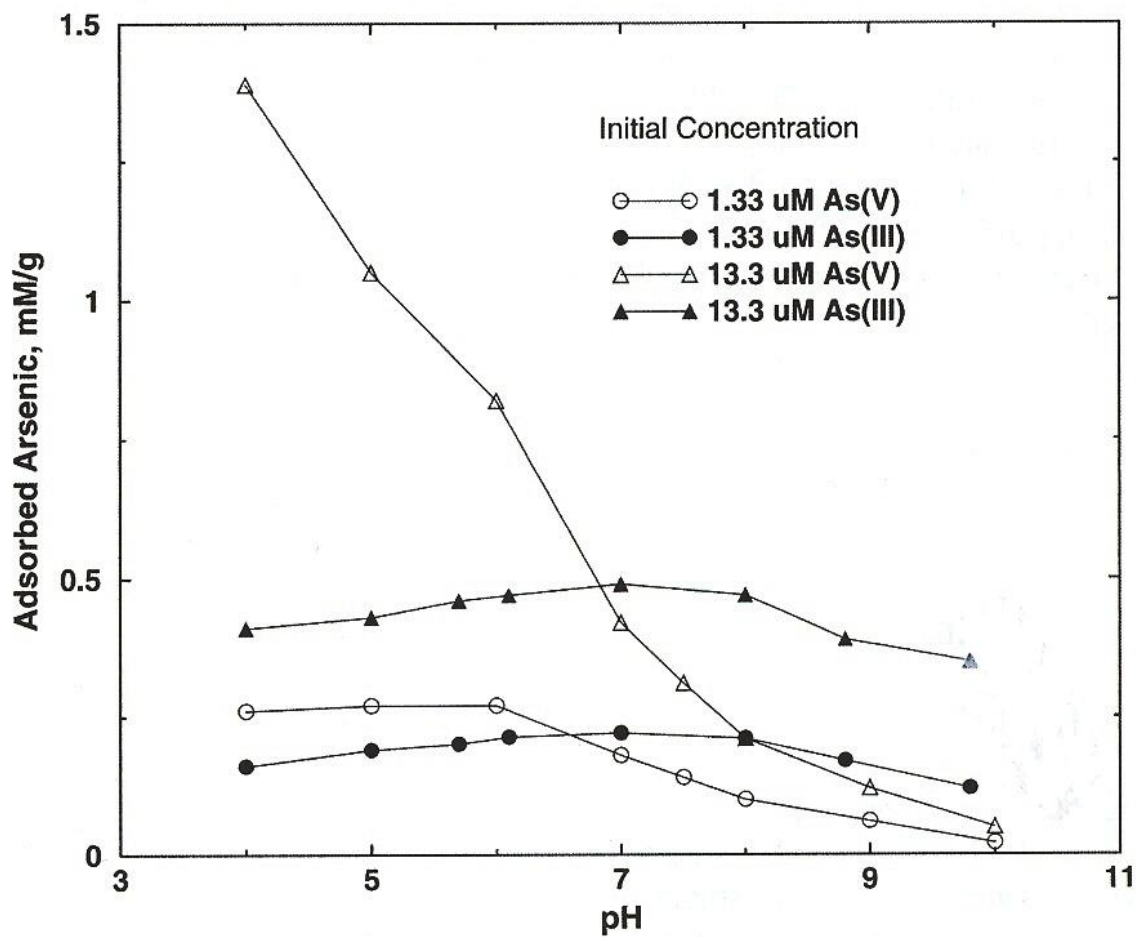


Figure 18 – pH dependency on adsorption on ferrihydrite for As(III) and As(V) (Stollenwerk, 2003)

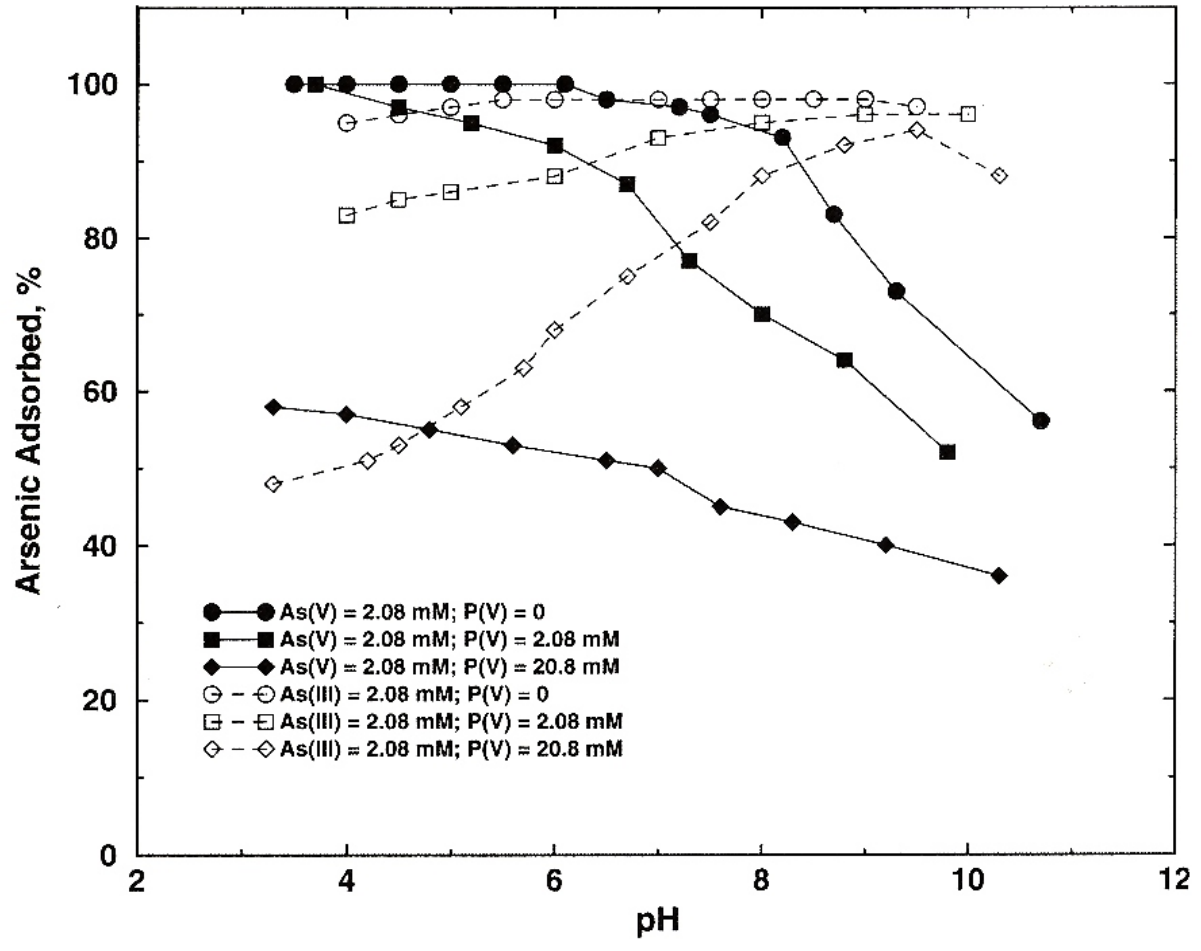


Figure 19 – Arsenic adsorption with phosphate (Stollenwerk, 2003)

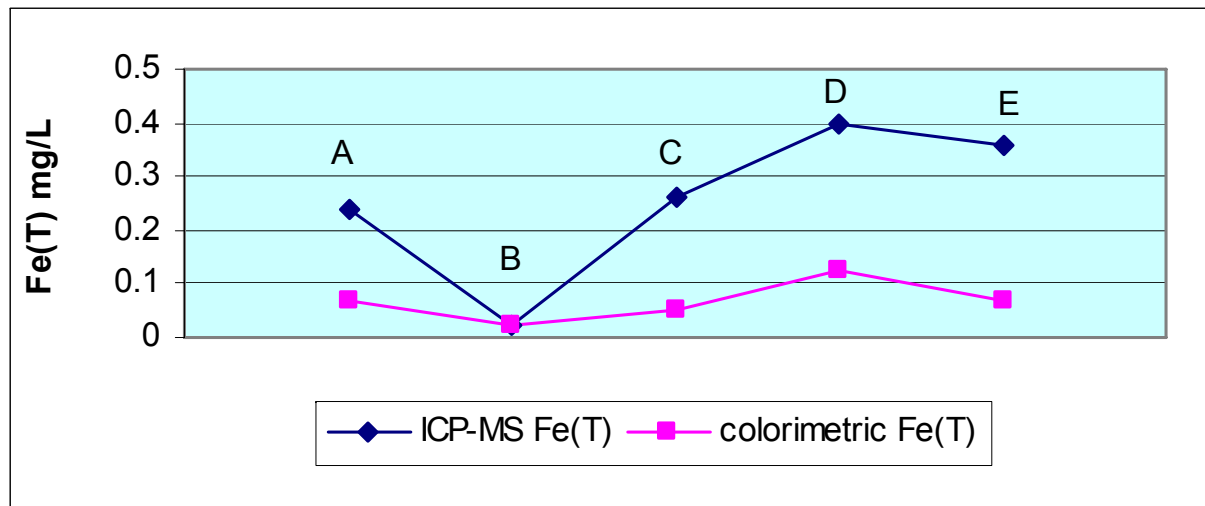


Figure 20 - ICP-MS Fe(T) and colorimetric Fe(T) compared for Wells A-E.

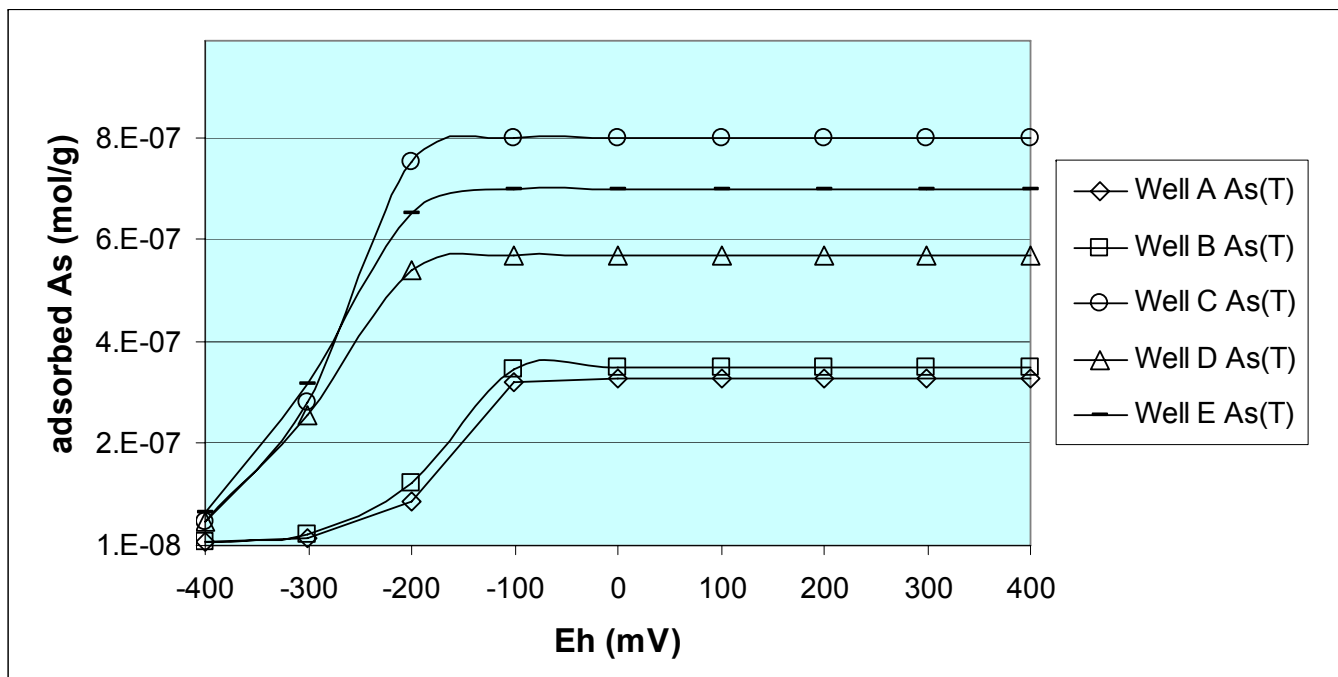


Figure 21 - As(T) adsorption as a function of Eh at average pH for all wells (8.79) as modeled by Visual MINTEQ 2.3.

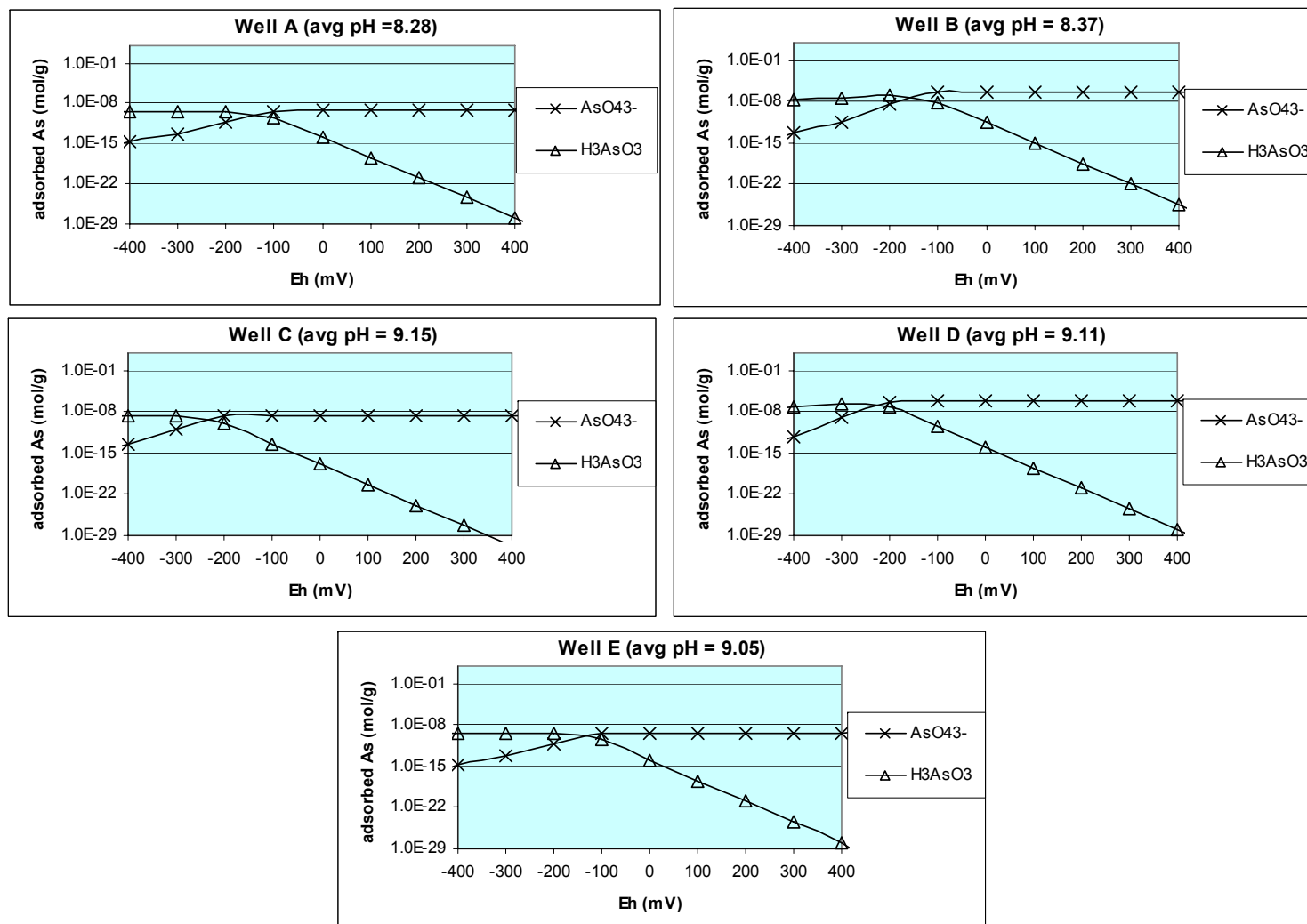


Figure 22 - Arsenate and arsenite adsorption as a function of Eh at average pH for all wells (pH=8.79) modeled by Visual MINTEQ 2.3.

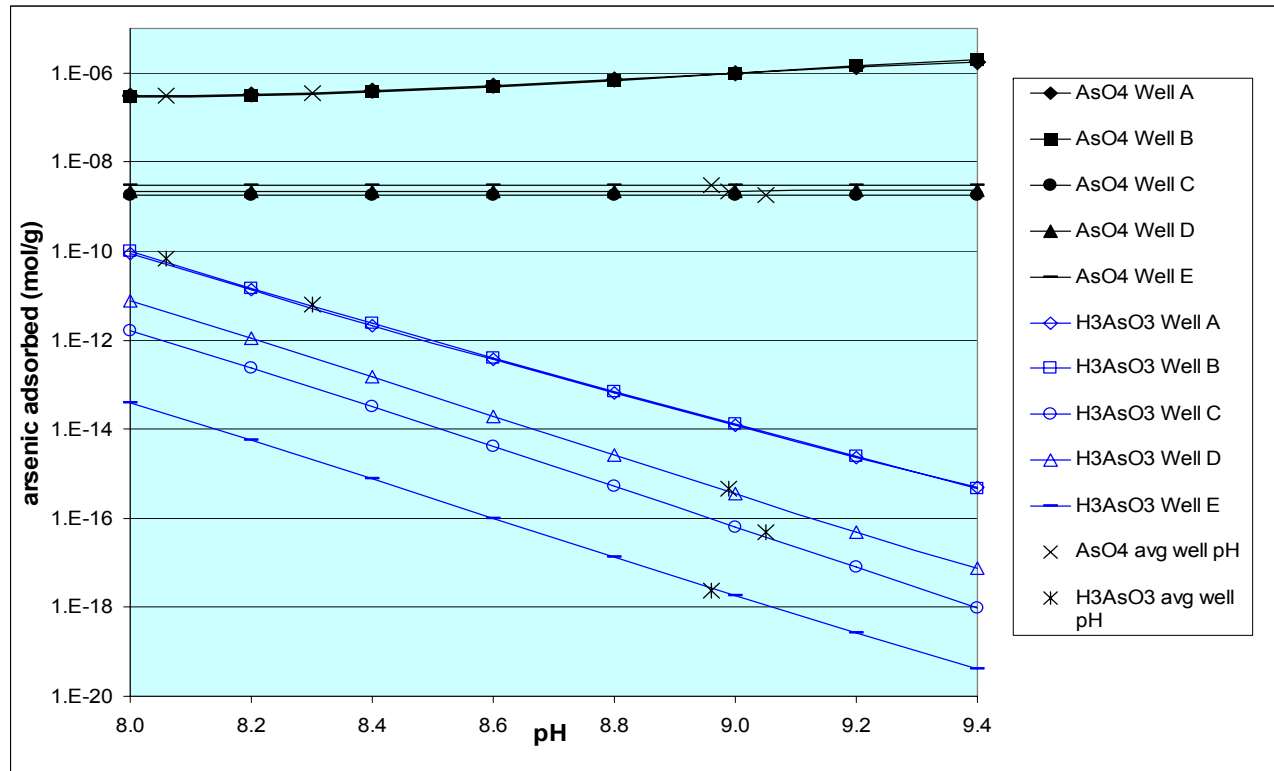


Figure 23 - MINTEQ modeled As adsorption as a function of pH at field-measured Eh values as modeled by Visual MINTEQ 2.3.

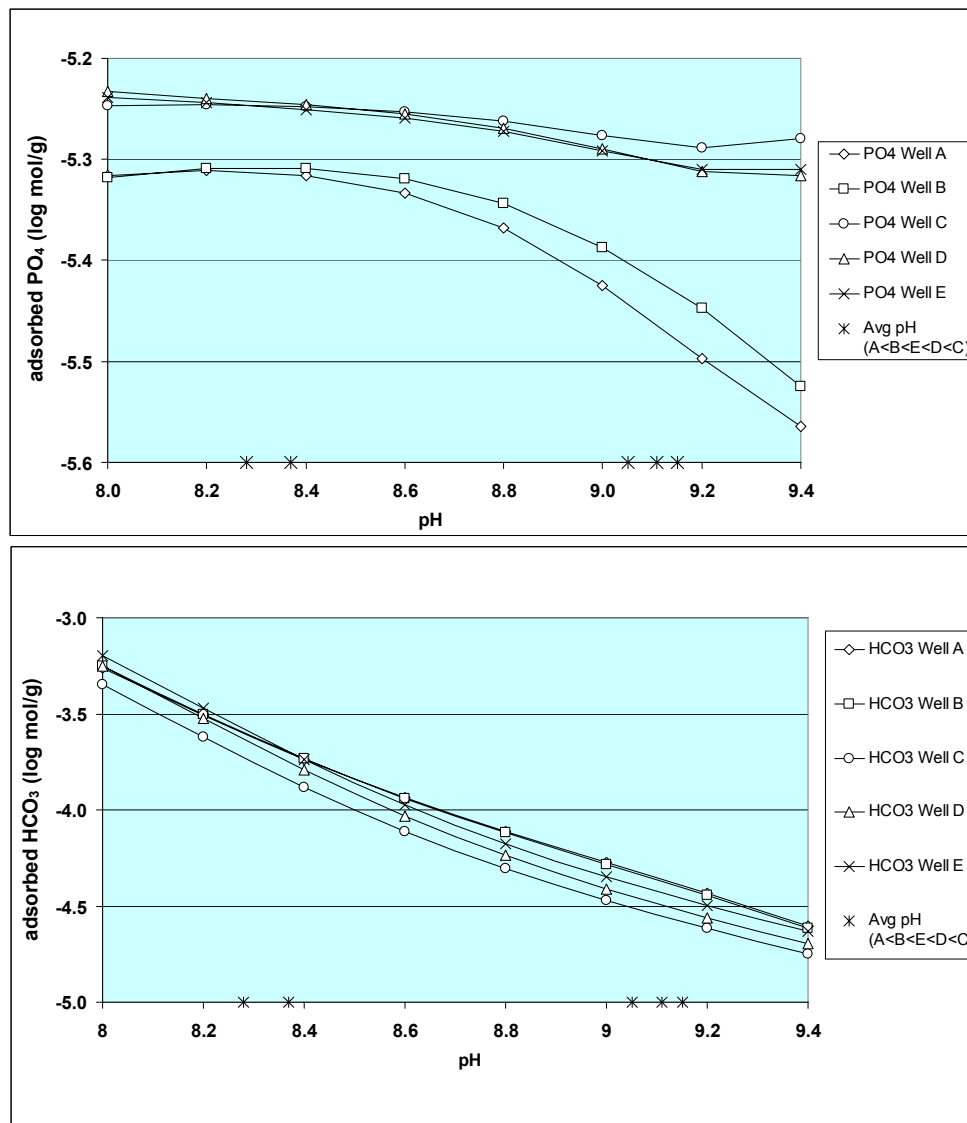


Figure 24 – PO₄ and HCO₃ adsorption on HFO as a function of pH at field-measured Eh as modeled by Visual MINTEQ 2.3.

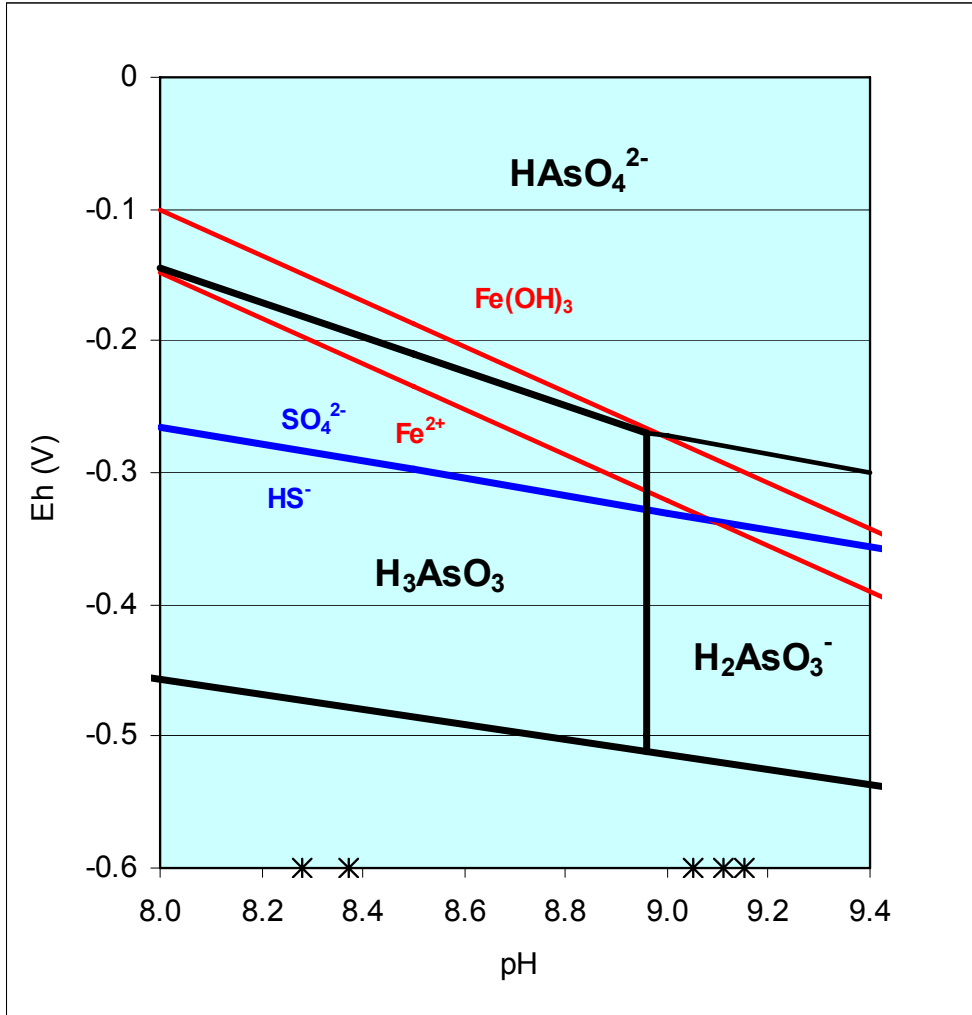


Figure 25 - Eh/pH stability field for selected redox couples at pH range of study. Average pH values for wells are shown with an "x" and $pH_A < pH_B < pH_E < pH_D < pH_C$. Arsenic equilibria (Brookins 1988 ; Langmuir 1997).

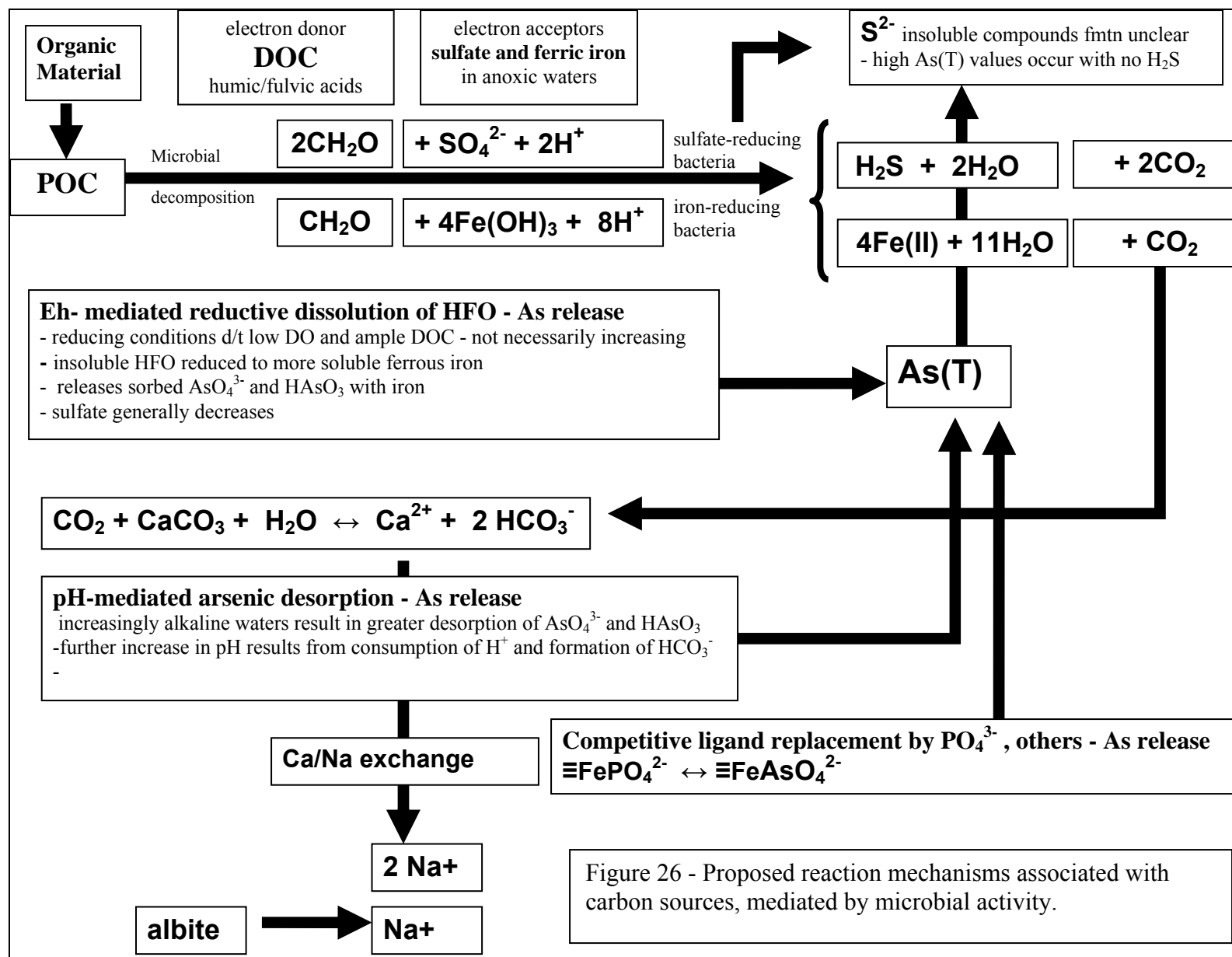


Figure 26 - Proposed reaction mechanisms associated with carbon sources, mediated by microbial activity.

Chapter 4 - Future Work

The biogeochemistry of arsenic in both shallow and intermediate aquifers of Lahontan Valley should be pursued. Future studies should incorporate iron couple data throughout the sampling period to estimate Eh values that could improve upon those used for the analyses in Chapter 3. Field instruments like the YSI Multimeter used in the study should be field-calibrated more than once per sampling day so that uncertainties about readings could be reduced for Eh, pH and other values.

To examine the vertical variability of As concentrations in the aquifer, newly-drilled wells should be logged and sampled along their entire depth to help locate water-bearing units, and potential groundwater channels. Extraction and analysis of bulk As and Fe from drill cores and subsurface samples would be critical to any study that seeks to understand As mobilization. In addition, detailed identification of resident microbes could help determine whether spatial As variability, and $\text{Fe}(\text{OH})_3$ and SO_4 reduction are biologically mediated. It would be possible to aseptically collect sediment samples from or near newly-drilled wells. Analysis of stable isotopes of sulfur may also help determine the origin of sampled sulfides.

More than five wells should be incorporated along any future flow-path study, and they should allow access to water from equal depths or within similar facies to remove some uncertainties about the water's origin.

The strong correlation between As_T , HCO_3^- and DOC should be further researched, especially with respect to their complexation and their mutual interference with each other. Radiocarbon-dating of DOC and DIC should be undertaken to determine if, indeed, aqueous HCO_3^- is the direct result of present-day DOC oxidation.

In-depth modeling of groundwater samples, including that for DOC complexation would also help describe As mobility. The utilization of more than one modeling program would be useful. Other substrates besides ferrihydrite have been implicated in arsenic adsorption and should be considered. These include goethite, gibbsite, montmorillonite, and DOC.

Literature Cited

- Ahmed, K. M., P. Bhattacharya, et al. (2004). "Arsenic enrichment in groundwater of the alluvial aquifers in Bangladesh: an overview." Applied Geochemistry 19: 11.
- APHA (1989). Standard Methods for the Examination of Water and Wastewater, The American Public Health Association.
- Assam, J. (2007). Tungsten. Reno, Nevada, University of Nevada, Reno. Masters Hydrogeology.
- ATSDR (2000). Arsenic Toxicological Profile. Atlanta, Georgia, U.S. Department of Health and Human Services: 468.
- Baedecker, M. J. and I. M. Cozzarelli (1992). "The determination and fate of unstable constituents in contaminated groundwater." Groundwater Quality and Analysis at Hazardous Waste Sites 425-461.
- Ball, J. W. and D. K. Nordstrom (1991). User's manual for WATEQ4, with revised thermodynamic data base and test cases for calculation of major, trace, and redox elements in natural waters., U.S. Geological Survey Open-File Report 91-183.
- Benson, M. (2003). Arsenic in Churchill County, Nevada: Risk Factors Associated with Consumption of Tap Water. Environmental and Natural Resources. Reno, University of Nevada, Reno: 98.
- Brookins, D. G. (1988). Eh-pH diagrams for geochemistry, Springer-Verlag.
- Brown, T. L., H. E. LeMay, et al. (2000). Chemistry - The Central Science. Upper Saddle River, NJ.
- Carillo, A. and J. I. Drever (1998). "Adsorption of arsenic in natural aquifer material in the San Antonio-El Triunfo mining area, Baja California, Mexico." Environmental Geology 35: pp. 251-257.
- Cherry, J. A., A. U. Shaikh, et al. (1979). "Arsenic species as an indicator of redox conditions in groundwater." Journal of Hydrology Vol. 43: p. 373-392.
- Clark, I. D. and P. Fritz (1997). Environmental Isotopes in Hydrogeology, Lewis Publishers, New York.
- Council, N. R. (2000). Arsenic in Drinking Water, National Academy Press.
- Deuel, L. E. and A. R. Swoboda (1972). "Arsenic Solubility in a Reduced Environment." Soil Science Society of America Journal 36.
- DeVore, J. L. (2004). Probability and Statistics for Engineering and the Sciences, Brooks/Cole.
- Dzombak, D. A. and F. M. M. Morel (1990). Surface Complexation Modeling, John Wiley and Sons, Inc.
- EPA, U. (2008). "Primary Drinking Water standards."
- EPA, U. (2009). "Standardized Analytical Methods."
- Fitzgerald, B. (2003). Arsenic Occurrence and Speciation in Domestic Wells: Churchill County, Nevada. Environmental Sciences. Reno, Nevada, University of Nevada, Reno: 100.
- Fosbury, D. (2007). Methods for recognizing distinct source-waters and mixing in the shallow aquifer, Stillwater, Nevada. Hydrology. Reno, University of Nevada, Reno. Masters

- Frost, F., D. Frank, et al. (1993). A seasonal study of arsenic in groundwater, Snohomish County, Washington, USA, Snohomish Health District Washington State Department of Health.
- Gao, S., R. Fujii, et al. (2004). "Evaluation of Adsorbed Arsenic and Potential Contribution to Shallow Groundwater in Tulare Lake Bed Area, Tulare Basin, California." Soil Science Society of America Journal 68: 89-95.
- Gao, Y. and A. Mucci (2001). "Acid base reactions, phosphate and arsenate complexation, and their competitive adsorption at the surface of goethite in 0.7 M NaCl solution." Geochimica et Cosmochimica Acta 65(14): 2361-2378.
- Garbarino, J. R., A. J. Bednar, et al. (2002). Methods of Analysis by the U.S. Geological Survey National Water Quality Laboratory - Arsenic Speciation in Natural Water Samples Using Laboratory and Field Methods, U.S. Geological Survey.
- Glancy, P. A. (1986). Geohydrology of the basalt and unconsolidated sedimentary aquifers in the Fallon area, Churchill County, Nevada, U.S. Geological Survey Water Supply Paper 2263: 62 p.
- Goldberg, S. (2002). "Competitive adsorption of arsenate and arsenite on oxides and clay minerals." Journal of the Soil Science Society of America 66: p. 413-421.
- Goyer, R. A., Ed. (2000). Arsenic in Drinking Water. Arsenic in Drinking Water. Washington, D.C., National Academy of Sciences, National Research Council.
- Grafe, M., M. J. Eick, et al. (2002). "Adsorption of Arsenate and Arsenite on Ferrihydrite in the Presence and Absence of Dissolved Organic Carbon." Journal of Environmental Quality 31: 1115-1123.
- Gustafsson, J. P. (2006). Visual MINTEQ ver. 2.5.
- Harvey, C. F. and R. D. Beckie (2005). "Arsenic: Its Biogeochemistry and Transport in Groundwater." Metal Ions in Biological Systems 44: 145-169.
- Helsel, D. R. and R. M. Hirsch (1992). Statistical Methods in Water Resources, Elsevier Science Publishers.
- Herrera, N. B., R. L. Seiler, et al. (2000). Conceptual Evaluation of Ground-water Flow and Simulated Effects of Changing Irrigation Practices on the Shallow Aquifer in the Fallon and Stillwater Areas, Churchill County, Nevada. Water-Resources Investigations Report 99-4191. Carson City, Nevada, U.S. Geological Survey.
- Kehew, A. E. (2001). Applied Chemical Hydrogeology, Prentice-Hall.
- Kirk, M. F., T. R. Holm, et al. (2004). "Bacterial sulfate reduction limits natural arsenic contamination in groundwater." Geology Vol 32., No. 11: pp. 953-956.
- Korte, N. E. F., Quintus (1991). "A Review of Arsenic (III) in Groundwater." Critical Reviews in Environmental Control 21(1): 39.
- Langmuir, D. (1997). Aqueous Environmental Geochemistry, Prentice-Hall, Inc.
- Lepkowski, W. (1998). "Arsenic Crisis in Bangladesh." Chemical and Engineering Newsletter/ACS.
- Lico, M. S. and R. L. Seiler (1994). Ground-Water Quality and Geochemistry, Carson Desert, Western Nevada. Carson City, U. S. Geological Survey Open-File Report 94-31: 91.
- Lico, M. S., A. H. Welch, et al. (1987). Geochemistry of Ground Water in the Shallow Alluvial Aquifer, Carson Desert, Western Nevada, Lewis Publishers.

- Lombi, E., W. W. Wenzel, et al. (1999). "Arsenic adsorption by soils and iron-oxide coated sand: kinetics and reversibility." Journal of Plant Nutrition Science 162: 451-456.
- Magalhaes, M. C. F. (2002). "Arsenic. An environmental problem limited by solubility." Pure and Applied Chemistry 74(10): 1843-1850.
- Manning, B. A. and S. Goldberg (1997). "Adsorption and Stability of Arsenic (III) at the Clay Mineral-Water Interface." Environmental Science and Technology 31: 2005-2011.
- Manning, B. A. and S. Goldberg (1997). "Arsenic (III) and arsenic (V) adsorption on three California soils." Soil Science 162(12): 886-895.
- Masscheleyn, P. H., R. D. Delaune, et al. (1991). "Effect of Redox Potential and pH on Arsenic Speciation and Solubility in a Contaminated Soil." Environmental Science and Technology 25(8): 1414-1419.
- Maurer, D. K., A. K. Johnson, et al. (1996). Hydrogeology and Potential Effects of Changes in Water Use, Carson Desert Agricultural Area, Churchill County, Nevada, U.S. Geological Survey Water-Supply Paper 2436.
- Newlands, P. (2004). "Newlands Project Data." 2004.
- Nordstrom, D. K. and D. G. Archer (2003). Arsenic Thermodynamics Data and Environmental Geochemistry. Arsenic in Groundwater - Geochemistry and Occurrence. K. A. Publishers.
- Penrose, W. R. (1974). "Arsenic in the marine and aquatic environments: Analysis, occurrence, and significance." CRC Critical Reviews in Clinical Laboratory Science 4: 465-482.
- Peters, G. R., R. F. McCurdy, et al. (1996). "Environmental aspects of arsenic toxicity." CRC Critical Reviews in Clinical Laboratory Science 33: 457-457.
- Pierce, M. L. and C. B. Moore (1980). "Adsorption of Arsenite on Amorphous Iron from Dilute Aqueous Solution." Environmental Science and Technology 21(2).
- Pierce, M. L. and C. B. Moore (1982). "Adsorption of Arsenite and Arsenate on Amorphous Iron Hydroxide." Water Resources 16: 1247-1253.
- Plummer, L. N., E. C. Prestemon, et al. (1994). An Interactive Code (NETPATH) for Modeling Net Geochemical Reactions Along a Flowpath - Version 2.0. Reston, Virginia, US Geological Survey: 128.
- Polizzotto, M. L., C. F. Harvey, et al. (2006). "Solid-phases and desorption processes of arsenic within Bangladesh sediments." Chemical Geology 228: 97-111.
- Poulson, S. (2008). Personal communication.
- Saranko, C. J., N. C. Halmes, et al. (1998). The Toxicity of Arsenite and Arsenate Fact Sheet, Center for Environmental and Human Toxicology, University of Florida; prepared for the Division of Waste Management, Florida Department of Environmental Protection.
- Seiler, R. L. (2004). "Temporal changes in water quality at a childhood leukemia cluster." Ground Water 42(3): 446-455.
- Seiler, R. L. (2005). Geochemistry of 79 wells.
- Seiler, R. L. and K. K. Allander (1993). Water-Level Changes and Directions of Ground-Water Flow in the Shallow Aquifer, Fallon Area, Churchill County, Nevada, U.S. Geological Survey.

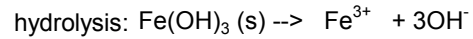
- Seiler, R. L., K. G. Stollenwerk, et al. (2005). "Factors controlling tungsten concentrations in ground water, Carson Desert, Nevada." Applied Geochemistry 20: 423-441.
- Smedley, P. L. and D. G. Kinniburgh (2002). "A Review of the sources, behavior, and distribution of arsenic in natural waters." Applied Geochemistry 17(5): 517-568.
- Sracek, O., Bhattacharya, P., Jacks, G., Gustafsson, J-P., von Bromssen, M. (2004). "Behavior of arsenic and geochemical modeling of arsenic enrichment in aqueous environments." Applied Geochemistry 19(2004): 169-180.
- Steinmaus, C., Y. Yuan, et al. (2005). "The temporal stability of arsenic concentrations in well water in western Nevada." Environmental Research 99: 164-168.
- Stollenwerk, K. G. (2003). Geochemical Processes Controlling Transport of Arsenic in Groundwater: A Review of Adsorption. Arsenic in Groundwater. Geochemistry and Occurrence. A. Welch and K. G. Stollenwerk. Boston, Massachusetts, Kluwer Academic Publishers: 475 pgs.
- Thomas, M. A. (2007). The Association of Arsenic with Redox Condition, Depth, and Ground-water Age in the Glacial Aquifer System of the Northern United States. Reston, Virginia, United States Geological Survey: 36.
- Thundiyil, J. G., Y. Yuan, et al. (2007). "Season variation of arsenic concentration in wells in Nevada." Environmental Research 104.
- Walker, M., M. Benson, et al. (2003). Coping with high concentrations of arsenic in private wells.
- Walker, M. and D. Fosbury (2003). Exposure to Tungsten, Arsenic, and As(III) through private domestic wells, University of Nevada, Reno.
- Walker, M., R. L. Seiler, et al. (2007). "Arsenic exposure from well water treated with reverse osmosis." Science of the Total Environment: 24.
- Waltham, C. A. and M. J. Eick (2002). "Kinetics of Arsenic Adsorption on Goethite in the Presence of Sorbed Silicic Acid." Soil Science Society of America Journal 66: 818-825.
- Wassenaar, L. I., R. Aravena, et al. (1990a). "Isotopic composition (^{13}C , ^{14}C , ^2H) and geochemistry of aquatic humic substances from groundwater." Organic Geochemistry 15: 383-396.
- Waychunas, G. A., C. C. Fuller, et al. (1993). "Surface chemistry of ferrihydrite: Part 2. Kinetics of arsenate adsorption and coprecipitation " Geochimica et Cosmochimica Acta 57: 2271-2282.
- Welch, A. H. and M. S. Lico (1998). "Factors Controlling As and U in shallow ground water, southern Carson Desert, Nevada." Applied Geochemistry 13(4): p. 18.
- Welch, A. H. and K. G. Stollenwerk (2003). Arsenic in ground water, Springer.
- Welch, A. H., D. B. Westjohn, et al. (2000). "Arsenic in ground water of the United States: occurrence and geochemistry." Ground Water 38(4): 589-604.

Appendix B: Ionic strength calculations for Wells A-E

Ionic strength (I) calculations for A-E

average for I: 0.0201

WELL A							WELL B						
Species	avg conc (mg/L)	formula weight (g)	molarity (mol/L)	valence (z _i)	(m _i) (meq/L) m _i *z _i ²		Species	avg conc (mg/L)	formula weight (g)	molarity (mol/L)	valence (z _i)	(m _i) (meq/L) m _i *z _i ²	
Ca ²⁺	4.90	40.1	0.00012	2	0.00024	0.00098	Ca ²⁺	4.75	40.1	0.00012	2	0.00024	0.00095
Mg ²⁺	4.60	24.3	0.00019	2	0.00038	0.00151	Mg ²⁺	4.50	24.3	0.00019	2	0.00037	0.00148
Na ⁺	95.80	23.0	0.00417	1	0.00417	0.00417	Na ⁺	128.00	23.0	0.00557	1	0.00557	0.00557
K ⁺	6.90	39.1	0.00018	1	0.00018	0.00018	K ⁺	4.85	39.1	0.00012	1	0.00012	0.00012
						Σ m_c*z_c							Σ m_c*z_c
CO ₃ ²⁻	4.25	60.0	0.00007	-2	-0.00014	0.00057	CO ₃ ²⁻	4.65	60.0	0.00008	-2	-0.00016	0.00062
HCO ₃ ⁻	148.85	61.0	0.00244	-1	-0.00244	0.00244	HCO ₃ ⁻	197.65	61.0	0.00324	-1	-0.00324	0.00324
SO ₄ ²⁻	68.30	96.1	0.00071	-2	-0.00142	0.00569	SO ₄ ²⁻	37.95	96.1	0.00040	-2	-0.00079	0.00316
Cl ⁻	18.10	35.5	0.00051	-1	-0.00051	0.00051	Cl ⁻	6.25	35.5	0.00018	-1	-0.00018	0.00018
						Σ m_a*z_a							Σ m_a*z_a
charge balance (Σ m _c *z _c - Σ m _a *z _a)/(Σ m _c *z _c + Σ m _a *z _a)							charge balance (Σ m _c *z _c - Σ m _a *z _a)/(Σ m _c *z _c + Σ m _a *z _a)						
% error = 4.78 %							% error = 18.2 %						
I = 1/2 * Σ mi*zi ² = 0.0160							I = 1/2 * Σ mi*zi ² = 0.0153						
WELL C							WELL D						
Species	avg conc (mg/L)	formula weight (g)	molarity (mol/L)	valence (z _i)	(m _i) (meq/L) m _i *z _i ²		Species	avg conc (mg/L)	formula weight (g)	molarity (mol/L)	valence (z _i)	(m _i) (meq/L) m _i *z _i ²	
Ca ²⁺	5.00	40.078	0.00012	2	0.00025	0.00100	Ca ²⁺	4.75	40.078	0.00012	2	0.00024	0.00095
Mg ²⁺	5.00	24.305	0.00021	2	0.00041	0.00165	Mg ²⁺	4.75	24.305	0.00020	2	0.00039	0.00156
Na ⁺	197.89	22.98977	0.00861	1	0.00861	0.00861	Na ⁺	173.50	22.98977	0.00755	1	0.00755	0.00755
K ⁺	5.00	39.0983	0.00013	1	0.00013	0.00013	K ⁺	4.85	39.0983	0.00012	1	0.00012	0.00012
						Σ m_c*z_c							Σ m_c*z_c
CO ₃ ²⁻	37.55	60.0	0.00063	-2	-0.00125	0.00501	CO ₃ ²⁻	48.95	60.0	0.00082	-2	-0.00163	0.00653
HCO ₃ ⁻	352.53	61.017	0.00578	-1	-0.00578	0.00578	HCO ₃ ⁻	300.30	61.017	0.00492	-1	-0.00492	0.00492
SO ₄ ²⁻	38.53	96.0636	0.00040	-2	-0.00080	0.00321	SO ₄ ²⁻	33.80	96.0636	0.00035	-2	-0.00070	0.00281
Cl ⁻	10.00	35.453	0.00028	-1	-0.00028	0.00028	Cl ⁻	6.60	35.453	0.00019	-1	-0.00019	0.00019
						Σ m_a*z_a							Σ m_a*z_a
charge balance (Σ m _c *z _c - Σ m _a *z _a)/(Σ m _c *z _c + Σ m _a *z _a)							charge balance (Σ m _c *z _c - Σ m _a *z _a)/(Σ m _c *z _c + Σ m _a *z _a)						
% error = 7.33 %							% error = 5.44 %						
I = 1/2 * Σ mi*zi ² = 0.0257							I = 1/2 * Σ mi*zi ² = 0.0246						
WELL E													
Species	avg conc (mg/L)	formula weight (g)	molarity (mol/L)	valence (z _i)	(m _i) (meq/L) m _i *z _i ²								
Ca ²⁺	5.85	40.078	0.0001	2	0.00020	0.00117							
Mg ²⁺	4.35	24.305	0.0002	2	0.00036	0.00143							
Na ⁺	73.50	22.98977	0.0032	1	0.00320	0.00320							
K ⁺	7.90	39.0983	0.0002	1	0.00020	0.00020							
						Σ m_c*z_c							
CO ₃ ²⁻	50.11	60.0	0.0008	-2	-0.00160	0.00668							
HCO ₃ ⁻	150.15	61.017	0.0025	-1	-0.00246	0.00246							
SO ₄ ²⁻	43.25	96.0636	0.0005	-2	-0.00090	0.00360							
Cl ⁻	7.60	35.453	0.0002	-1	-0.00021	0.00021							
						Σ m_a*z_a							
charge balance (Σ m _c *z _c - Σ m _a *z _a)/(Σ m _c *z _c + Σ m _a *z _a)													
% error = -12.9 %													
I = 1/2 * Σ mi*zi ² = 0.0190													

Appendix C - Eh-pH digram calculations for Figure 25 **$\Delta G^\circ_{\text{formation}}$ from $\Delta G^\circ_{\text{hydrolysis}}$ for $\text{Fe}(\text{OH})_3$ (s)**

$$\text{with } K_{\text{sp}} = [\text{Fe}^{3+}][\text{OH}^-]^3 = 10^{-38.5} \quad (\text{Langmuir, 1997})$$

assuming "fresh solid, amorphous precipitate"

$$\Delta G^\circ_{\text{hydrolysis}} = -RT \ln K_{\text{sp}}$$

$$= (-0.00199 * 298.15) * 2.303 * \log(10^{-38.5})$$

$$\Delta G^\circ_{\text{hydrolysis}} = 52.58 \quad \text{kcal/mol}$$

$$\Delta G^\circ_{\text{hydrolysis}} = \Delta G^\circ_{\text{f products}} - \Delta G^\circ_{\text{reactants}}$$

$$= [(\text{Fe}^{3+}) + 3(\text{OH}^-)] - \text{Fe}(\text{OH})_3$$

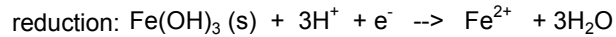
$$52.58 = [-2.52 + 3(-37.63)] - (\Delta G^\circ_{\text{formation Fe}(\text{OH})_3})$$

$$\Delta G^\circ_{\text{formation Fe}(\text{OH})_3} = -167.99 \text{ kcal/mol} \quad (-169.9 \text{ kcal/mol from Majzlan et al., 2004})$$

species	ΔG_f° (kcal/mol)	(Brown, et al., 2000)
$\text{Fe}(\text{OH})_3$ (s)	-168.00	calc
H^+ (aq)	0	
Fe^{2+} (aq)	-20.32	
H_2O (l)	-56.73	
OH^- (aq)	-37.63	
Fe^{3+} (aq)	-2.52	

constants

R	0.00199 kcal/mol K
	8.314 J/mol/K

 $\Delta G^\circ_{\text{reduction}}$ for $\text{Fe}(\text{OH})_3$ (s)

$$\Delta G^\circ_{\text{reduction}} = \Delta G_f^\circ_{\text{products}} - \Delta G_f^\circ_{\text{reactants}}$$

$$= [(\text{Fe}^{2+} + 3(\text{H}_2\text{O})) - ((\text{Fe}(\text{OH})_3 + 3(\text{H}^+)))]$$

$$= [(-20.3182) + 3(-56.7297)] - [-169.9 + 3(0)]$$

$$\Delta G^\circ_{\text{reduction}} = -20.61 \text{ kcal/mol} = -86220.43 \text{ J/mol}$$

 E° for $\text{Fe}(\text{OH})_3$ (s) reduction

$$\Delta G^\circ_{\text{reduction}} = -nFE^\circ$$

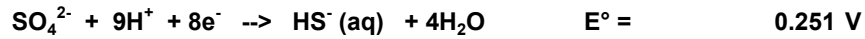
$$E^\circ = -\Delta G^\circ_{\text{reduction}}/nF = 0.894 \text{ V}$$

constants

n	1 mole e-
F	96450 C/mol e-
mass Fe	55.847 g/mol

Appendix C - continued

slope-intercept for sulfate reduction:



$$Q = [\text{HS}^-] / ([\text{SO}_4^{2-}][\text{H}^+]^9)$$

$$Eh = E^\circ - (2.303RT/nF) * \log Q$$

$$Eh = 0.251 + (0.0000248T * (\log(([\text{SO}_4^{2-}][\text{H}^+]^9)/[\text{HS}^-])))$$

$$Eh = 0.251 + (0.000719 * ((\log [\text{H}^+]^9) + \log (\{\text{SO}_4^{2-}\}/\{\text{HS}^-\}))) \quad \text{used T = 290 K for all}$$

$$Eh = 0.251 - (0.000719 * (9 \text{ pH} - \log (\{\text{SO}_4^{2-}\}/\{\text{HS}^-\})))$$

$$Eh = 0.251 - (0.0647 \text{ pH} - 0.000719 \log (\{\text{SO}_4^{2-}\}/\{\text{HS}^-\})) \quad a = \gamma * c \quad \gamma \sim 0.6$$

	(mg/L)	conc. (c) (M)	activity (a) (M)	log SO ₄ ²⁻ /HS ⁻
Eh = 0.253 - 0.0647 pH	high SO4 72	0.00075	0.00045	2.9
	low HS 0.032	9.41E-07	5.6471E-07	
Eh = 0.251 - 0.0647 pH	low SO4 31	0.000323	0.00019375	0.798
	high HS 1.75	5.15E-05	3.0882E-05	

for plot

high SO₄²⁻/low HS⁻
Eh = 0.253 - 0.0647 pH

low SO4²⁻/high HS⁻
Eh = 0.251 - 0.0647 pH

H₃AsO₃ upper (pH 6.88-8.96)
Eh = 0.893 - 0.130 pH

pH	Eh (V)	Eh (V)
8	-0.2646	-0.2666
8.5	-0.29695	-0.29895
9	-0.3293	-0.3313
9.5	-0.36165	-0.36365

H₂AsO₃⁻ upper (pH 8.96-0.88)
Eh = 0.337 - 0.0677 pH

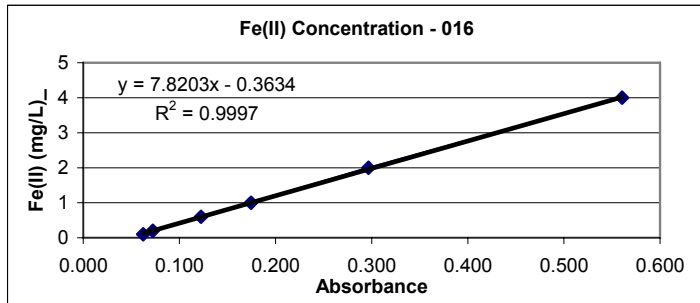
Appendix D - Colorimetric iron

Sample 016 Date: 5/18/05

016 Sample/analysis data Date: 5/18 and 5/25/05

Fe (II)

Sample	absorbance							Avg abs.	corrected abs	calc conc.	
	y (mg/L)	x (abs) 1	x (abs) 2	x (abs) 3	x (abs) 5	x (abs) 6	x (abs) 7	avg x	x corrected	y = 7.8203x - 0.3634 y calc	% error
DI		0.0474	0.0473	0.0472				0.0473	0.0458	-0.0055	
1% HNO3		0.0492	0.0488	0.0492	0.0488			0.0490	0.0475	0.0078	
DI w/ reagent		0.0487	0.0491	0.0486	0.0489			0.0488	0.0473	0.0065	
0.1		0.0640	0.0637	0.0640	0.0640			0.0639	0.0624	0.1245	-24.55
0.2		0.0739	0.0737	0.0742	0.0739	0.0736		0.0739	0.0723	0.2022	-1.12
0.6		0.1238	0.1242	0.1237	0.1238	0.1239		0.1239	0.1224	0.5934	1.10
1		0.1764	0.1761	0.1763	0.1758	0.1759		0.1761	0.1746	1.0018	-0.18
2		0.2982	0.2986	0.2983	0.2982	0.2983		0.2983	0.2968	1.9576	2.12
4		0.5619	0.5620	0.5623	0.5621	0.5621		0.5621	0.5606	4.0203	-0.507
											corrected y (+0.00625))
A		0.0543	0.0543	0.0540	0.0542			0.0542	0.0527	0.0485	0.0547
B		0.0496	0.0495	0.0495	0.0496			0.0496	0.0480	0.0121	0.0184
C		0.0523	0.0524	0.0524	0.0524			0.0524	0.0508	0.0342	0.0405
D		0.0643	0.0644	0.0645	0.0646			0.0645	0.0629	0.1287	0.1349
E		0.0546	0.0546	0.0551	0.0546	0.0548	0.0545	0.0547	0.0532	0.0524	0.0587
								0.00153	DI abs difference		mg/L



Obtained an absorbance for the DI and the DI w/reagent. Their difference was 0.00153, meaning this is the absorbance increase by adding the reagent. Therefore, this value was subtracted from each absorbance to get a "corrected" absorbance. These are the values used to determine the concentration of Fe(II). The avg DI is -0.00625 (neglecting the 0.0258), so added 0.00625 to all values since DI should be 0 corresponding to 0 mg/L Fe. The fit is perfect without it. Added 0.0164 mg/L to each value (y) since the DI water averaged this negative value and it ought to be 0 mg/L.

**016 Sample/analysis data Date: 5/18 and 5/25/05
Fe (II+III)**

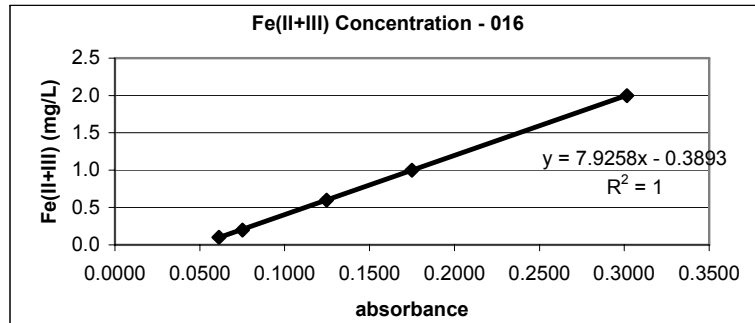
Sample	absorbance					
	y (mg/L)	x (abs) 1	x (abs) 2	x (abs) 3	x (abs) 5	x (abs) 6
DI		0.048	0.0475	0.0475	0.0475	
1% HNO3		0.0482	0.0482	0.0482		
DI w/ reagent		0.0485	0.0482	0.0482		
0.1		0.062	0.062	0.062		
0.2		0.0761	0.0758	0.0757	0.0757	0.0757
0.6		0.1256	0.1254	0.1253	0.1252	
1.0		0.1756	0.1757	0.1757	0.1757	
2.0		0.3026	0.3022	0.3022	0.3022	
4.0		0.3958	0.3955	0.3955	0.3955	
A		0.0552	0.0553	0.0553	0.0553	
B		0.0524	0.0523	0.0529	0.0522	0.0525
C		0.0533	0.0534	0.0535		
D		0.0609	0.0608	0.0608	0.0608	
E		0.0564	0.0564	0.0563	0.0563	

Avg abs corrected a calc conc.

$x_{corr} = y - 0.0007$

$y = 7.9258x - 0.3893$

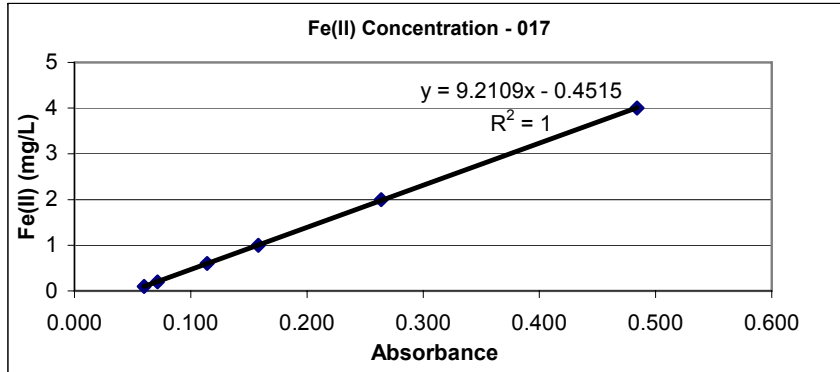
x	x corrected	y calc	% error
0.0476	0.0469	-0.0174	
0.0482	0.0475	-0.0128	
0.0483	0.0476	-0.0120	
0.0620	0.0613	0.0966	3.4
0.0758	0.0751	0.2059	-3.0
0.1254	0.1247	0.5988	0.2
0.1757	0.1750	0.9975	0.2
0.3023	0.3016	2.0011	-0.1
0.3956	0.3949	2.7404	31.5
			corrected y
			(+0.0164)
0.0553	0.0546	0.0433	0.0597
0.0525	0.0518	0.0209	0.0373
0.0534	0.0527	0.0284	0.0448
0.0608	0.0601	0.0872	0.1036
0.0564	0.0557	0.0518	0.0682
0.0007	DI abs difference		mg/L



Suspect the 4.0 standard is bad. Threw out the absorbance value for 4.0 mg/L. The fit is perfect without it.

017 Sample/analysis data: 6/6/ and 6/12/05
Fe (II)

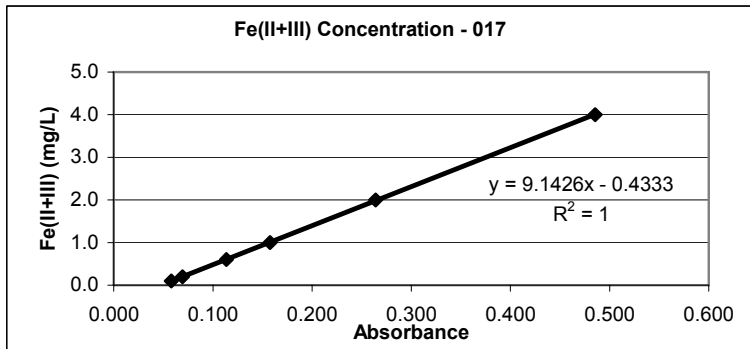
Sample	absorbance						Avg abs.	corrected abs xcorr=x-0.00123	calc conc.		
	y (mg/L)	x (abs)	x (abs)	x (abs)	x (abs)	x (abs)			y = 9.2109x - 0.4515	% error	
(Did calc conc by x=y corrected/0.1278)											
		1	2	3	5	6	7	x	x corrected	y calc	% error
DI		0.0484	0.0484	0.0483				0.0484	0.0471	-0.0173	
1% HNO3		0.049	0.0491	0.0491				0.0491	0.0478	-0.0109	
DI w/ reagent		0.0495	0.0497	0.0495	0.0497			0.0496	0.0484	-0.0060	
0.1		0.061	0.0611	0.0613	0.0614	0.0612	0.061	0.0612	0.0599	0.1006	-0.571
0.2		0.0726	0.0726	0.0726				0.0726	0.0714	0.2059	-2.941
0.6		0.1154	0.1153	0.1154				0.1154	0.1141	0.5998	0.033
1		0.1593	0.1595	0.1594				0.1594	0.1582	1.0054	-0.539
2		0.2652	0.2652	0.2653				0.2652	0.2640	1.9802	0.990
4		0.4854	0.4854	0.4854				0.4854	0.4842	4.0081	-0.204
corrected y (+0.0173)											
A		0.0536	0.0536	0.0538	0.0537			0.05368	0.05245	0.0316	0.0488
B		0.0503	0.0503	0.0503				0.05030	0.04907	0.0005	0.0177
C		0.0531	0.053	0.0531				0.05307	0.05184	0.0260	0.0432
D		0.0646	0.0645	0.0643				0.06447	0.06324	0.1310	0.1482
E		0.0555	0.0556	0.0555				0.05553	0.05430	0.0487	0.0659
								0.00123	DI Difference		mg/L



Suspect the 4.0 standard is bad. Threw out the absorbance value for 4.0 mg/L. The fit is perfect without it.

017 Sample/analysis data: 6/6 and 6/12/05
Fe (II+III)

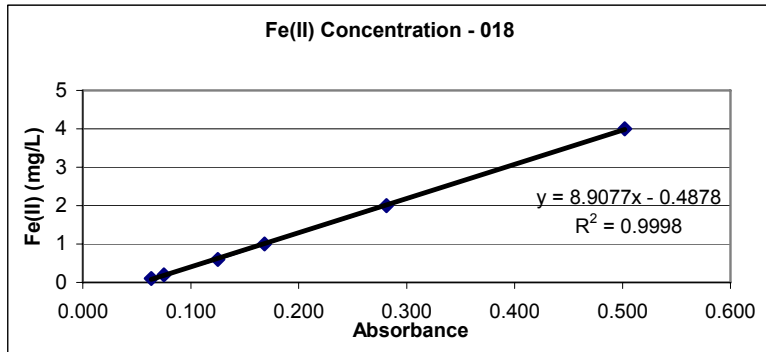
Sample	absorbance					Avg abs corrected a calc conc.			
	y (mg/L)	x (abs)	x (abs)	x (abs)	x (abs)	x	x corrected	y calc	% error
DI		0.0483	0.048	0.0481	0.0481	0.0481	0.0468	-0.0052	
1% HNO3		0.0499	0.0502	0.05	0.0501	0.0501	0.0488	0.0124	
DI w/ reagent		0.0494	0.0493	0.0495	0.0494	0.0494	0.0481	0.0065	
0.1		0.0595	0.0595	0.0594		0.0595	0.0582	0.0985	1.51
0.2		0.0707	0.0708	0.0706		0.0707	0.0694	0.2012	-0.60
0.6		0.1149	0.1147	0.1149	0.115	0.1149	0.1136	0.6053	-0.88
1.0		0.1588	0.1589	0.1586	0.1587	0.1588	0.1575	1.0062	-0.62
2.0		0.2655	0.2655	0.2655		0.2655	0.2642	1.9822	0.89
4.0		0.4869	0.4869	0.4869		0.4869	0.4856	4.0063	-0.16
									corrected y (+0.0035)
A		0.0577	0.0577	0.0577		0.0577	0.0564	0.0823	0.0858
B		0.0516	0.0515	0.0515	0.0515	0.0515	0.0502	0.0259	0.0294
C		0.0555	0.0553	0.0554		0.0554	0.0541	0.0613	0.0648
D		0.0619	0.0618	0.0618		0.0618	0.0605	0.1201	0.1236
E		0.0576	0.0576	0.0574	0.0576	0.0576	0.0563	0.0810	0.0845
						0.0013	DI Difference		mg/L



Suspect the 4.0 standard is bad. Threw out the absorbance value for 4.0 mg/L. The fit is perfect without it.

**018 Sample/analysis date 6/20 and 6/23//05
Fe(II)**

Sample	absorbance						Avg abs.	corrected abs xcorr=x-0.00088	calc conc.		
	y (mg/L)	x (abs)	x (abs)	x (abs)	x (abs)	x (abs)			y = 8.9077x - 0.4878	% error	
		(Did calc conc by x=y corrected/0.1278)									
		1	2	3	5	6	7	x	x corrected	y calc	% error
DI		0.0509	0.0509	0.0508				0.05087	0.0500	-0.0425	
1% HNO3		0.052	0.0519	0.052	0.0521			0.05200	0.0511	-0.0324	
DI w/ reagent		0.0519	0.0518	0.0515	0.052	0.0516	0.0517	0.05175	0.0509	-0.0347	
0.1		0.0642	0.0644	0.0643	0.0643	0.0644		0.06432	0.0634	0.0773	22.70
0.2		0.076	0.0758	0.0761	0.0763	0.0762		0.07608	0.0752	0.1821	8.97
0.6		0.1258	0.1259	0.1259				0.12587	0.1250	0.6255	-4.26
1		0.1693	0.1692	0.1691				0.16920	0.1683	1.0115	-1.15
2		0.282	0.2824	0.2823	0.2822			0.28223	0.2813	2.0183	-0.92
4		0.503	0.503	0.503				0.50300	0.5021	3.9849	0.38
A		0.0585	0.0586	0.0586	0.0586	0.0585		0.05856	0.0577	0.0260	0.0672
B		0.0532	0.0534	0.0534	0.0535	0.0534		0.05338	0.0525	-0.0201	0.0211
C		0.0556	0.0557	0.0557				0.05567	0.0548	0.0002	0.0414
D		0.0641	0.0637	0.0637	0.0638			0.06383	0.0629	0.0729	0.1141
E		0.0585	0.0584	0.0583	0.0583	0.0585	0.0583	0.05838	0.0575	0.0244	0.0656
								0.00088	DI abs difference		mg/L



**018 Sample/analysis date 6/20 and /23//05
Fe (II+III)**

Sample	absorbance					
	y 9mg/L	x (abs) 1	x (abs) 2	x (abs) 3	x (abs) 5	x (abs) 6
DI		0.0512	0.0512	0.0513		
1% HNO3		0.0571	0.057	0.0569		
DI w/ reagent		0.0524	0.0524	0.0525	0.0526	0.0526
0.1		0.0628	0.0627	0.0627	0.0628	
0.2		0.0734	0.0735	0.0735	0.0735	
0.6		0.1202	0.1201	0.1202	0.1201	
1.0		0.1665	0.1666	0.1666		
2.0		0.2755	0.2755	0.2754		
4.0		0.4885	0.4886	0.4887		
1% HNO3		0.05	0.0499	0.0499	0.0499	

A	0.0591	0.0594	0.0592	0.0592	0.0593
B	0.0525	0.0524	0.0524		
C	0.0578	0.0577	0.0578		
D	0.0643	0.0642	0.0642		
E	0.0577	0.0578	0.0579		

Avg abs corrected a calc conc.

$x = x - 0.00187$

$y = 9.1553x - 0.4775$

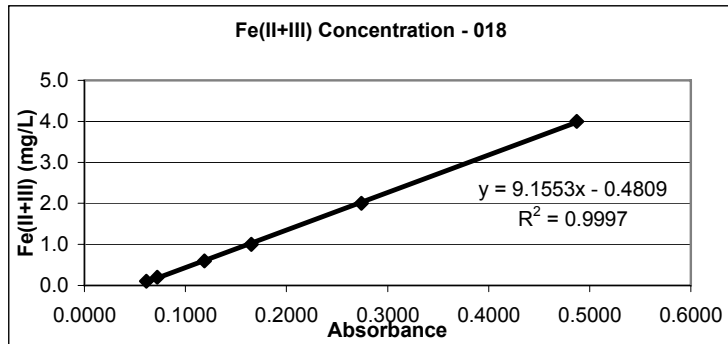
x	x corrected	x calc	% error
0.05123	0.0497	-0.0221	
0.05700	0.0555	0.0307	
0.05272	0.0510	-0.0105	
0.06275	0.0613	0.0834	16.65
0.07348	0.0720	0.1815	9.23
0.12015	0.1187	0.6089	-1.48
0.16657	0.1651	1.0338	-3.38
0.27547	0.2740	2.0308	-1.54
0.48860	0.4871	3.9821	0.45
0.04993	0.0484	-0.0341	

corrected y
(+0.0221)

0.05924	0.0578	0.0512	0.0733
0.05243	0.0509	-0.0111	0.0110
0.05777	0.0563	0.0377	0.0583
0.06423	0.0627	0.0969	0.1190
0.05780	0.0563	0.0380	0.0601

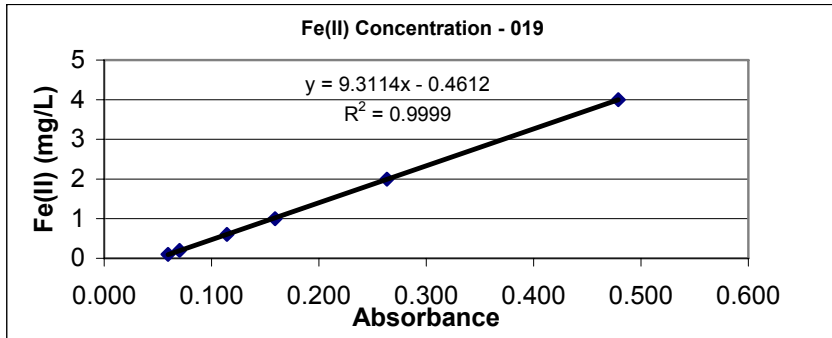
0.00149 DI abs difference

mg/L



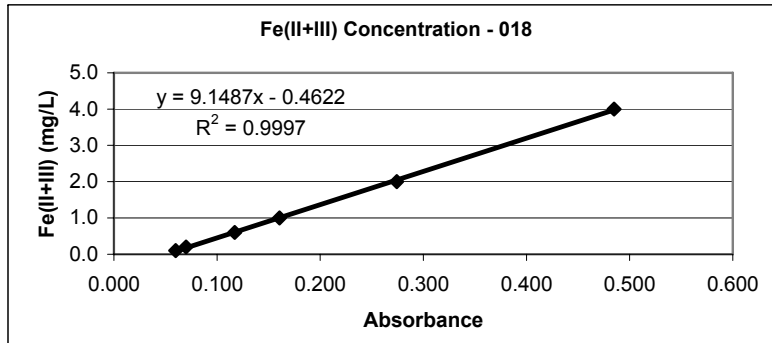
019 Sample/analysis date: 7/20 and 7/26/05
Fe (II)

Sample	absorbance						Avg abs.	corrected abs xcorr=x-0.0007	calc conc.	
	y (mg/L)	(Did calc conc by x=y corrected/0.1278)							x	x corrected
	x (abs)	x (abs)	x (abs)	x (abs)	x (abs)	x (abs)				
	1	2	3	5	6	7				
DI	0.0487	0.0487	0.0487				0.0487	0.0480	-0.0143	
1% HNO3	0.0494	0.0493	0.0495	0.0496			0.0495	0.0488	-0.0073	
DI w/ reagent	0.0494	0.0493	0.0495	0.0494			0.0494	0.0487	-0.0077	
0								0.0494		
0.1	0.0602	0.0602	0.0602				0.0602	0.0595	0.0928	7.172
0.2	0.0708	0.0709	0.0709	0.0708			0.0709	0.0702	0.1920	4.003
0.6	0.1151	0.1151	0.1149	0.115	0.1148	0.1151	0.1150	0.1143	0.6031	-0.516
1	0.1599	0.16	0.1599	0.16			0.1600	0.1593	1.0216	-2.164
2	0.2641	0.2641	0.2641				0.2641	0.2634	1.9914	0.429
4	0.4799	0.4796	0.4796	0.4796			0.4797	0.4790	3.9987	0.032
9	0.0559	0.0559	0.0559				0.0559	0.0552	0.0528	0.0671
104	0.0585	0.0583	0.0585	0.0583			0.0584	0.0577	0.0761	0.0904
163	0.0576	0.0575	0.0577				0.0576	0.0569	0.0686	0.0829
179	0.0646	0.0647	0.0646				0.0646	0.0639	0.1341	0.1484
319	0.052	0.052	0.052				0.0520	0.0513	0.0165	0.0308
							0.00070			DI abs difference
										corrected y (+0.0143)
										mg/L



019 Sample/analysis date: 7/20 and 7/26/05
Fe (II+III)

Sample	absorbance					Avg abs corrected a calc conc.				
	y (mg/L)	x (abs)	x (abs)	x (abs)	x (abs)	x (abs)	x	x corrected	y calc	% error
		1	2	3	5	6			$y = 9.1487x - 0.4622$	
DI		0.0492	0.0491	0.0492			0.0492	0.0487	-0.0164	
1% HNO3		0.05	0.0502	0.0503	0.0502	0.0504	0.0502	0.0498	-0.0068	
DI w/ reagent		0.0502	0.0501	0.0503			0.0502	0.0498	-0.0070	
0.1		0.0603	0.0604	0.0604	0.0605		0.0604	0.0600	0.0864	13.644
0.2		0.0705	0.0703	0.0703	0.0703		0.0704	0.0699	0.1774	11.307
0.6		0.1174	0.1176	0.1173	0.1175		0.1175	0.1170	0.6083	-1.382
1.0		0.1611	0.1611	0.1611			0.1611	0.1607	1.0076	-0.763
2.0		0.2745	0.2746	0.2746			0.2746	0.2741	2.0457	-2.285
4.0		0.4854	0.4854	0.4854			0.4854	0.4850	3.9746	0.636
										corrected y (+0.0164)
A		0.0558	0.0558	0.056	0.0561	0.0559	0.05592	0.0555	0.0454	0.0618
B		0.0512	0.0514	0.0515	0.0514		0.05138	0.0509	0.0038	0.0202
C		0.0545	0.0546	0.0545			0.05453	0.0541	0.0327	0.0491
D		0.0655	0.0648	0.0645	0.0647	0.0645	0.06480	0.0644	0.1266	0.1430
E		0.0567	0.0567	0.0569	0.057	0.0569	0.05684	0.0564	0.0538	0.0702
							0.00044	DI abs difference		mg/L



Appendix D - continued

Fe(III) reduction: $\text{Fe(III)} + e^- \rightarrow \text{Fe(II)}$ $E_h^\circ = 0.771 \text{ V}$

Nernst Equation: $E_h = E_h^\circ - (2.303RT/nF) \cdot \log Q$

Where: E_h° is standard electric potential at 25 °C, 1 atm, and 1 M
 R is the gas constant, 8.314 J/mol K
 T is water temperature in Kelvin
 n is moles of electrons transferred for the redox reaction
 F is Faraday's constant: 96,500 coulombs/mole e-
 Q is reaction quotient or ion activity product (IAP)

and

$$Q = \{\text{Fe(II)}\} / \{\text{Fe(III)}\} \quad \text{activities in molarity}$$

Activities for Fe(II) and Fe(III) and ionic strength (I) for the solutions were

calculated as follows:

Ionic strength (I) is: $I = \frac{1}{2} \sum (m \cdot Z^2)$

Where: m is milliequivalents per liter for each ion;
 1 milliequivalent = 1 millimole of electrons
 Z is ion valence

The Extended Debye-Huckel equation is: $\log \gamma = -AZ^2 I^{1/2} / (1 + BaI^{1/2})$

Where: γ is activity coefficient
 A and B are 0.5091 and 0.3286, respectively
 a is effective size of the hydrated ion in angstroms

Activity {a} is: $\{a\} = C \cdot \gamma$

Where: C is concentration in molarity

A summary of these calculations follows.

Appendix D (continued)

Eh calculations from colorimetric iron (samples 016-019)

Data was obtained from colorimetric iron analysis in the Stilling lab.

Iron activities {Fe} using Extended Debye-Huckel:

$$\log g = -Az^{1/2}/(1+Ba^{1/2})$$

	Well	I	default dielectric constants	ion size parameter	(Langmuir, 1997)
Fe ³⁺ + 1 e- ----> Fe ²⁺	A	0.0155	A 0.5091	Fe2+	6
E° = 0.771 V	B	0.0147	B 0.3286	Fe3+	9
F = 96485 C/mol e-	C	0.0206			
n = 1 mol e-	D	0.0181			
	E	0.0123			

Nernst Equation (Brown and Lemay, 2000)

$$Eh = E° - (2.303RT/nF) \cdot \log(Fe^{2+}/Fe^{3+})$$

	Fe(T) (mg/L)	Fe(T) (M)	Fe(II) (mg/L)	conc Fe(II) (M)	log γ	γ	a = γ * c Fe(II) {M}	Fe(III) (mg/L)	conc Fe(III) (M)	log γ	γ	a = γ * c Fe(III) {M}	temp (K)	Eh (V)
Well A														
16	0.0597	1.07E-06	0.0547	9.80E-07	-0.20	0.63	6.13E-07	0.0049	8.78E-08	-0.42	0.38	3.36E-08	289.02	0.699
17	0.0858	1.54E-06	0.0488	8.73E-07	-0.20	0.63	5.46E-07	0.0371	6.64E-07	-0.42	0.38	2.54E-07	289.11	0.752
18	0.0733	1.31E-06	0.0672	1.20E-06	-0.20	0.63	7.53E-07	0.0061	1.10E-07	-0.42	0.38	4.20E-08	289.08	0.699
19	0.0671	1.20E-06	0.0618	1.11E-06	-0.20	0.63	6.92E-07	0.0053	9.52E-08	-0.42	0.38	3.65E-08	289.17	0.698
avg	0.0715	1.28E-06	0.0581	1.04E-06	-0.20	0.63	6.51E-07	0.0134	2.39E-07	-0.42	0.38	9.16E-08	289.10	0.722
Well B														
16	0.0272	4.87E-07	0.0213	3.81E-07	-0.20	0.63	2.41E-07	0.0059	1.06E-07	-0.41	0.39	4.12E-08	290.28	0.739
17	0.0294	5.26E-07	0.0177	3.17E-07	-0.20	0.63	2.00E-07	0.0117	2.10E-07	-0.41	0.39	8.18E-08	290.21	0.761
18	0.0211	3.77E-07	0.0110	1.97E-07	-0.20	0.63	1.25E-07	0.0101	1.80E-07	-0.41	0.39	7.02E-08	290.22	0.769
19	0.0322	5.76E-07	0.0124	2.22E-07	-0.20	0.63	1.40E-07	0.0198	3.54E-07	-0.41	0.39	1.38E-07	290.29	0.783
avg	0.0275	4.92E-07	0.0156	2.79E-07	-0.20	0.63	1.76E-07	0.0119	2.12E-07	-0.41	0.39	8.28E-08	290.25	0.764
Well C														
16	0.0448	8.02E-07	0.0405	7.25E-07	-0.23	0.59	4.29E-07	0.0043	7.73E-08	-0.46	0.35	2.67E-08	288.94	0.715
17	0.0603	1.08E-06	0.0438	7.84E-07	-0.23	0.59	4.64E-07	0.0165	2.95E-07	-0.46	0.35	1.02E-07	288.87	0.747
18	0.0583	1.04E-06	0.0422	7.56E-07	-0.23	0.59	4.47E-07	0.0161	2.88E-07	-0.46	0.35	9.96E-08	289.04	0.747
19	0.0904	1.62E-06	0.0491	8.79E-07	-0.23	0.59	5.20E-07	0.0413	7.39E-07	-0.46	0.35	2.55E-07	289.14	0.767
avg	0.0634	1.14E-06	0.0439	7.86E-07	-0.23	0.59	4.65E-07	0.0196	3.50E-07	-0.46	0.35	1.21E-07	289.00	0.751
Well D														
16	0.1349	2.42E-06	0.1036	1.86E-06	-0.22	0.61	1.13E-06	0.0313	5.60E-07	-0.44	0.36	2.03E-07	289.28	0.741
17	0.1482	2.65E-06	0.1236	2.21E-06	-0.22	0.61	1.34E-06	0.0245	4.39E-07	-0.44	0.36	1.59E-07	289.16	0.731
18	0.1190	2.13E-06	0.1141	2.04E-06	-0.22	0.61	1.24E-06	0.0049	8.84E-08	-0.44	0.36	3.20E-08	289.26	0.693
19	0.1484	2.66E-06	0.1430	2.56E-06	-0.22	0.61	1.56E-06	0.0054	9.67E-08	-0.44	0.36	3.50E-08	289.26	0.689
avg	0.1376	2.46E-06	0.1211	2.17E-06	-0.22	0.61	1.32E-06	0.0165	2.96E-07	-0.44	0.36	1.07E-07	289.24	0.721
Well E														
16	0.0682	1.22E-06	0.0587	1.05E-06	-0.19	0.65	6.85E-07	0.0095	1.70E-07	-0.38	0.41	7.06E-08	290.23	0.726
17	0.0845	1.51E-06	0.0659	1.18E-06	-0.19	0.65	7.70E-07	0.0186	3.33E-07	-0.38	0.41	1.38E-07	290.16	0.739
18	0.0656	1.18E-06	0.0601	1.08E-06	-0.19	0.65	7.03E-07	0.0055	9.83E-08	-0.38	0.41	4.07E-08	290.39	0.711
19	0.0829	1.48E-06	0.0702	1.26E-06	-0.19	0.65	8.20E-07	0.0127	2.28E-07	-0.38	0.41	9.45E-08	290.67	0.728
avg	0.0753	1.35E-06	0.0637	1.14E-06	-0.19	0.65	7.45E-07	0.0116	2.07E-07	-0.38	0.41	8.59E-08	290.36	0.728

Appendix E - NETPATH model results

Well A - Well D colorimetric Fe(T); field Eh values: Eh = -4.75 mV and -13.7 mV for Wells A and D, respectively									
constraints: C, Ca, S, Na, Fe, redox, Al, K									
phase	model								
	1	2	3	4	5	6	7	8	9
calcite	1.33	1.27	2.34	2.34	2.34	1.33	1.33	1.33	
gypsum	0.00	0.06	-1.02	-1.02	-1.02		0.80		1.33
albite (+)	0.80	0.80	0.80	0.80	0.80	0.80		0.80	0.80
exchange	1.29	1.29	1.29	1.29	1.29	1.29	1.29	1.29	1.29
CH ₂ O (+)	1.02	1.07				1.02	1.02	1.02	2.34
goethite	0.04		0.79	0.42		0.04	0.04		-0.93
Fe-S		0.04	-0.75		0.83	0.00		0.08	0.97
montmorillonite	-0.40	-0.40	-0.40	-0.40	-0.40	-0.40	-0.40	-0.40	-0.40
H ₂ S	-1.66	-1.67	-1.56	-2.12	-2.74	-1.66	-1.66	-1.72	-1.79
pyrite (-)				-0.37	-0.79		0.00	-0.04	
all values in mmol/kg									

Well A - Well D colorimetric Fe(T); MINTEQ Eh values: Eh = -284 mV and -339 mV for Wells A and D, respectively									
constraints: C, Ca, S, Na, Fe, redox, Al, K									
phase	model								
	1	2	3	4	5	6	7	8	9
calcite	1.33	1.27	2.34	2.34	2.34	1.33	1.33	1.33	
gypsum	0.00	0.06	-1.02	-1.02	-1.02		0.80		1.33
albite (+)	0.80	0.80	0.80	0.80	0.80	0.80		0.80	0.80
exchange	1.29	1.29	1.29	1.29	1.29	1.29	1.29	1.29	1.29
CH ₂ O (+)	1.02	1.07				1.02	1.02	1.02	2.34
goethite	0.04		0.79	0.42		0.04	0.04		-0.93
Fe-S		0.04	-0.75		0.83	0.00		0.08	0.97
montmorillonite	-0.40	-0.40	-0.40	-0.40	-0.40	-0.40	-0.40	-0.40	-0.40
H ₂ S	-1.66	-1.67	-1.56	-2.12	-2.74	-1.66	-1.66	-1.72	-1.79
pyrite				-0.37	-0.79		0.00	-0.04	
all values in mmol/kg									

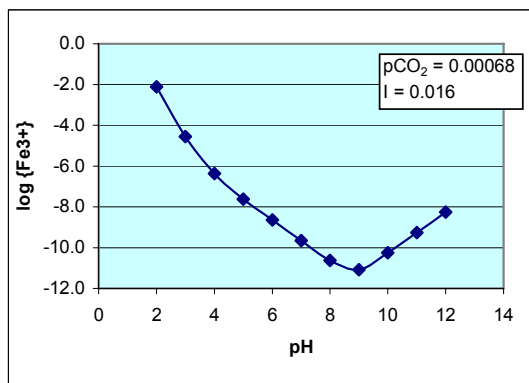
Appendix E - continued

Well A - Well E colorimetric Fe(T); field Eh values: Eh = -4.75 mV and -13.7 mV for Wells A and E, respectively									
constraints: C, Ca, S, Na, Fe, redox, Al, K									
phase	model								
	1	2	3	4	5	6	7	8	9
calcite	1.89	1.84	3.13	3.13	3.13	1.89	1.89	1.89	
gypsum	0.00	0.05	-1.24	-1.24	-1.24				1.89
albite (+)	0.74	0.74	0.74	0.74	0.74	0.74	0.74	0.74	0.74
exchange	1.85	1.85	1.85	1.85	1.85	1.85	1.85	1.85	1.85
CH₂O (+)	1.30	1.29				1.24	1.24	1.24	3.13
goethite	0.04		0.95	0.49		0.04	0.04		-1.35
Fe-S		0.04	-0.91		0.98	0.00		0.08	1.39
montmorillonite	-0.37	-0.37	-0.37	-0.37	-0.37	-0.37	-0.37	-0.37	-0.37
H₂S	-2.19	2.20	-2.07	-2.75	-3.49	-2.19	-2.19	-2.25	-2.38
pyrite (-)				-0.46	-0.95		0.00	-0.04	
all values in mmol/kg									

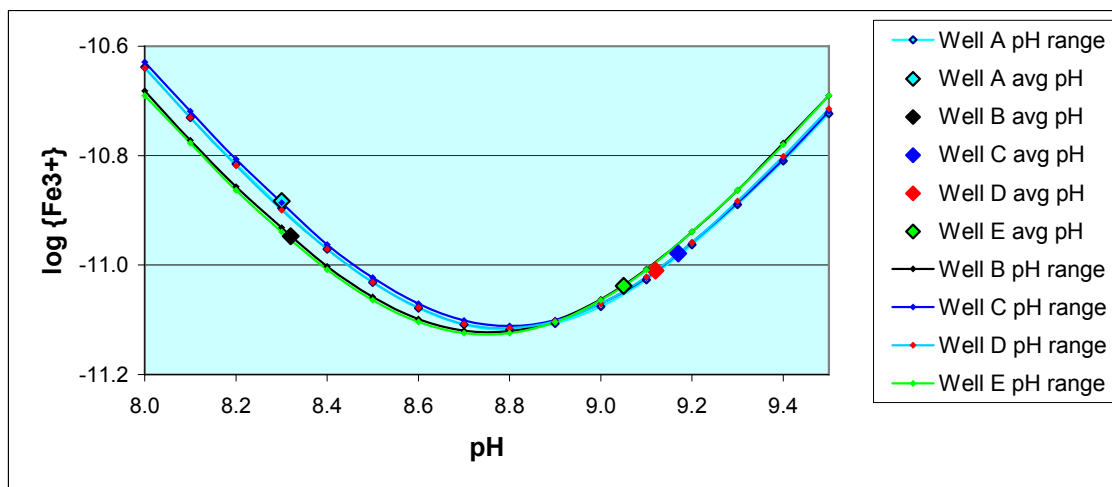
Well A - Well E colorimetric Fe(T); MINTEQ Eh values: Eh = -284 mV and -339 mV for Wells A and E, respectively									
constraints: C, Ca, S, Na, Fe, redox, Al, K									
phase	model								
	1	2	3	4	5	6	7	8	9
calcite	1.89	1.84	3.13	3.13	3.13	1.89	1.89	1.89	
gypsum	0.00	0.05	-1.24	-1.24	-1.24				1.89
albite (+)	0.74	0.74	0.74	0.74	0.74	0.74	0.74	0.74	0.74
exchange	1.85	1.85	1.85	1.85	1.85	1.85	1.85	1.85	1.85
CH₂O (+)	1.24	1.29				1.24	1.24	1.24	3.13
goethite	0.04		0.95	0.49		0.04	0.04		-1.35
Fe-S		0.04	-0.91		0.98	0.00		0.08	1.39
montmorillonite	-0.37	-0.37	-0.37	-0.37	-0.37	-0.37	-0.37	-0.37	-0.37
H₂S	-2.19	2.20	-2.07	-2.75	-3.49	-2.19	-2.19	-2.25	-2.38
pyrite				-0.46	-0.95		0.00	-0.04	
all values in mmol/kg									

Appendix F - ferrihydrite as "infinite solid" in equilibrium with Fe(III). Well chemistry from Table 7

pH	A		B		C		D		E	
	Fe3+ (m)	log Fe3+	Fe3+ (m)	log Fe3+	Fe3+ (m)	log Fe3+	Fe3+ (m)	log Fe3+	Fe3+ (m)	log Fe3+
8.0	2.30E-11	-10.64	2.08E-11	-10.68	2.35E-11	-10.63	2.29E-11	-10.64	2.04E-11	-10.69
8.1	1.86E-11	-10.73	1.69E-11	-10.77	1.91E-11	-10.72	1.86E-11	-10.73	1.67E-11	-10.78
8.2	1.53E-11	-10.82	1.39E-11	-10.86	1.56E-11	-10.81	1.52E-11	-10.82	1.37E-11	-10.86
8.3	1.27E-11	-10.90	1.17E-11	-10.93	1.30E-11	-10.89	1.26E-11	-10.90	1.15E-11	-10.94
8.4	1.07E-11	-10.97	9.95E-12	-11.00	1.09E-11	-10.96	1.07E-11	-10.97	9.81E-12	-11.01
8.5	9.30E-12	-11.03	8.75E-12	-11.06	9.49E-12	-11.02	9.30E-12	-11.03	8.63E-12	-11.06
8.6	8.34E-12	-11.08	7.97E-12	-11.10	8.50E-12	-11.07	8.36E-12	-11.07	7.88E-12	-11.10
8.7	7.79E-12	-11.11	7.59E-12	-11.12	7.92E-12	-11.10	7.80E-12	-11.11	7.51E-12	-11.12
8.8	7.62E-12	-11.12	7.57E-12	-11.12	7.74E-12	-11.11	7.67E-12	-11.12	7.51E-12	-11.12
8.9	7.82E-12	-11.11	7.92E-12	-11.10	7.93E-12	-11.10	7.89E-12	-11.10	7.87E-12	-11.10
9.0	8.40E-12	-11.08	8.66E-12	-11.06	8.50E-12	-11.07	8.50E-12	-11.07	8.63E-12	-11.06
9.1	9.40E-12	-11.03	9.83E-12	-11.01	9.49E-12	-11.02	9.52E-12	-11.02	9.80E-12	-11.01
9.2	1.09E-11	-10.96	1.15E-11	-10.94	1.10E-11	-10.96	1.10E-11	-10.96	1.15E-11	-10.94
9.3	1.29E-11	-10.89	1.37E-11	-10.86	1.30E-11	-10.89	1.31E-11	-10.88	1.37E-11	-10.86
9.4	1.55E-11	-10.81	1.67E-11	-10.78	1.56E-11	-10.78	1.58E-11	-10.80	1.66E-11	-10.78
9.5	1.89E-11	-10.72	2.04E-11	-10.69	1.91E-11	-10.72	1.93E-11	-10.71	2.04E-11	-10.69



I	pH	temp (K)	{Fe3+}	
			MINTEQ	log {Fe3+}
A	0.0155	8.3	289.1	1.31E-11 -10.8827
B	0.0147	8.32	290.25	1.13E-11 -10.9469
C	0.0206	9.17	289	1.05E-11 -10.9788
D	0.0181	9.12	289.24	9.78E-12 -11.0097
E	0.0123	9.05	290.36	9.16E-12 -11.0381



Appendix G - Fe substrate data for wells in the Lahontan Valley, used for MINTEQ analyses.

Lateral flow wells - Fallon area - all shallow

Assam (Assam, 2007)
W&L (Welch and Lico, 1998)

M (As) is adsorbed As in µg extracted per g of sediment material
M (Fe) is Fe (assumed as HFO) in µg of Fe extracted per g of sediment material
G (As) is concentration of As in g/L
G (Fe) is concentration of Fe in g/L
C (As observed) is mol/L after extraction from sediment surface
D is specific gravity of sediment ~ 2.6
Ø is porosity

The value for 4(#15) from W&L was 0.000260 mol/L corresponding to 3.2 µg/g As. This is just 2 sd away from the mean.
Discarding it according to Chauvenet's criterion.
The corresponding Fe value was retained.

W is GAM of As (74.92 g/mol) or Fe (55.85 g/mol)

As predicted is from adsorption models

$$G = M * D * (1 - \emptyset) * (1000 \text{ cm}^3 / \text{L}) * (10^{-6} \text{ g} / \mu\text{g}) / \emptyset$$

and $C = G/W$

(from Welch and Lico, 1998)

W
As 74.92
Fe 55.85

W&L lateral	M Fe (µg/g)	G Fe g/L	observed value to compare to mine		(from adsorption modeling)		
			M As (µg/g)	G As g/L	C As adsorbed mol/L	modeling As predicted mol/L	
1 (#6)	1440	8.74	1.3	0.0079	0.000100	0.00150	
2 (#13)	1180	7.16	1.5	0.0091	0.000120	0.00026	
3 (#14)	880	5.34	0.9	0.0055	0.000073	0.00060	
4 (#15)	1170	7.10	3.2			0.00031	
5 (#17)	680	4.13	0.7	0.0042	0.000057	0.00050	
6 (#18)	1000	6.07	1.1	0.0067	0.000089	0.00063	
W&L avg	1058	6.42	1.1	0.0067	0.000088	0.000633	
Assam 40	2978		1.473				
Assam 70	889		0.94				
Assam 110	29.00		0.79				
Assam avg	1298.67	7.88	1.068	0.0065	0.000086		
W&L&J avg		Fe (g/L) 7.15 Fe	MINTEQ input value	As (g/L) 0.006575 As	As _{ads} (mol/L) 0.000087	As _{ads} (mg/L) 6.528	As _{ads} (µg/L) 6528
					Arsenic adsorbed onto HFO		